
# Vibration isolation under isolator-structure interaction

Submitted by Jorge Pérez-Aracil to the University of Exeter as a thesis for the degree of Doctor of Philosophy in Engineering in November 2020



I certify that all material in this thesis which is not my own work has been identified and that no material has previously been submitted and approved for the award of a degree by this or any other University

Signature .....
(Jorge Pérez-Aracil)

*A mis padres, Luis y Carmen,*
*y a mis abuelas, Monserrate y Carmen.*

# Abstract

This thesis analyses a general case of the vibration isolation (VI) problem, considering both a rigid and non-rigid supporting structures. The aim is to study changes on the behaviour of both systems isolators and supporting structure when the interaction phenomenon between them is considered. The influence of the VI task on the base response is evaluated. In addition, the effect of the base dynamics on the the VI and alignment problem is studied.

The novel contribution to the knowledge of this thesis is formulation of a novel VI approach, which facilitates a holistic analysis of the problem considering all the systems involved on it. This approach is valid for any number of isolators and for any type of base structure. Moreover, different control objectives can be easily defined; evaluation of the interaction phenomenon on both the platform and base response for different VI techniques; demonstration of the importance of the isolator damping ratio on the influence that the VI task has on the base response; evaluation of the effects of the supporting structure dynamics on the VI and alignment problem when multiple isolators are involved; analysis of the Multiple-Input-Multiple-Ouput (MIMO) control strategy by comparison with the Single-Input-Single-Output (SISO) control strategy. This comparative has been made for the VI and alignment problem of multiple isolators on a non-rigid supporting structure and includes analysis of the effectiveness of the Coral Reefs Optimization algorithms to find nearly-optimal control gains in VI and alignment problems.

Through the investigation made for this thesis, a number of significant results have been reached, which show the importance of the supporting structure dynamics on the VI and alignment task. Moreover, the interaction phenomenon, and its consequence on the base response, has been investigated experimentally. The results

derived from this thesis conclude that, for most scenarios, the dynamics of the base affects the VI task. Also, the active VI (AVI) technique shows a greater influence on the base response than passive VI (PVI) technique, for most cases. It has been observed that the use of AVI technique can additionally be oriented to control vibrations of the supporting structure, while the VI task is developed. Significant differences have been found when multiple isolators are involved in the same task for the alignment and VI problem, depending on whether or not the dynamics of the base are considered. The best set of control gains for the rigid-support case (which lead to maximum damping ratio) differ from those obtained when the supporting structure is considered as a flexible system, for different cases analysed in this thesis. The MIMO control strategy has shown great improvement with respect to the use of the SISO control strategy. Also, the Coral Reefs Optimization algorithms have been demonstrated to be a suitable tool to find nearly-optimal solutions for this type of problems.

# Acknowledgements

Paul, thank you so much for giving me the most challenging and fascinating professional opportunity of my life. This is something I will always remember. Thanks to you I have had the opportunity to live in UK, where now I feel as at home. The confidence and support you have shown to me have been really important. Thank you for guiding me during the research process, showing the importance of finding a "real application", and always leading the work to the correct way. It has been a pleasure to learn from you.

The importance of knowing people in the academic world is now high. But the importance of making new friends is even higher: Emiliano, thank you so much. Your guidance has been very important, but not only for thesis, for my life. Thanks for your patience. Thanks for the enthusiasm you show every day in your work. Thank you for having time to respond questions with obvious answers for you about control systems. Thanks for being humble, and thank you for showing me the importance of taking a beer break.

I also want to thank Iván, who has been an inspiration for me. Thank you for having time to teach me about how to carry out an experimental test, and how to address a paper. Thank you for motivating me to do more. Also, thank for being critical with the work.

Sancho, thank you for the support. I have learnt a lot from you. Also, you received me at Univeristy of Alcalá as one of your team, and it was very important for me.

I also would like to thank Carlos, Sara and Laura for all the good moments we have lived in and out the office. I hope this has been just the beginning of much more!

Thanks to the Univerisy of Alcalá for giving me the possibility of doing a research stay. This opportunity has been very important for me, not only for my research development, but also for my personal experience.

I would like to thank Mubarak Patel for being best friend. Thank you for all the good moments we have lived there. I am looking forward to see what is coming on now! Thank you for showing me the UK life, and of course, thank you for loving too much the chicken!

I also want to thank my friend James Bassit. I will always remember the time in lab thanks of you. You made it easier and more fun. Thank you for your enthusiasm in your work, and for coming to Spain to live great moments! I am waiting for you again!

I want to thank Pedro Castrillo. His advices have helped me during the thesis. Your experienced perspective has lead to me to take the correct way. Thank you.

I would like to thank Katy Manning. She has helped me with many different things since I arrived until today. Thank you for arranging all the stuff in the office and for always having a kind answer.

*Me gustaría agradecer, muy especialmente, a mi mujer, Beatriz. Gracias por haber estado ahí siempre. Gracias por venir conmigo a UK, por hacerlo fácil. Gracias por vivir estos años, algo locos, conmigo. Has sido el pilar fundamental de apoyo durante todo este tiempo.*

*Quiero agradecer a toda mi familia el apoyo que han mostrado durante la tesis, especialmente a mis padres, a mis hermanos, Luis y Carmen, y a Helena. Y por supuesto, a mis sobrinos, Luis y Leo, que con su llegada han alegrado aún más nuestros encuentros. El apoyo de todos ellos durante la tesis ha sido fundamental para su desarrollo.*

# Contents

# List of Figures

# List of Tables

# List of Abbreviations

| | |
|---|---|
| 2Px | 2-Points crossover |
| AF | Acceleration Feedback |
| AVC | Active Vibration Control |
| AVI | Active Vibration Isolation |
| CRO | Coral Reefs Optimization |
| CRO-SL | Coral Reefs Optimization algorithm with Substrate Layers |
| DE | Differential Evolution |
| DVF | Direct Velocity Feedback |
| ER | Electro-Rheological |
| FA | Firefly Algorithm |
| FF | Force Feedback |
| FRF | Frequency Response Function |
| GM | Gaussian Mutation |
| HMCR | Harmony Memory Considering Rate |
| HS | Harmony Search |
| LQG | Linear Quadratic Gaussian |
| MIMO | Multiple-Input-Multiple-Output |
| MPx | Multi-points crossover |
| MR | Magneto-Rheological |
| NaFa | Neighbourhood Attraction Firefly Algorithm |
| PAR | Pitch Adjusting Rate |
| PF | Position Feedback |
| PFF | Positive Force Feedback |

| | |
|---|---|
| PID | Proportional Integral Derivative |
| PVI | Passive Vibration Isolation |
| SAVI | Semi-Active Vibration Isolation |
| SDOF | Single Degree of Freedom |
| SISO | Single-Input-Single-Output |
| TF | Transfer Function |
| TMD | Tuned Mass Damper |
| VI | Vibration Isolation |
| WWo | Water Wave Optimization |

# Symbols

**Uppercase letters**

$\boldsymbol{A}_B$ State space matrix of the supporting structure system

$A_{GM}$ Linear dimension of the domain search for the Gaussian Mutation algorithm

$\boldsymbol{A}_I$ State space matrix of the vibration isolation system

$\boldsymbol{A}_{I_j}$ State space matrix of the $j^{th}$ isolator

$\boldsymbol{B}_{BD}$ Disturbance force input state space matrix of the supporting structure system

$\boldsymbol{B}_{BI}$ Isolator force input state space matrix of the supporting structure system

$\boldsymbol{B}_{IB}$ Base disturbance input state space matrix of the vibration isolation system

$\boldsymbol{B}_{IB_j}$ Base disturbances input state space matrix of the $j^{th}$ isolator

$\boldsymbol{B}_{IF}$ Force disturbances input state space matrix of the vibration isolation system

$\boldsymbol{B}_{IF_j}$ Force disturbances input state space matrix of the $j^{th}$ isolator

$C_1$ Arbitrary value of the mode shape amplitude in a pinned-pinned supported beam

$\boldsymbol{C}_B$ Output state space matrix of the supporting structure system

$\boldsymbol{C}_f(s)$ Controller matrix

$C_f(s)$ Generic controller

$C_{f_{jr}}(s)$ Controller element applied to the platform of the $j^{th}$ isolator from the platform of the $r^{th}$ isolator

$\boldsymbol{C}_I$ Output state space matrix of the vibration isolation system

$\boldsymbol{C}_{I_j}$ Output state space matrix of the $j^{th}$ isolator

$\boldsymbol{D}_{BD}$ Feed-through term of disturbance forces input of the supporting structure system

$\boldsymbol{D}_{BI}$ Feed-through term of isolator forces input of the supporting structure system

$\boldsymbol{D}_{IF}$ Feed-through term of the vibration isolation system

$\boldsymbol{D}_{IF_j}$ Feed-through term of the $j^{th}$ isolator

$E_x$ Young's module

$F$ Evolution factor weighting the perturbation amplitude for the Differential Evolution algorithm

$\boldsymbol{F}_a(s)$ Active force vector in Laplace domain

$F_{a_j}(s)$ Active force of the $j^{th}$ isolator in Laplace domain

$F_{ad}$ Percentage of asexual reproduction

$F_b$ Frequency of broadcast spawning

$\boldsymbol{F}_d(s)$ Disturbance force vector in Laplace domain

$F_{d_k}(s)$ $k^{th}$ disturbance force applied on the supporting structure in Laplace domain

$F_{dep}$ Fraction of corals for depredation

$\boldsymbol{G}_{AVI,F}(s)$ Feedback control matrix

$G_{AVI,F}[j,r]$ Feedback control element applied to the platform of the $j^{th}$ isolator from the platform of the $r^{th}$ isolator

$\boldsymbol{G}_{AVI,F_w}(s)$ Feedforward control matrix

$G_{AVI,F_w}[j,r]$ Feedforward control element applied to the platform of the $j^{th}$ isolator from the platform of the $r^{th}$ isolator

$\boldsymbol{G}_B^{AVI}(s)$ Transfer function from disturbance forces to base movement considering active vibration isolation technique

$\boldsymbol{G}_B^{PVI}(s)$ Transfer function from disturbance forces to base movement considering passive vibration isolation technique

$\boldsymbol{G}_{BD}(s)$ Transfer function from disturbance forces to base movement

$\boldsymbol{G}_{BI}(s)$ Transfer function from isolator forces to base movement

$\boldsymbol{G}_I(s)$ Generic transmissibility transfer function of the isolator

$\boldsymbol{G}_I^{AVI}(s)$ Transmissibility transfer function of the isolator considering active vibration isolation technique

$\boldsymbol{G}_I^{PVI}(s)$ Transmissibility transfer function of the isolator considering passive vibration isolation technique

$\boldsymbol{G}_{IB}(s)$ Transfer function from base movement to platform movement

$\boldsymbol{G}_{IF}(s)$ Transfer function from active force to platform movement

$\boldsymbol{I}_{2m}(s)$ Identity $2m \times 2m$ matrix

$\boldsymbol{I}_n(s)$ Identity $n \times n$ matrix

$\boldsymbol{I}_{2n}(s)$ Identity $2n \times 2n$ matrix

$I_x$ Moment of inertia of the cross section respect to the horizontal axis

$\boldsymbol{K}_B^C$ Generic control gain matrix for $C$ type of control and $B$ type of supporting structure

$\boldsymbol{K}_V^S$ Control gain matrix for a rigid supporting structure considering a Single-Input-Single-Output control technique

$\hat{\boldsymbol{K}}_V^S$ Optimal control gain matrix for a rigid supporting structure considering a Single-Input-Single-Output control technique

$\boldsymbol{K}_{FV}^S$ Control gain matrix for a non-rigid supporting structure considering a Single-Input-Single-Output control technique

$\hat{\boldsymbol{K}}_{FV}^{S}$ Optimal control gain matrix for a non-rigid supporting structure considering a Single-Input-Single-Output control technique

$\boldsymbol{K}_{FV}^{M}$ Control gain matrix for a non-rigid supporting structure considering a Multiple-Input-Multiple-Output control technique

$\hat{\boldsymbol{K}}_{FV}^{M}$ Optimal control gain matrix for a non-rigid supporting structure considering a Multiple-Input-Multiple-Output control technique

$L_{12}$ Length between left-end and mid-span isolators

$L_{23}$ Length between right-end and mid-span isolators

$L_b$ Length of the beam supporting structure

$L_{sl}$ Distance from the left-end isolator to the left support in a the beam supporting structure

$L_{sr}$ Distance from the right-end isolator to the right support in a the beam supporting structure

$\boldsymbol{M}_m$ Modal mass of the supporting structure

$\boldsymbol{M}_l$ Mass per unit length of the supporting structure

$\boldsymbol{M}_p$ Isolators system mass matrix

$M_\Lambda$ Linear dimension of the of the rectangular shaped reef

$N_\Lambda$ Linear dimension of the of the rectangular shaped reef

$\mathbb{N}$ Natural numbers set

$N_i$ Random number following Gaussian distribution

$P_d$ Probability of depredation

$\boldsymbol{X}_b(s)$ Base displacement vector in Laplace domain

$X_b(s)$ Base displacement of a single degree of freedom supporting structure in Laplace domain

$X_{b_j}(s)$ Base displacement at the location of the $j^{th}$ isolator in Laplace domain

$\boldsymbol{X}_p(s)$ Platform displacement vector in Laplace domain

$X_p(s)$ Platform displacement of a generic isolator in Laplace domain

$X_{p_j}(s)$ Platform displacement of the $j^{th}$ isolator in Laplace domain

$\boldsymbol{Y}_b(s)$ Output vector of the supporting structure system in Laplace domain

$Y_{b_j}(s)$ Output of the supporting structure at the location of the $j^{th}$ isolator in Laplace domain

$\boldsymbol{Y}_I(s)$ Output vector of the vibration isolation system in Laplace domain

$Y_{I_j}(s)$ Output of the $j^{th}$ isolator in Laplace domain

$\boldsymbol{Z}$ Diagonal matrix of damping ratios

---

**Lowercase letters**

$c_b$ Damping of a generic supporting structure

$c_f(t)$ Generic controller in time domain

$c_p$ Damping of a generic isolator

$c_{p_j}$ Damping of the $j^{th}$ isolator

$f_{G(0,\sigma^2)}(x)$ Gaussian probability density function

$\boldsymbol{f}_a(t)$ Active force vector in time domain

$f_a(t)$ Active force of a generic isolator in time domain

$f_{a_j}(t)$ Active force of the $j^{th}$ isolator in time domain

$\boldsymbol{f}_d(t)$ Disturbance force vector in time domain

$f_d(t)$ Disturbance force in time domain for a single degree of freedom supporting structure

$f_{d_k}(t)$ $k^{th}$ disturbance force applied on the supporting structure in time domain

$f_{sp}(t)$ Spring force in time domain

$f_{dp}(t)$ Damper force in time domain

$\boldsymbol{f}_I(t)$ Vector of isolator forces in time domain

$f_{I_j}(t)$ Force of the $j^{th}$ isolator in time domain

$j$ Imaginary unit

$k_b$ Generic control gain

$k_{b_{jr}}$ Generic control gain applied to the platform of the $j^{th}$ isolator from the $[j,r]$ controller

$k_{fv_{jr}}$ Control gain applied to the platform of the $j^{th}$ isolator from the $[j,r]$ controller for a flexible supporting structure type

$\hat{k}_{fv_{jr}}$ Optimal control gain applied to the platform of the $j^{th}$ isolator from the $[j,r]$ controller for a flexible supporting structure type

$k_{v_{jr}}$ Control gain applied to the platform of the $j^{th}$ isolator from the $[j,r]$ controller for a rigid supporting structure type

$\hat{k}_{v_{jr}}$ Optimal control gain applied to the platform of the $j^{th}$ isolator from the $[j,r]$ controller for a rigid supporting structure type

$k_p$ Stiffness of a generic isolator

$k_{p_j}$ Stiffness of the $j^{th}$ isolator

$m$ Number of modes considered

$m_b$ Mass of the supporting structure

$m_p$ Payload mass of a generic isolator

$m_{p_j}$ Payload mass of the $j^{th}$ isolator

$n$ Number of isolators

$n_s$ Number of substrate layers considered

$r_m$ Mass ratio

$r_\omega$ Frequency ratio

$t$ Time variable

$x'$ Mutated larva

$x^*$ Best solution found in a specific iteration in Water Wave optimization algorithm

$x_{B_q}(t)$ State-space variable of the supporting structure system for the $q^{th}$ mode

$\dot{x}_{B_q}(t)$ Derivative of the state-space variable of the supporting structure system for the $q^{th}$ mode

$\boldsymbol{x}_B(t)$ State-space vector of the supporting structure

$\dot{\boldsymbol{x}}_B(t)$ Derivative of the state-space vector of the supporting structure

$x_b(t)$ Base position in time domain of a generic isolator

$x_{b_j}(t)$ Base position of the $j^{th}$ isolator in time domain

$\ddot{\boldsymbol{x}}_b(t)$ Base acceleration vector in time domain

$\ddot{x}_b(t)$ Base acceleration of a generic isolator in time domain

$\ddot{x}_{b_j}(t)$ Base acceleration of the $j^{th}$ isolator in time domain

$\boldsymbol{x}_I(t)$ State-space vector of the vibration isolation system

$\dot{\boldsymbol{x}}_I(t)$ Derivative state-space vector of the vibration isolation system

$\boldsymbol{x}_{I_j}(t)$ State-space vector of the $j^{th}$ isolator

$\dot{\boldsymbol{x}}_{I_j}(t)$ Derivative state-space vector of the $j^{th}$ isolator

$\boldsymbol{x}_k$ Coral of the Coral Reefs with Substrate Layers algorithm

$x_p(t)$ Platform displacement of a generic isolator in time domain

$x_{p_j}(t)$ Platform displacement of the $j^{th}$ isolator in time domain

$\ddot{\boldsymbol{x}}_p(t)$ Platform acceleration vector in time domain

$\ddot{x}_p(t)$ Platform acceleration of a generic isolator in time domain

$\ddot{x}_{p_j}(t)$ Platform acceleration of the $j^{th}$ isolator in time domain

$x_{r_j}$ Relative position between platform and base of the $j^{th}$ isolator

$\dot{x}_{r_j}$ Relative velocity between platform and base of the $j^{th}$ isolator

$\ddot{x}_{r_j}$ Relative acceleration between platform and base of the $j^{th}$ isolator

$\boldsymbol{y}_b(t)$ Output vector of the supporting structure system in time domain

$\boldsymbol{y}_I(t)$ Output vector of the vibration isolation system in time domain

$y_{I_j}(t)$ Output of the $j^{th}$ isolator in time domain

---

**Greek letters**

$\alpha$ Functional weight corresponding with the transmissibility

$\alpha_c$ Maximum number of iterations of the Coral Reefs Optimization with Substrate Layers algorithm

$\beta$ Functional weight corresponding with the alignment

$\beta_f$ Breaking coefficient in Water Waver Optimization

$\beta_o$ Attractiveness at distance $r = 0$

$\gamma$ Influence parameter on the supporting structure response

$\omega_b$ Natural frequency of the supporting structure

$\omega_c$ Cut-off frequency of the feedback controller

$\omega_p$ Natural frequency of a generic isolator

$\omega_{p_j}$ Natural frequency of the $j^{th}$ isolator

$\zeta_b$ Damping ratio of the supporting structure

$\zeta_p$ Damping ratio of a generic isolator

$\zeta_{p_j}$ Damping ratio of the $j^{th}$ isolator

$\zeta_{p_j}^{AVI}$ Damping ratio of the $j^{th}$ isolator due to the effect of the AVI control

$\theta_{j,r}$ Angle between platforms of the $j^{th}$ and $r^{th}$ isolators

$\sigma$ Standard deviation of the Gaussian probability density function

$\rho$ Density of the material

$\rho_o$ Fraction of reef capacity initially occupied

$\mathbf{\Omega}$ Matrix of natural frequencies of the supporting structure

$\phi_{b_q}$ Modal shape of the $q^{th}$ mode

$\mathbf{\Phi}_D$ Modal shape matrix of the supporting structure at disturbance forces locations

$\mathbf{\Phi}_I$ Modal shape matrix of the supporting structure at isolator locations

$\mathbf{\Phi}_I^T$ Tranpose of the modal shape matrix of the supporting structure at isolator locations

$\Lambda_T$ Transmissibility functional

$\Lambda_A$ Alignment functional

$\Lambda$ Domain of the rectangle shaped reef

---

**Subscripts**

$B$ Generic type of supporting structure in control gain matrix, it can be either $V$ (rigid) or $FV$ (flexible)

$FV$ Flexible supporting structure type in control gain matrix

$fv$ Flexible supporting structure type in control gain element

$j$ Isolator number

$l$ Number of disturbance forces

$lk$ Spring deflection at lock-up

$m$ Number of modes considered

$q$ Mode number

$r$ Number of the isolator used to generate the control signal

$V$ Rigid supporting structure type in control gain matrix

$v$ Rigid supporting structure type in control gain element

---

**Superscripts**

$C$ Generic control matrix strategy, it can be either $S$ (Single-Input-Single-Output) or $M$ Multiple-Input-Multiple-Output

$M$ Multiple-Input-Multiple-Output control strategy

$S$ Single-Input-Single-Output control strategy

---

**Math symbols**

$*$ Convolution operator

$\mathbf{0}_m$ Zero $m \times m$ matrix

$\mathbf{0}_n$ Zero $n \times n$ matrix

$\mathbf{0}_{m,l}$ Zero $m \times l$ matrix

$\|\bullet\|_\infty$ H-infinity norm of $\bullet$

$\sum_a^b \bullet$ Summation from $a$ to $b$ of the elements of $\bullet$

$(\bullet)^T$ Transpose of $\bullet$

$\mathcal{U}(a, b)$ Uniformly distributed function beteween $a$ and $b$

# Chapter 1

# Introduction

## 1.1 Background

There is an ever increasing need to provide the highest quality vibration environments for extremely sensitive scientific and manufacturing processes. Application areas as diverse as bioengineering and biotechnology, medical imaging, materials science, nano- and quantum engineering, communications technology, deep space observation and precision manufacturing rely on our ability to provide stable platforms for this most sensitive instrumentation ever produced. A key technology for delivering these stable platforms is vibration isolation (VI).

The VI task implies the use of an isolator, situated between the payload, and the base on which is situated [Preumont, 2018a] (Figure 1.1). Vibration propagation occurs in two main scenarios: scenario 1 - Equipment generates vibrations that are transferred onto the supporting structure, and scenario 2 - Support structure propagates vibration onto the sensitive equipment it supports, [Preumont, 2018a]. Research aimed at AVI for Scenario 1 is significantly mature, [Gardonio et al., 1997a, Gardonio et al., 1997b]. Owing to the current thrust towards precise, noise-free measurements, micro- and nanoscale machining and high-density electronic device manufacturing where sensitive equipment needs to be isolated from vibrations propagating through the supporting structure, improved VI techniques aimed at Scenario 2 are needed. The contribution to scenario 2 is the aim of this thesis.

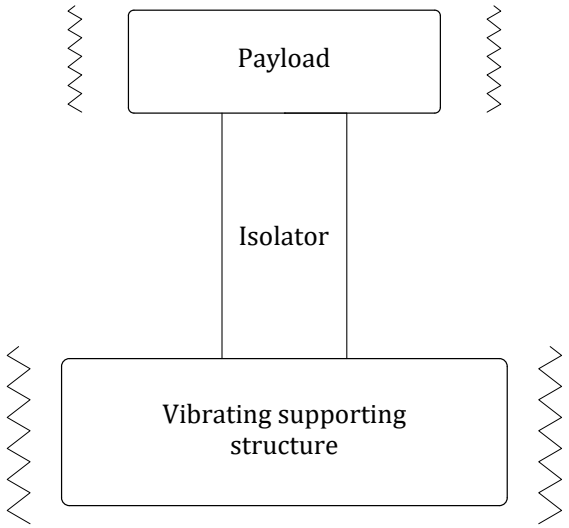


Figure 1.1: Illustrative example of the VI problem.

### 1.1.1 Isolator-supporting structure interaction

The common hypothesis for scenario 2, in classic isolator system design, is to consider the supporting structure as an infinitely rigid system compared with the isolator. This assumption is reasonable when the *control force* (i.e., the force applied on both the payload and the supporting structure) exerted by the isolation system does not affect significantly the base response, [Kaplow and Velman, 1980, Wang et al., 2016a, Mikhailov and Bazinenkov, 2017]. However, this hypothesis is false in a wide range of practical examples [Inman, 1990, Huang et al., 2003, Liu et al., 2012, Farshidianfar et al., 2012, Venanzi et al., 2017, Jiang et al., 2018, Alujević et al., 2019, Allaoua and Guenfaf, 2019]. This interaction phenomenon may change the response of the supporting structure. Thus, vibration reduction on the supporting structure can also improve the isolation performance, since the absolute vibration isolation level may be reduced.

Scenario 2, with interaction between the isolator system and the supporting structure, can be defined as a hybrid scenario. In this case, the supporting structure vibration may occur due to two disturbance inputs: i) the disturbance forces and ii) the control force from the isolators. These vibrations affect the absolute vibration measured on the payload. Thus, if the interaction between both system

is significant, the isolator can contribute, positively or negatively, to mitigate the supporting structure vibration. Then, isolator and supporting structure dynamics might be considered together in order to achieve the payload vibration requirements. It is necessary to know when the hypothesis of considering the base as an infinitely rigid and heavy system is not valid. This information may be useful to select and to design the isolation system. This thesis studies how the interaction also depends on the VI technique, the control objective and the number and location of the isolators. The consideration of this interaction can improve the performance of the VI. Thus, this thesis shows that the rigid hypothesis is not valid in a significant and not obvious number of practical cases.

### 1.1.2 Vibration isolation techniques

Depending on the way in which the isolator generates the force to control the payload movement, the so called control force or *controlled force*, it is possible to distinguish three different techniques: i) passive VI (PVI), ii) semi-active VI (SAVI), iii) active VI (AVI).

For PVI, the controlled force is just a reaction to the relative movement between the base and the platform (where the payload is situated) of the isolator. The dynamic properties of the isolator are constant [Rivin, 2003, Sun et al., 2015a], as they have to be specifically designed for the task. One of the main issues of this technique is the narrow rejection bandwidth, since VI does not occur for disturbance frequencies lower than $\sqrt{2}\omega_p$, where $\omega_p$ is the natural frequency of the isolator. This has motivated the development of non-linear techniques, which can lead to an increase in the rejection bandwidth. A virtual reduction of the natural frequency of the isolator can be reached by changing its stiffness. This technique is usually combined with AVI [Kamesh et al., 2012, Alujević et al., 2018].

When the stiffness and/or viscous damping of the isolator can be changed during operation, the technique is SAVI [Karnopp et al., 1974, Liu et al., 2008, Jiang et al., 2020]. This technique solves one of the main problems of PVI technique, since it is possible to adapt the dynamic properties of the isolator to the task requirements. For

that purpose, the use of magneto-rheological dampers has been widely investigated [Liao and Lai, 2002, Zhang et al., 2009, Ho et al., 2013], which can change the dynamic properties through the application of an electromagnetic field.

The use of PVI and SAVI techniques is suitable for many applications. However, the AVI technique presents numerous advantages over them, such as [Ruzicka, 1968]: i) the possibility to adapt the control strategy to the task requirements, ii) zero static deflection and iii) the possibility to follow trajectories. The use of this technique implies the application of an *active force* on the platform, and by consequence, on the supporting structure.

### 1.1.3 Optimization problem involved in multiple isolators

In scenarios in which multiple isolators are involved in the same task, the control strategy must deal with this more complex problem. For example, in manufacturing industries or in research centres, such as Diamond Light Source (DLS), in which multiple laser devices must be aligned between them. In these cases, AVI strategies are required, as occurs multi-degree of freedom systems (e.g. Stewart platforms) or applications where the alignment between equipment is necessary [Bastaits et al., 2009, Kong and Huang, 2018, Li et al., 2018]. Note that, if the hypothesis of a rigid base is considered, the alignment problem may be considered analogous to obtaining the best VI performance in terms of platform movement with respect to the supporting structure. Thus, each isolator can be considered as an individual system that does not interact with other isolators or with the supporting structure. However, if the isolators are situated on a non-rigid supporting structure, the problem must be analysed from a wider perspective, considering the effect that the isolator makes on the supporting structure response. This effect may involve improvements in the VI performance and in the alignment between these multiple devices. Therefore, the model used to design AVI control must consider the supporting structure model, which is excited by both external disturbances and by each isolator system, in order to improve the performance of the isolation and alignment control objectives.

When the VI system is comprised of multiple isolators, their responses are coupled by the supporting structure dynamics. Thus, the system is considered as a Multiple-Input-Multiple-Output (MIMO) AVI system. However, the controller system of each individual isolator can be either a Single-Input-Single-Output (SISO) system or a MIMO one, depending on the strategy adopted. This thesis proves that the use of MIMO control strategies leads to better solutions in AVI problems than SISO strategies, as occurs in other applications [Chanan et al., 2004, Beijen et al., 2018, Song et al., 2018, Xie et al., 2018]. The implementation of the MIMO controller may be difficult due to the following issues: i) there must be a trade off between the objectives of VI and alignment, ii) the stability of the intrinsic feedback loop must be guaranteed and iii) the number of controller parameters should be optimally tuned. Thus, the optimal control design of the MIMO AVI controllers subjected to stability restrictions is a very complex problem, which may not be solved by traditional optimization approaches. This thesis explores the use of the recently proposed Coral Reefs Optimization (CRO) algorithms [Gao et al., 2019, Tsai et al., 2019]. The optimization of MIMO AVI controllers shows that vibration isolation under isolator-structure interaction is a complex and not obvious problem. Thus, this thesis tries to be a reference work, which can be used to develop more complex control laws and design criteria can be explored and implemented in the future.

## 1.2 The research problem

As was mentioned in the background, the main objective of this thesis is to show the effect of the interaction phenomenon between the isolator and the supporting structure on the VI and alignment performance. The following novel approaches, to the author's best knowledge, are developed in this research work related with this issue:

1. A formulation of the VI framework is developed. It allows defining control objectives, which can be accomplished by the definition of the functional.

2. The interaction phenomenon through the mathematical formulation is proved by simulation and experimental results. A proof of concept, which is based on a single isolator situated on a single degree of freedom (SDOF) supporting structure, is included.

3. Generalisation of the problem. Instead of considering a single isolator and a simplified supporting structure model, the problem of multiple isolators located on a general supporting structure is studied.

4. Based on the knowledge of the VI response, which is coupled by the base structure, the evaluation of SISO and MIMO control strategies is made.

5. Search of optimal control gain values, based on a functional definition, considering stability conditions of both systems: isolator and supporting structure systems. The recently proposed CRO is used to optimally design this multivarible problem .

## 1.3 Organisation of the Thesis

The remainder of the thesis is as follows: Chapter 2 shows the formulation of the vibration isolation problem. Also, a literature review, focused on the different vibration isolation techniques is included. This state of the art also includes works where the interaction phenomenon theory is also developed. The proof of concept is shown in Chapter 3, in which an isolator is situated on a SDOF supporting structure. The influence of both techniques PVI and AVI on the base response are compared. Also, an experimental test is carried out to validate the theory developed. Chapter 4 formulates the VI and alignment problem considering the general framework presented in Chapter 2. In addition, Chapter 4 particularises this framework to three isolators situated on a flexible supporting structure. A SISO control strategy is followed, and the results are compared with the case in which a rigid supporting structure is considered. Chapter 5 analyses the same example as in Chapter 4, but instead a MIMO control strategy is proposed. The control gains are tuned using the CRO

algorithms. The conclusions derived from the research made for this thesis, and the proposed future works, are shown in Chapter 6.

# Chapter 2

# Related Work

## 2.1 Introduction

This chapter shows a literature review of the main VI techniques used in the aforementioned scenario 2. The related works are divided into two groups. The first group presents the most relevant works when the supporting structure is considered as a rigid system. In this subsection, the works are classified as PVI, SAVI and AVI techniques. In order to present these contributions in a clear way, this chapter begins with an introduction of the classic VI approach. In addition, the transmissibility Transfer Function (TF) between the acceleration measured at the payload and at the supporting structure is defined when feedback and/or feedforward AVI control strategies are used.

The second group presents the related works when the supporting structure is considered as a non-rigid system. The chapter ends with the first contribution of this thesis: a common framework for vibration isolation problems under isolator-structure interaction, which is based on [Balas, 1978]. This new formulation allows the generalization of the VI problem for any number of isolators and for any modal model of flexible supporting structure. This novel approach is used to present the rest of the thesis contributions, which have been accepted in international congress and indexed journals or have been submitted to indexed journals.

## 2.2 Modelling the vibration isolation problem

The transmissibility model of a generic isolator $j$[1], such that $\{1 \leq j \leq n, j \in \mathbb{N}\}$, is shown in Figure 2.1. The mass to be isolated is $m_{p_j}$, which is situated on the isolator platform. As was mentioned above, the control force is the force applied to the platform, which it is also applied to the supporting structure with opposite sign, and its value is given by $m_{p_j}\ddot{x}_{p_j}$. The dynamic properties of the isolator are modelled with its stiffness $k_{p_j}$ and its viscous damping $c_{p_j}$. The active force $f_{a_j}(t)$ is obtained either by a feedback and/or feedforward technique, which may consider any variable of the isolator and/or the supporting structure. The variables $\ddot{x}_{p_j}(t)$ and $\ddot{x}_{b_j}(t)$ are the accelerations of the payload mass, $m_{p_j}$, and of the base, respectively. If the variable $x_{r_j}(t) = x_{p_j}(t) - x_{b_j}(t)$ is defined, the differential equation that describes the motion of $m_{p_j}$ is expressed as:

$$f_{a_j}(t) - m_{p_j}\ddot{x}_{b_j}(t) = m_{p_j}\ddot{x}_{r_j}(t) + c_{p_j}\dot{x}_{r_j}(t) + k_{p_j}x_{r_j}(t). \tag{2.1}$$

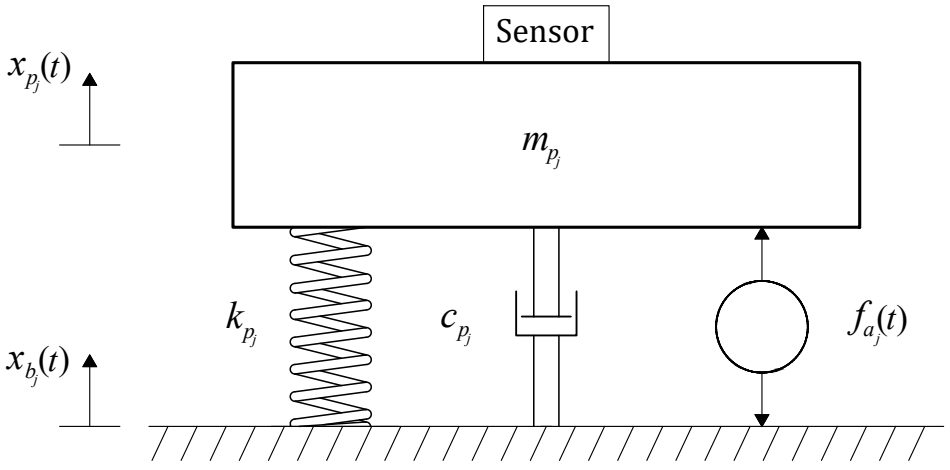


Figure 2.1: Dynamic isolation system model with a rigid base structure.

It is desired to have a general representation of all isolators of the system to formulate the design criteria. Thus, the state-space model of Equation (2.1) can be

[1]Note that the subscript $j$ may be suppressed from the notation when the problem refus to a single isolator.

defined as:

$$\begin{aligned} \dot{\boldsymbol{x}}_{I_j}(t) &= \boldsymbol{A}_{I_j}\boldsymbol{x}_{I_j}(t) + \boldsymbol{B}_{IB_j}\ddot{x}_{b_j}(t) + \boldsymbol{B}_{IF_j}f_{a_j}(t) \\ y_{I_j}(t) &= \ddot{x}_{p_j}(t) = \boldsymbol{C}_{I_j}\boldsymbol{x}_{I_j}(t) + \boldsymbol{D}_{IF_j}f_{a_j}(t), \end{aligned} \tag{2.2}$$

where the time derivative of the state vector is defined as $\dot{\boldsymbol{x}}_{I_j}(t) = [\dot{x}_{r_j}(t), \ddot{x}_{r_j}(t)]^T$, and the matrices of the system are:

$$\begin{aligned} \boldsymbol{A}_{I_j} &= \begin{bmatrix} 0 & 1 \\ -\omega_{p_j}^2 & -2\zeta_{p_j}\omega_{p_j} \end{bmatrix}, \ \boldsymbol{B}_{IB_j} = \begin{bmatrix} 0 \\ 1 \end{bmatrix}, \ \boldsymbol{B}_{IF_j} = \begin{bmatrix} 0 \\ 1/m_{p_j} \end{bmatrix}, \\ \boldsymbol{C}_{I_j} &= \begin{bmatrix} -\omega_{p_j}^2 & -2\zeta_{p_j}\omega_{p_j} \end{bmatrix}, \ \boldsymbol{D}_{IF_j} = 1/m_{p_j}, \end{aligned} \tag{2.3}$$

in which $\omega_{p_j}$ is the natural frequency of the $j^{\text{th}}$ isolator, obtained by $\omega_{p_j}^2 = k_{p_j}/m_{p_j}$, and $\zeta_{p_j}$ is its damping ratio, obtained by $\zeta_{p_j} = c_{p_j}/(2m_{p_j}\omega_{p_j})$. Each isolator system then has two inputs: the base acceleration $\ddot{x}_{b_j}(t)$ and the active force $f_{a_j}(t)$, which depends on the AVI controller used.

If Equations (2.2) and (2.3) are generalised for $n$ isolators, the state-space model of the isolators system is:

$$\begin{aligned} \dot{\boldsymbol{x}}_I(t) &= \boldsymbol{A}_I\boldsymbol{x}_I(t) + \boldsymbol{B}_{IB}\ddot{\boldsymbol{x}}_b(t) + \boldsymbol{B}_{IF}\boldsymbol{f}_a(t) \\ \boldsymbol{y}_I(t) &= \boldsymbol{C}_I\boldsymbol{x}_I(t) + \boldsymbol{D}_{IF}\boldsymbol{f}_a(t), \end{aligned} \tag{2.4}$$

in which the state variables of each isolator are defined in the vector $\boldsymbol{x}_I(t) = [\boldsymbol{x}_{I_1}(t), \boldsymbol{x}_{I_2}(t), \ldots, \boldsymbol{x}_{I_n}(t)]^T$; the output vector is $\boldsymbol{y}_I(t) = [y_{I_1}(t), y_{I_2}(t), \ldots, y_{I_n}(t)]^T$; the system matrix is a diagonal matrix of the system matrices of the $n$ isolators, such that $\boldsymbol{A}_I = \text{diag}(\boldsymbol{A}_{I_1}, \boldsymbol{A}_{I_2}, \ldots, \boldsymbol{A}_{I_n})$; the disturbance input matrix is $\boldsymbol{B}_{IB} = \text{diag}\ (\boldsymbol{B}_{IB_1}, \boldsymbol{B}_{IB_2}, \ldots, \boldsymbol{B}_{IB_n})$; the controlled input matrix is $\boldsymbol{B}_{IF} = \text{diag}(\boldsymbol{B}_{IF_1}, \boldsymbol{B}_{IF_2}, \ldots, \boldsymbol{B}_{IF_n})$; the output matrix is $\boldsymbol{C}_I = \text{diag}(\boldsymbol{C}_{I_1}, \boldsymbol{C}_{I_2}, \ldots, \boldsymbol{C}_{I_n})$; and the feedthrough matrix is defined as $\boldsymbol{D}_{IF} = \text{diag}(\boldsymbol{D}_{IF_1}, \boldsymbol{D}_{IF_2}, \ldots, \boldsymbol{D}_{IF_n})$. The inputs of the system are defined by the vectors $\ddot{\boldsymbol{x}}_b(t) = [\ddot{x}_{b_1}(t), \ddot{x}_{b_2}(t), \ldots, \ddot{x}_{b_n}(t)]^T$ and $\boldsymbol{f}_a(t) = [f_{a_1}(t), f_{a_2}(t), \ldots, f_{a_n}(t)]^T$.

The model of Equation (2.4) can be expressed in the Laplace domain as follows:

$$\boldsymbol{Y}_I(s) = \boldsymbol{G}_{IB}(s)s^2\boldsymbol{X}_b(s) + \boldsymbol{G}_{IF}(s)\boldsymbol{F}_a(s), \tag{2.5}$$

in which the Laplace variable is denoted by $s$, and the variables $\boldsymbol{Y}_I(s)$, $\boldsymbol{X}_b(s)$ and $\boldsymbol{F}_a(s)$ are the Laplace transforms of $\boldsymbol{y}_I(t)$, $\boldsymbol{x}_b(t)$ and $\boldsymbol{f}_a(t)$, respectively, and the matrices $\boldsymbol{G}_{IB}(s)$ and $\boldsymbol{G}_{IF}(s)$ are defined as the following TFs:

$$\boldsymbol{G}_{IB}(s) = \boldsymbol{C}_I \left[s\boldsymbol{I}_{2n} - \boldsymbol{A}_I\right]^{-1} \boldsymbol{B}_{IB}, \tag{2.6}$$

$$\boldsymbol{G}_{IF}(s) = \boldsymbol{C}_I \left[s\boldsymbol{I}_{2n} - \boldsymbol{A}_I\right]^{-1} \left(\boldsymbol{B}_{IF} + \boldsymbol{D}_{IF}\right), \tag{2.7}$$

where $\boldsymbol{I}_{2n}$ is a $2n \times 2n$ identity matrix.

### 2.2.1 Feedback and feedforward control strategies

The active force applied by the isolator can be generated using feedback and/or feedforward techniques. If a feedback control strategy is considered, the expression of this force, in Laplace domain, is:

$$\boldsymbol{F}_a(s) = \boldsymbol{G}_{AVI,F}(s)\boldsymbol{Y}_I(s). \tag{2.8}$$

If a feedforward control strategy is followed, the active force can be expressed as:

$$\boldsymbol{F}_a(s) = \boldsymbol{G}_{AVI,F_w}(s)\boldsymbol{Y}_b(s), \tag{2.9}$$

in which $\boldsymbol{Y}_b(s)$ is a vector comprised of the base accelerations measured at the isolator locations, $\boldsymbol{G}_{AVI,F}(s)$ is the control matrix for the feedback control strategy and $\boldsymbol{G}_{AVI,F_w}(s)$ is the control matrix for the feedforward control technique.

Thus, the TF between the base acceleration and the platform acceleration at the same point, the called transmissibility, for the $j^{th}$ isolator can be expressed as:

$$\frac{X_{p_j}(s)}{X_{b_j}(s)} = \frac{G_{AVI,F_w}[j,j]s^2 + 2\zeta_{p_j}\omega_{p_j}s + \omega_{p_j}^2}{(1 - G_{AVI,F}[j,j]/m_{p_j})s^2 + 2\zeta_{p_j}\omega_{p_j}s + \omega_{p_j}^2}. \tag{2.10}$$

where $G_{AVI,F}[j,j]$ and $G_{AVI,F_w}[j,j]$ represent the TFs of the feedback and feedforward AVI controllers, respectively.

Equation (2.10) can be used if the objective is to design the controller of AVI to improve the transmissibility performance of a particular isolator. In addition, this equation can be used to study the influence of each AVI on the base structure. In other words, Equation (2.10) represents the $j^{th}$ SISO AVI.

## 2.3 Vibration isolation techniques

This section presents the most relevant works when the supporting structure is considered as a rigid system. In this subsection, the works are classified in PVI, SAVI and AVI techniques.

### 2.3.1 Passive vibration isolation

The PVI technique aims to reduce the movement transmission by interposing an isolator, with constant dynamic properties, between the structure and/or device to be isolated and the noisy base. In this technique, no controllers are used $\boldsymbol{G}_{AVI,F}(s) = \mathbf{0}_n, \boldsymbol{G}_{AVI,F_w}(s) = \mathbf{0}_n$, and the dynamic properties of the isolator, $k_{p_j}, c_{p_j}$, are constant. Then, Equation (2.10) is reduced to:

$$\frac{X_{p_j}(s)}{X_{b_j}(s)} = \frac{2\zeta_{p_j}\omega_{p_j}s + \omega_{p_j}^2}{s^2 + 2\zeta_{p_j}\omega_{p_j}s + \omega_{p_j}^2}. \tag{2.11}$$

Effective VI occurs when $|X_{p_j}(j\omega)| < |X_{b_j}(j\omega)|$. Thus, for PVI system, it only happens for disturbance frequencies such that $\omega > \sqrt{2}\omega_{p_j}$ (Figure 2.2). However, this does not make PVI an unsuitable technique, since in some applications, the reduction of the peak magnitude by the addition of damping, is enough to accomplish the task [Preumont, 2018b].

If Equation (2.11) is analysed, it can observed that the addition of damping $\zeta_{p_j}$ is not always the best solution from the VI perspective. As it is increased, the peak of the TF reduces, but also does the decay ratio. For small damping ratio values it is -40 dB / dec. However, it can be observed that the rejected bandwidth

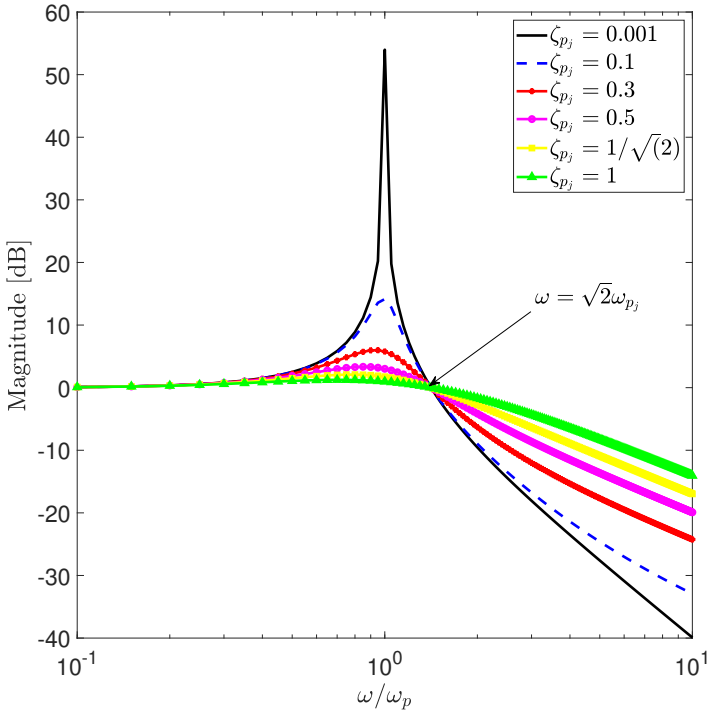


Figure 2.2: Representation of the transmibility TFs of a PVI system with different damping ratios $\zeta_{p_j}$.

is considerably reduced for increased damping as shown in Figure 2.2 where the transmissibility TFs for an isolator with different damping ratios $\zeta_{p_j}$ are shown.

The two main problems of PVI can be then summarised as: i) VI occurs only for disturbance frequencies greater than $\sqrt{2}\omega_{p_j}$, and ii) an increase in the damping ratio $\zeta_{p_j}$ reduces the peak transmissibility, but it also reduces the beneficial attenuation at higher frequencies. The solution of the first problem can be solved using non-linear techniques. Their application leads to a virtual reduction of the natural frequency of the isolator, hence increasing the rejection bandwidth. Different non-linear applications are found in [Ibrahim, 2008]. The solution to the second problem may be the AVI, which can increase the damping and yet keep -40 dB / dec reduction in transmissibility. This technique is explained further in Section 2.3.3.

There is a wide variety of applications in which PVI has been used, especially those which include non-linear elements. Some PVI applications will be mentioned to show the importance that this technique has in some engineering applications.

### PVI applications

Some applications of the PVI technique can be found in civil structures, where the VI technique is known as *base isolation*. The particular characteristic in this type of structures is that the isolator acts mainly in the horizontal direction, since the vertical component of response to earthquake excitation is not significant compared with the horizontal. The PVI process consists of the introduction of a device between the structure to be isolated and the ground, with the aim of creating a discontinuity between them. Different techniques can be encountered for base isolation purposes [Rosaria, 2008], although based on the type the isolator, they can be divided in two: i) sliding-based isolators [Tsai et al., 2006], ii) rubber-based isolators [Bhandari et al., 2018].

The sliding-based isolators are based on the friction pendulum system, an idea applied a long time ago by the engineer David Stevenson [Carpani, 2017], who applied this concept to a lighthouse in Japan [Stevenson, 1868]. This technique consists in an articular slider that moves on a spherical surface, which is usually coated by a low-friction material (Figure 2.3a). When the base is excited, the slider is moved between both top and bottom semicircular surfaces. A friction force is exerted to the superstructure and it is displaced to the lateral (upper) position. When this occurs, the restoring force resumes the superstructure to its initial position. It may occur that the maximum displacement is too high which promoted the use of this technique in combination with inerters [De Domenico and Ricciardi, 2018, Zhao et al., 2019], hence reducing the maximum displacement at the isolator location, due to the shifting.

The rubber-based isolation system used in civil structures uses PVI technique interposing a rubber device between the structure and the ground. Three different techniques can be encountered for this type of technique: i) low-damping rubber bearing isolators, ii) lead-plug bearing isolators, and iii) high-damping rubber bearing isolators [Naeim and Kelly, 1999].

In the first group, low-damping rubber bearing isolators, the device has two end plates. The bottom one is attached to the ground, and the top one is fixed to the

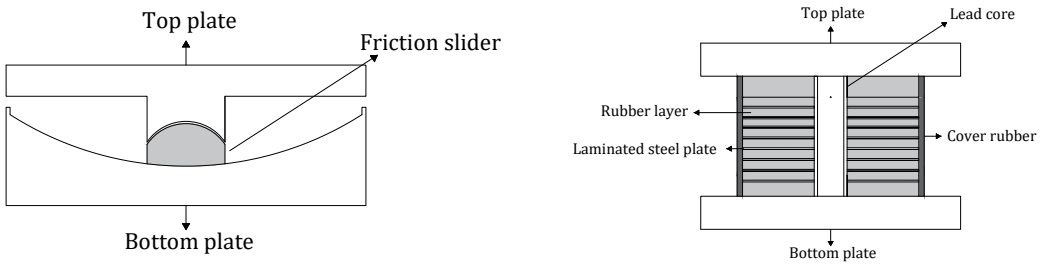


(a) (b)

Figure 2.3: Friction pendulum scheme (a), and rubber bearing base isolation systems (b).

structure. Also, intermediate thin steel shims are used. The device usually presents a damping ratio of about 2 %. Although they are designed to correspond with a linear viscous dynamic model, they usually need additional energy-absorbing devices to reach effective damping ratios of 10-20 % [Fujita, 1991].

The second group of rubber-based isolation is the lead-plugs bearing. The devices are very similar to those of the first group, but they contain holes in which one or more lead plugs are collocated (Figure 2.3b). This element works as an internal hysterical damper [Fujita, 1991]. Tests and design procedures are shown in [Robinson, 1982]. The influence of the lateral displacement on its vertical stiffness is shown in [Warn et al., 2007], and a sensitivity analysis of the mechanical properties has been made in [Ahmadipour and Alam, 2017].

For the third group, high-damping rubber isolators, the device is made in such a way that it has enough damping to avoid the use of an extra device. This damping is reached by the inclusion of extrafine carbon block, oils, or resins, and other proprietary fillers [Naeim and Kelly, 1999]. Thus, the response at the frequency of the isolator device is reduced [Fuller et al., 1997]. One of the main issues of this type of isolator is its numerical model. Different proposal have been made in [Markou and Manolis, 2016, Oliveto et al., 2019].

In another applications, such as laser interferometer which are used to detect gravity waves, one of the main problems is low-frequency disturbances, as occurs in the VIRGO or LIGO research facilities [Bradaschia et al., 1990, Abbott et al., 2009].

In these cases, the application of the concept of *negative stiffness* is made. This technique was introduced by Platus in 1992 [Platus, 1992]. It consists in a virtual reduction of the stiffness, with the aim of increasing the rejection bandwidth of the isolator when PVI is being used. For that, a vertical spring is connected to two Euler columns, see Figure 2.4. The columns are loaded with their critical load, hence producing a virtual reduction of the stiffness. This concept has been widely used in numerous VI applications: isolation and positioning platform in LIGO observatory [Matichard et al., 2015a, Matichard et al., 2015b]; construction of metastructures composed by unit cells with quasi-zero stiffness [Fan et al., 2020]; in fluid-conveying pipes [Ding et al., 2019]; in floating raft systems [Li and Xu, 2017]; its use has been analysed to reduce dynamic loads on the foundation of machines [Anvar et al., 2017].

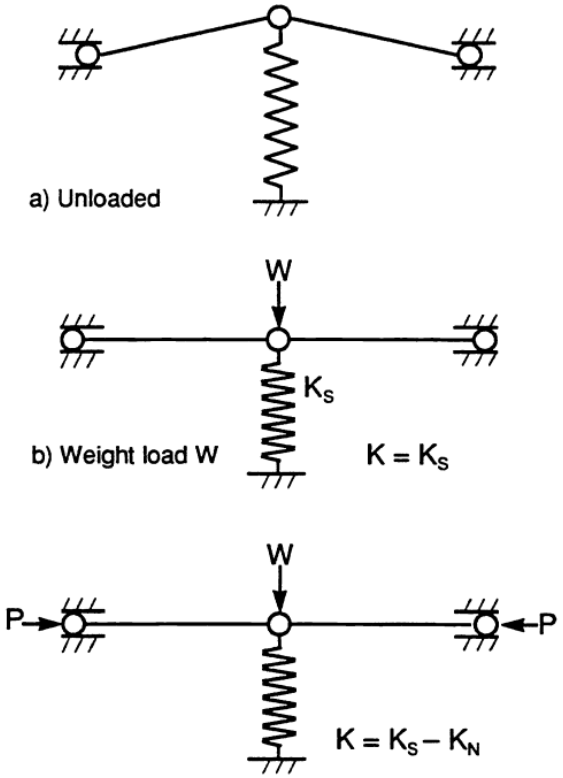


Figure 2.4: Negative stiffness scheme. [Platus, 1992].

Another field in which PVI has been used is in space applications. In particular [Davis et al., 1995]:

- Microgravity experiments require low acceleration spectrum. Vibration isolation is required to reduce accelerations produced by machinery and astronaut-induced forces.

- Disturbance source isolation is required in surveillance and communications satellites. Devices as reaction wheels, cyrocoolers or tape drivers cause on-orbit jitter. This problem can be solved by isolating the disturbance from the spacecraft.

- Payload isolation and pointing is required in satellites demanding a stable base for precision pointing. In addition, the spacecraft attitude control can be relaxed.

The following works related with PVI applications in payload isolation are significant contributions to the scenario 2 studied in this thesis. In space applications, the payloads are connected through struts to the spacecraft, which act as isolators. A common design is called D-strut, which is a passive isolator (see Figure 2.5). A design with very low fundamental frequency was presented in [Davis et al., 1994]. In this work, the damper has a viscous fluid flowing through a controlled annulus between two hermetically scaled chambers. In an alternative design, the fluid is replaced with gas in the pneumatic the D-strut. The orifice which the gas flows is longer with a smaller cross area [George W. Wilson and Patrick J. Wolke, 1997].

Another way of implementing the PVI technique is made by low frequency flexible space platform, which consists of folded continuous beams (Figure 2.6), for mounting of a reaction wheel assembly [Kamesh et al., 2012]. This can be used to isolate the disturbances from the reaction wheel into high precision payloads. This type of device provides good isolation performance below 30 Hz without using additional energy dissipation devices [Liu et al., 2015].

The automotive industry requires the use of VI techniques to isolate passengers and some parts of vehicles from vibrations. The application of PVI has been made by using elastomeric (or rubber) materials [Schmitt and Leingang, 1976, Yu et al., 2001]. They allow isolation in all directions. Also, they are compact, cost-effective and maintenance free. Better performance is reached using hydraulic mounts (Figure 2.7), patented in 1962 by Richard Rasmusssen [Marjoram, 1985], where a spring with a hydraulic damper is combined. The use of hydraulic mounts considering the non-linear behaviour due to the fluid they contain, was shown in

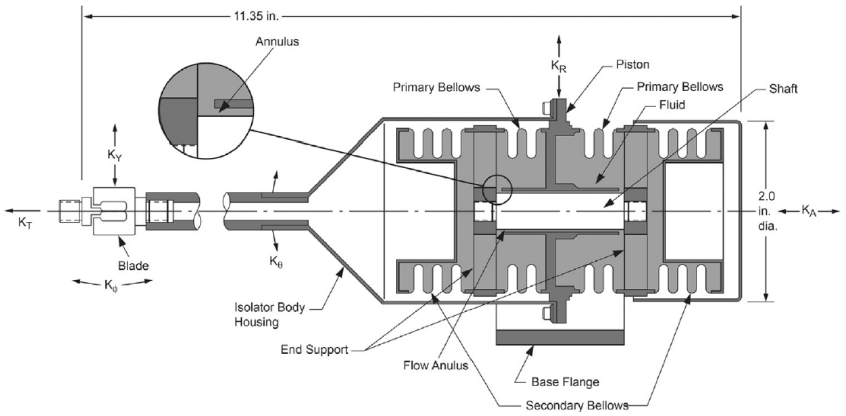


Figure 2.5: Schematic of a D-strut. [Liu et al., 2015].

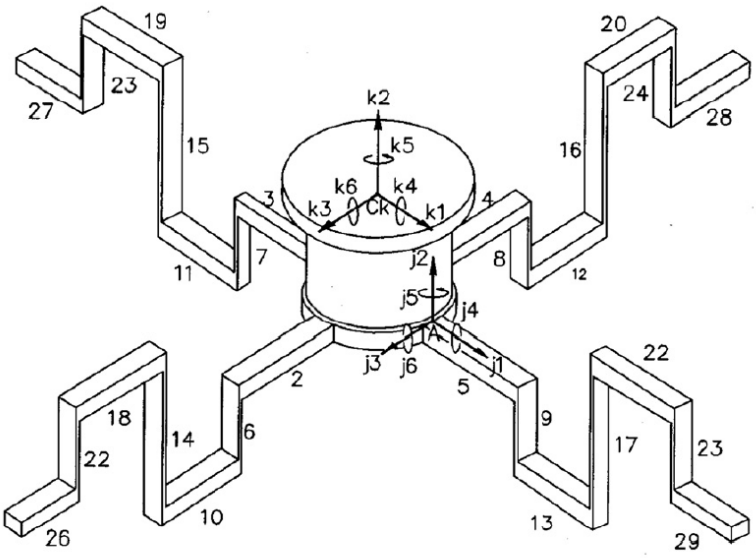


Figure 2.6: Folded beam. [Kamesh et al., 2012].

[Kim and Singh, 1993, Colgate et al., 1995, Golnaraghi and Nakhaie Jazar, 2001].

### 2.3.2 Semi-active vibration isolation

This VI strategy has generated enormous interest in a range of different areas. This arises from the high VI performance that this technique is able to reach. In some cases, it allows isolation of vibrations with similar performance to the AVI technique, but with low-level power supply.

The SAVI technique is based on the same principle as PVI, in that the controlled force is generated as a consequence of the relative movement between the platform and the base. There is no active control, so $\boldsymbol{G}_{AVI,F} = \boldsymbol{0}_n$, $\boldsymbol{G}_{AVI,F_w} = \boldsymbol{0}_n$. However, the dynamic properties of the isolator $\zeta_{p_j}$ and $\omega_{p_j}$ can be changed in real time during

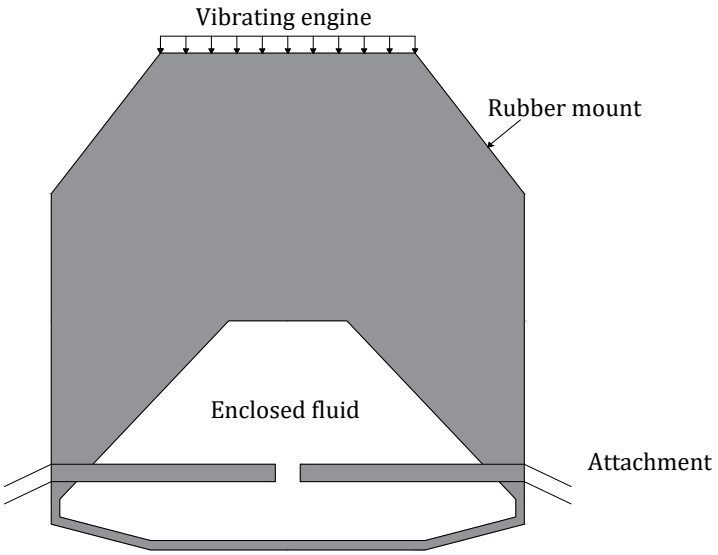


Figure 2.7: Schematic of a hydraulic mount.

the task development.

Firstly it is necessary to introduce how this technique is developed. One of the most important works related with the SAVI technique was made by Karnopp [Karnopp et al., 1974]. An isolator was proposed which used feedback signals to change its dynamic properties, but only low level external power supplied was necessary. The aim was to emulate the behaviour of the *sky-hook* damper. This is a damper which uses the platform velocity, $\dot{x}_{p_j}(t)$, to control its movement, instead of the relative velocity, $\dot{x}_{p_j}(t) - \dot{x}_{b_j}(t)$, as a classic damper does. Figure 2.8 shows the schematic of an ideal sky-hook damper.

For that purpose, Karnopp proposed the isolator of Figure 2.9. The device has the capability of changing its damping coefficient, by modulating the fluid-flow, then the damping coefficient, $c_{p_j}$. The power associated with the force $f_{dp_j}(t)$ must always be positive, so that:

$$f_{dp_j}(t)(\dot{x}_{p_j}(t) - \dot{x}_{b_j}(t)) \geq 0. \tag{2.12}$$

In this case, the coefficient $c_{p_j}$ changes as the fluid fills the damper. Only full ($\max(c_{p_j})$) and empty ($c_{p_j} = 0$) cases were considered in that work. The ideal force then would be $f_{dp_j}(t) = \max(c_{p_j})\dot{x}_{p_j}(t)$. However, to ensure the isolator does not

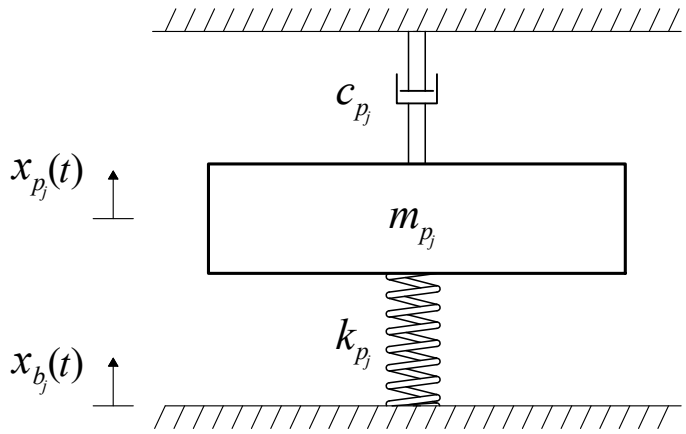


Figure 2.8: Schematic of the ideal sky-hook damper.

supply power to the system, the sign of $(\dot{x}_{p_j}(t) - \dot{x}_{b_j}(t))$ must be proper. Then, the next cases were considered:

$$f_{dp_j}(t) = \begin{cases} \max(c_{p_j})\dot{x}_{p_j}(t) & \text{if } \dot{x}_{p_j}(t)(\dot{x}_{p_j}(t) - \dot{x}_{b_j}(t)) > 0 \\ 0 & \text{if } \dot{x}_{p_j}(t)(\dot{x}_{p_j}(t) - \dot{x}_{b_j}(t)) < 0. \end{cases} \tag{2.13}$$

If the sign of $(\dot{x}_{p_j}(t) - \dot{x}_{b_j}(t))$ is the same that the sign of $\dot{x}_{p_j}(t)$, then the damping of the isolator must reach its maximum value. However, if $(\dot{x}_{p_j}(t) - \dot{x}_{b_j}(t))$ and $\dot{x}_{p_j}(t)$ have opposite signs, it would be necessary to apply an opposite force to the desired one: $f_{dp_j}(t) = \max(c_{p_j})\dot{x}_{p_j}(t)$. Then, the best the isolator can do is not apply force at all, $f_{dp_j}(t) = 0$. It is possible that $\dot{x}_{p_j}(t)(\dot{x}_{p_j}(t) - \dot{x}_{b_j}(t)) = 0$, either because $\dot{x}_{p_j}(t) = 0$ or because the velocity of the platform is the same that the velocity of the base, $(\dot{x}_{p_j}(t) - \dot{x}_{b_j}(t)) = 0$. For the first case, the best value for the damper force would be 0, then $f_{dp_j}(t) = 0$. For the second case, the isolator attempts to apply the maximum damping force. It depends on the time history of $x_{b_j}(t)$ during the subsequent instants, that will make either the damper force changes to one of the cases shown in Equation (2.13), or the damper force can be large enough to lock-up

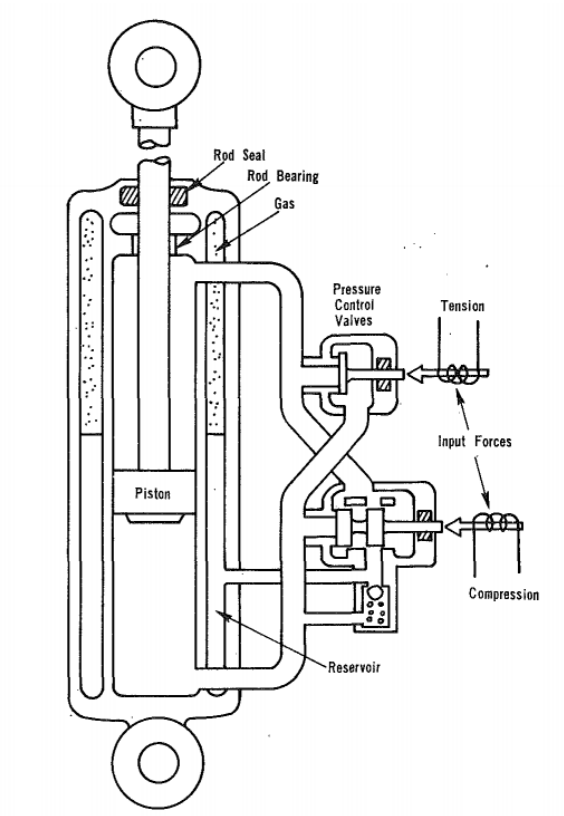


Figure 2.9: Semi-active isolator proposed by Karnopp. [Karnopp et al., 1974].

the system, it is $\ddot{x}_{p_j} = \ddot{x}_{b_j}$, the damper force is:

$$f_{dp_j}(t) = -m_{p_j}\ddot{x}_{p_j} - k_{p_j}(x_{p_j}(t) - x_{b_j}(t))_{lk} \tag{2.14}$$

in which $(x_{p_j}(t) - x_{b_j}(t))_{lk}$ is the spring deflection at lock-up.

Further works have been developed based on the idea of modulating the fluid-flow in dampers to control the damping coefficient in the isolator, such as the work of Rakheja in 1985, [Rakheja and Sankar, 1985], who introduced the concept of *on-off* damper. The concept was motivated by the idea of measuring the relative displacement and velocity between the platform and the base, instead of the velocity of the platform, since they are directly measurable signals. Through the analysis of the spring and damper forces, it is possible to observe the values for which the mass acceleration is increased during the vibration cycle. These forces are defined

as follows:

$$f_{sp_j}(t) = k_{p_j}\left(x_{p_j}(t) - x_{b_j}(t)\right) \tag{2.15}$$

$$f_{dp_j}(t) = \max(c_{p_j})\left(\dot{x}_{p_j}(t) - \dot{x}_{b_j}(t)\right), \tag{2.16}$$

and the acceleration of the mass to be isolated is defined as $\ddot{x}_{p_j} = -(f_{sp_j}(t)) + f_{dp_j}(t))/m_{p_j}$. If the three forces are represented (Figure 2.10), it is possible to observe that there is an increase in the inertial force, hence in the mass acceleration, when the spring and damper forces bear the same sign. Also, it is observed that the mass acceleration is decreased when the damper force is opposite to the spring force. Considering that the spring force is proportional to the relative displacement, and the damper force is proportional to the relative velocity, the proposed control scheme was as follows:

$$f_{dp_j}(t) = \begin{cases} \max(c_{p_j})(\dot{x}_{p_j}(t) - \dot{x}_{b_j}(t)) & \text{if } (\dot{x}_{p_j}(t) - \dot{x}_{b_j}(t))(x_{p_j}(t) - x_{b_j}(t)) < 0 \\ \min(c_{p_j})(\dot{x}_{p_j}(t) - \dot{x}_{b_j}(t)) & \text{if } (\dot{x}_{p_j}(t) - \dot{x}_{b_j}(t))(x_{p_j}(t) - x_{b_j}(t)) > 0, \end{cases} \tag{2.17}$$

the term $\min(c_{p_j})$ makes reference to the minimum damping coefficients, controlled by the orifice of the isolator device, since it was set that it is not possible to set zero damping. Based on this concept, further works were made with the aim of using a variable damping coefficient [Alanoly and Sankar, 1987]. When the spring and damper forces are in opposite directions, the damper force must be adjusted, with the aim of producing the same force that the spring one, but with opposite sign, thus the net force applied on the mass would be zero. Also, as occurs in the on-off control scheme, the lower damping coefficient is reached when the spring and damper forces have the same sign.

It was proved in [Wu et al., 1994] that using this control scheme, the damper force may exceed its limit. Hence proposing a new control strategy, in which instead of modulating the damping force, a maximum value of damping is set when a threshold damping coefficient is exceeded. This value was proposed to be 30 % of

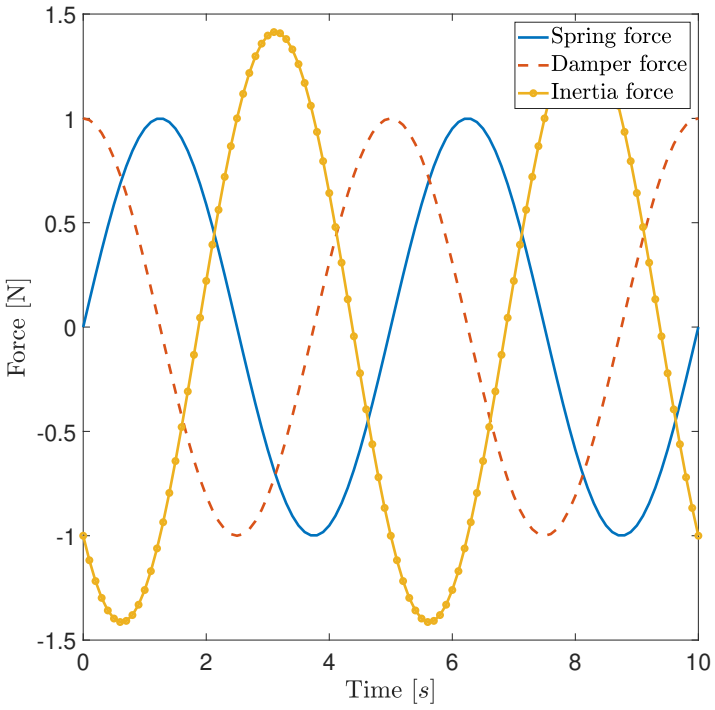


Figure 2.10: Spring, damper and inertia forces of a PVI isolator with a harmonic disturbance input.

the critical damping of the isolator. The use of on-off dampers carries the problem of the jerk by the mass, due to discontinuities in the movement. The problem was analysed, and a solution based on a continuously variable semi-active suspension was proposed [Miller and Nobles, 1990].

The use of SAVI tehcnique has also been applied by controlling the rheological properties of the fluid of the damper, also its internal structure [Parthasarathy and Klingenberg, 1996]. Depending on the nature of the input control, two different types are considered: i) magneto-rheological (MR) dampers , ii) electro-rheological (ER) dampers. In the first one, a magnet field is applied to the fluid (Figure 2.11), whilst for the second one, a electric field is applied to change its properties

Another way to implement the SAVI technique is by using piezoelectric materials. They have coupled mechanical-electrical characteristics. A piezoelectric material reacts to a mechanical force by generating an electric field and vice versa. Some examples of semi-active vibration control using piezoelectric materials can be found in [Qiu et al., 2009].

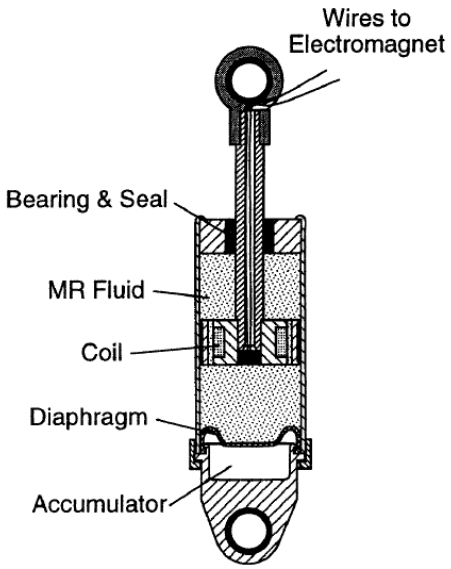


Figure 2.11: Schematic of a MR damper. [Dyke et al., 1996].

Although most SAVI applications are oriented to change the damping of the isolator, there are numerous works which have investigated a change in stiffness. The aim is to change the natural frequency of the isolator $\omega_{p_j}$. For example, in [Liu et al., 2008] the use of a Voight element is combined with a spring in series, thus the stiffness of the system can be controlled. The work [Pu et al., 2019] shows the use of the aforementioned negative stiffness concept, with the aim of changing the stiffness of the isolator using an electromagnetic spring. MR dampers with the capability of changing stiffness and damping are shown in [Sun et al., 2015b, Zhou et al., 2009].

### SAVI applications

The SAVI technique has been used in an extensive number of applications. For example, in civil engineering structures, base isolation is improved by modulating the damping coefficient in [Symans and Kelly, 1999]. A benchmark model for seismically excited base-isolated buildings for evaluating different control strategies was presented in [Narasimhan et al., 2006, Nagarajaiah and Narasimhan, 2006, Jung et al., 2006]. The effectiveness of the MR dampers for seismic isolation was evaluated in [Jung et al., 2006]. The work proposed control algorithms, such as clipped-optimal control [Tseng and Hedrick, 1994], the maximum energy dissipa-

tion, of the fuzzy logic-based control. Semi-active damping is also achieved by combining PVI with MR dampers, as shown in [Shook et al., 2008]. It combines elastomeric bearings, friction pendulums , shape memory alloys and MR dampers. A review of seismic control strategies, for both VI and vibration control is made in [Symans and Constantinou, 1999].

The SAVI technique is also applied in space applications, through the use of ER and MR dampers. [Oh et al., 2004] presented an isolator filled with liquid-crystal type ER-fluid, previously analyzed in [Oh et al., 2000], with the aim of improving pointing performance under disturbance by a momentum-wheel. The results were compared with PVI techniquesand much better performance was observed for the SAVI case with aforementioned on-off control laws . To improve the pointing performance of observation satellites, the use of SAVI isolators is presented in [Makihara et al., 2006]. The isolators are compounded by piezoelectric materials and a switch-controlled passive circuit. A detailed review of the SAVI techniques in micro-vibration isolation in space applications is made in [Liu et al., 2015].

Most of the SAVI developments aforementioned in the introduction of this technique were primarily developed for the automotive industry. An experiment of SAVI technique in car suspensions has been shown in [Yao et al., 2002], using MR dampers. Time and frequency control methodologies for SAVI technique MR dampers are investigated in [Zapateiro et al., 2012]. In [Zhang et al., 2014], extended state observer techniques are used for car suspension, using MR dampers.

### 2.3.3 Active vibration isolation

The main difference that AVI has with respect to PVI and SAVI is the addition of the active force. Its use leads to numerous advantages over PVI and SAVI techniques [Ruzicka, 1968], such as:

- Zero static deflection
- Very stiff system for applied loads of constant magnitude
- Return of the payload to the initial position during a constant load

- The VI performance is independent of the payload
- Capability of changing the controller during the task development

The acceleration of the platform $\ddot{x}_{p_j}(t)$, when AVI technique is used, can be expressed using Equation (2.5). From the TFs of Equations (2.6) and (2.7), the platform displacement can be expressed, for the $j^{th}$ isolator, as:

$$X_{p_j}(s) = \frac{2\zeta_{p_j}\omega_{p_j}s + \omega_{p_j}^2}{s^2 + 2\zeta_{p_j}\omega_{p_j}s + \omega_{p_j}^2} X_{b_j}(s) + \frac{1/m_{p_j}s^2}{s^2 + 2\zeta_{p_j}\omega_{p_j}s + \omega_{p_j}^2} F_{a_j}(s) \tag{2.18}$$

As can be observed, the main difference with respect to PVI and SAVI is the addition of an extra force, which is the active force $F_{a_j}(s)$. To generate it, it is necessary to use an external power supply, sensors, signal processors and actuator of some kind. Although the use of this technique has been typically oriented to very demanding applications, its us can be widely extended in numerous applications.

The AVI problem has been approached considering different control strategies and techniques. Depending on the position of the sensor, two different techniques can be distinguished: i) feedback control, Equation (2.8), ii) feedforward control Equation (2.9).

### AVI using feedback control

For the feedback technique, the platform movement is used by the controller to generate the active force signal. Thus, the movement of the mass to be isolated is used to generate the active force.

As was mentioned previously, one of the main purposes of SAVI technique is to use the velocity of the platform to generate the control force, as the ideal sky-hook damper does. The use of the AVI allows implementation of this technique, since the velocity of the platform can be measured. Its application is usually called *direct velocity feedback* (DVF) [Preumont, 2018a]. It is widely extended in numerous applications, since it is easy to implement it also guarantees stability of the system. Some applications can be encountered in the following works. For ex-

ample [Balas, 1979] in which the AVI with DVF was used to reduce vibration in a large space structure. A decentralised control strategy using DVF was used in [Kim et al., 2001, Huang et al., 2003]. In those cases, the VI system is formed by parallel actuators, which uses the velocity of equipment to be isolated, at the end of the actuator. An extensive analysis of the VI using velocity feedback is made in [Yan et al., 2006].

Alternatively, instead of measuring the velocity to emulate the sky-hook damper behaviour, the acceleration or the force received by the platform can be used. When the acceleration of the platform is used, the technique is called *acceleration feedback* (AF), whilst *force feedback* (FF) is used to refer that the force received by the platform is used by the controller. It was proven by Preumont [Preumont et al., 2002] that the use of both strategies is equivalent when the isolator connects to rigid bodies. However, the FF technique presents an advantage respect to the use of AF when the payload is a flexible body, since it always presents pole-zero pattern in the open-loop, hence leading to a stable closed-loop system. However, if AF is used, this pattern is not exhibited when the modes of the flexible payload interfere with the isolation system.

The position of the platform can also be fed back, and the technique is called *position feedback* (PF). The use of this technique leads to a *sky-hook spring* [Collette et al., 2011]. The principle is the same that the sky-hook damper, but instead of a damper attached to the inertial frame (the "sky"), a spring is attached. It arises from the idea that the displacement of the platform is used to generate the control force, as the spring does. In practical cases, the relative displacement between an inertial mass and the mass to be isolated can be measured using different techniques: collocating the inertial mass on the platform, and using a sensor to measure the relative displacement [Saulson, 1984, Nelson, 1991]; collocating the inertial mass on the ground and measuring the relative displacement [Vervoordeldonk et al., 2004]; using a strain gauge is shown in [Benassi and Elliott, 2004]. The neutral position of the sensor corresponds with the desired operating height of the actuator mass. The signal supplied by this sensor is proportional to the relative displacement. Then, the

controller generates a continuously increasing signal as the relative displacement is not zero.

Figure 2.12 shows a comparison of the effect that each technique has in the transmissibility function. As can be observed, the use of PF and AF virtually moves the natural frequency of the isolator, whereas for DVF the natural frequency is maintained, but a reduction of the peak response is obtained. One of the main drawbacks of the aforementioned PVI technique is that, as the damping ratio $\zeta_{p_j}$ increases , the absolute value of the decay rate is also reduced. With the use of AVI-DVF, high decay rates can be achieved, whilst simultaneous the peak is reduced, hence solving one of the main problems of PVI. A study of the different patented developments in AVI, considering the different strategies, is made in [Collette et al., 2011].

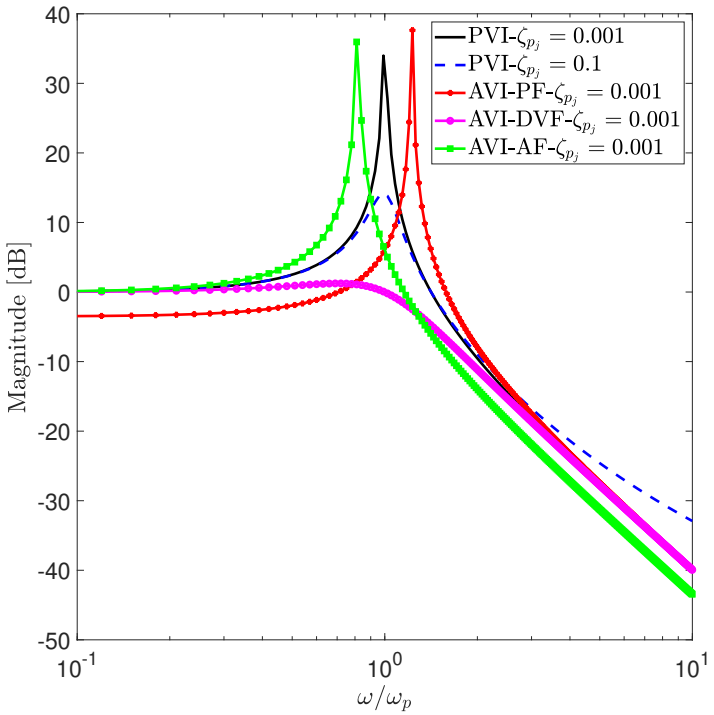


Figure 2.12: Comparison of different VI techniques: PVI, PF, DVF, AF.

### AVI using feedforward control

Although the use of feedback technique is widely practised in VI applications, the feedforward strategy has also generated interest among researchers. Instead of using the platform movement to generate the control signal, the feedforward technique uses the base movement, thus the transmissibility can be reduced to zero. According to

Equation (2.10), and considering just feedforward strategy (i.e. $\boldsymbol{G}_{AVI,F}(s) = \mathbf{0}_n$), the transmissibility TF is expressed as:

$$\frac{X_{p_j}(s)}{X_{b_j}(s)} = \frac{G_{AVI,F_w}[j,j]s^2 + 2\zeta_{p_j}\omega_{p_j}s + \omega_{p_j}^2}{s^2 + 2\zeta_{p_j}\omega_{p_j}s + \omega_{p_j}^2} \tag{2.19}$$

The aim of the control strategy is to reach $X_{p_j}(s) = 0$. This can be achieved if the numerator of Equation (2.19) is 0. Thus, the transfer function $G_{AVI,F_w}[j,j]$ must be as follows [Beijen, 2018]:

$$G_{AVI,F_w}[j,j] = \frac{-2\zeta_{p_j}\omega_{p_j}s - \omega_{p_j}^2}{s^2} \tag{2.20}$$

However, the implementation of this controller in real scenarios does not guarantee good performance. The following practical issues must be considered: i) the need for a very precise isolator model, ii) sensor noise, and iii) causality, since feedforward controllers are usually implemented in discrete-time. The disturbance has to be measured before compensation is applied, otherwise the cancellation of the isolator may come too late. Recent contributions have been made in this field [Beijen et al., 2017], including MIMO controllers [Beijen et al., 2018] and combining feedback and feedforward techniques [Beijen et al., 2019].

### AVI applications

The use of AVI is made in those applications in which stringiest vibration criteria are demanded, or when the performance of PVI and/or SAVI techniques is insufficient.

In civil structures, active control techniques have been combined with PVI to improve isolation performance. An example is shown in [Nagarajaiah et al., 1993], in which a hybrid control case is presented with application to a sliding-isolated bridge. The sliding isolators, situated at the abutments and pier of the bridge, act as passive isolators. An active actuator is interposed between the vibration source and the structure to be isolated (Figure 2.13). A significant reduction of peak deck acceleration can be achieved compared with the use of PVI only.

Experimental and numerical results for an isolated building, using a

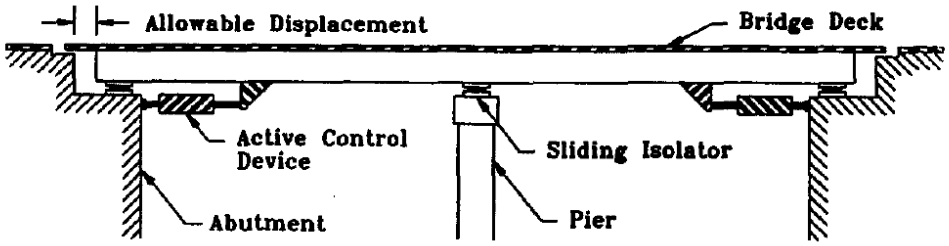


Figure 2.13: Hybrid VI in a sliding-isolated bridge. [Nagarajaiah et al., 1993].

low-friction pendulum bearing system combined with AVI, were shown in [Chang and Spencer, 2010]. In addition, the interaction between the controller and the structure was considered. The results derived from this work show the potential effectiveness of an active base isolation system, reducing both floor accelerations and base shear.

The addition of the active force in AVI allows reduction of the vibration of a platform whilst simultaneously accomplishing other control objectives, such as positioning or tracking position. The demanding requirements of many applications have led to the development of devices able to both reduce the vibration transmitted to the payload and also to change its position and orientation. This is usually accomplished using Stewart platforms [Stewart, 1965], which comprise parallel manipulators with six actuators with prismatic joints [Fichter, 1986] (Figure 2.14). Every strut of the platform is an isolator, which can be driven by voice coil motors [Cobb et al., 1999, Xu and Weng, 2013, Kong and Huang, 2018, Tang et al., 2019] or piezoelectric actuators [Loix et al., 2002, Xu and Weng, 2013, Wang et al., 2016b].

Stewart platforms have been widely used in space applications [Geng and Haynes, 1992, Rahman et al., 1998, Thayer et al., 2002]. Since strut responses are coupled, multiple control strategies are oriented to decentralise them. In [Preumont et al., 2007], a FF control strategy was used. The isolator was equipped with six force sensors, measuring axial forces in the legs. Another example is shown in [Yang et al., 2017], in which the FF technique is used to reach stability

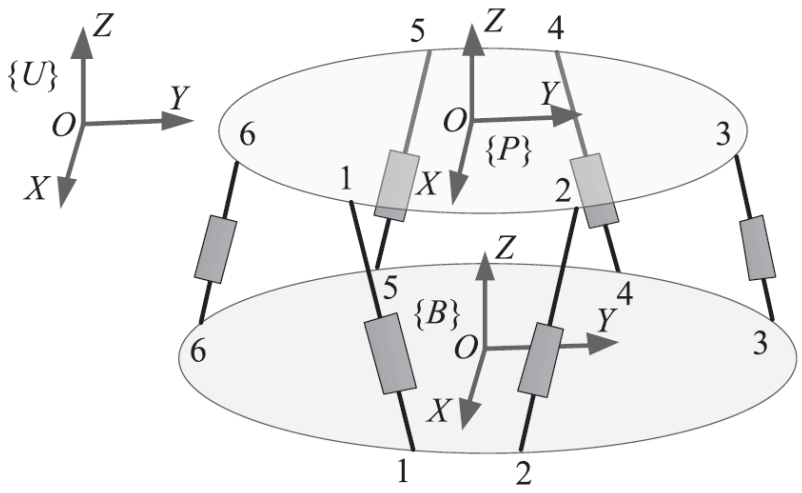


Figure 2.14: Schematic of a Stewart Platform. [Kong and Huang, 2018]

.

at nanoscale level. MIMO control strategies have also been utilised, as shown in [Beijen et al., 2018], which proposed a MIMO disturbance feedforward controller for high-precision machinery.

Some applications combine both objectives: vibration isolation and position/pointing control. A control method for optical payloads is proposed in [Li et al., 2018]. This is called Positive Force Feedback (PFF) and it is used in combination with AF to reject payload disturbances. This technique has the potential to improve the performance of the system if the subtraction of the external disturbances from the payload inputs is made. It is shown that, if the disturbances are measurable, the use of PFF can improve performance. However, it is very susceptible to measurement errors.

The automotive industry has also applied AVI techniques, which are usually called *active suspension*. The AVI must accomplish two objectives: passenger comfort and good road handling. The main disturbance input is a result of the irregularities of the terrain [Aly and Salem, 2013]. Different control techniques have been utilised to develop AVI in car suspensions, for example: classic control techniques are shown in [Thompson, 1970, Smith and Walker, 2000]; optimal control techniques are applied in [Wilson et al., 1986, Shirahatti et al., 2008, Rutledge et al., 1996]; nonlinear control is investigated in [Chen et al., 2005,

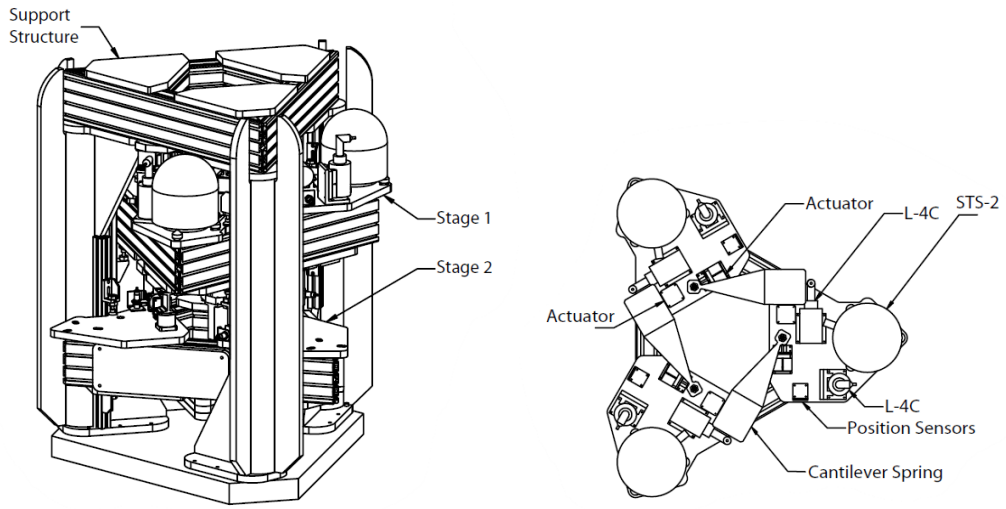


(a) (b)

Figure 2.15: Prototype of the vibration isolation system used in LIGO (a), Support structure and two stages level (b) Top view of the first stage. [Hua et al., 2004].

Alleyne and Hedrick, 1995]; the application of robust control is shown in [Gaspar et al., 2003, A. Chamseddine et al., 2006]; intelligent control techniques are shown in [Foda, 2000, Klement et al., 1999, Kuo et al., 2005].

Research centres, as LIGO observatory, have also used the AVI technique against seismic excitations. It is necessary to isolate the interferometer mirrors from ground motion below 0.1 Hz. The main problem to be addressed is the tilt-horizontal coupling, since inertial horizontal sensors cannot distinguish between horizontal acceleration from tilt motion [Hua et al., 2004]. The isolator system designed for this application is shown in Figure 2.15. It has two stages. There are three cantilever springs to link Stage 1 from the support structure and three more to join Stages 1 and 2. These cantilevers are also used to support the static load of the system. Only the Stage 2 has damping controllers. There are six actuators commanded by a SISO control strategy. The results meet with vibration isolation requirements of the task.

## 2.4 Vibration isolation on a flexible supporting structure

### 2.4.1 Previous works

There are numerous works which have studied the effect of the supporting structure dynamics on the VI performance. In [Plunkett, 1958, Blackwood, 1994], it was noted that failure to take into account the interaction phenomenon between the machine (i.e. the payload) and its base would lead to incorrect results, except at low frequencies. Also, a further two effects were considered as a consequence of the interaction phenomenon: i) the possibility of shifting resonant frequencies, which implies dangerous consequences in terms of machine health, and ii) the interaction may affect the vibration amplitude of either the machine or the foundation. The derivation of an equation governing the responses of a non-rigid machine, which is situated on a non-rigid supporting structure and excited by any number of forces, is presented in [Soliman and Hallam, 1968]. When the machine is situated on an undamped set of springs, it is possible to extract useful information, such as the optimal damping value of the isolators.

A high-bandwidth positioning and pointing of a payload situated on a flexible supporting structure was analysed in [Garcia et al., 1992], with application to the positioning of mirrors, which are connected to the base via piezoelectric actuators, in a space-based interferometer. The importance of the base flexibility in the control of positioning of the payload, with respect to an external or internal part of the flexible structure, was governed by $m_p/(M_m\zeta_b)$, in which $M_m$ is the effective modal mass at the isolator location and $\zeta_b$ is the modal damping of the base. It was defined that the interaction can be neglected when its value is much lower than one, i.e. if the payload mass is low. A multi-layer control approach of a baseline space interferometer was developed in [Spanos et al., 1992]. The control structure interaction was noted to be a key technology requirement, especially in optical class space missions. A three layer control approach was proposed, which involved: i) disturbance isolation, ii) base structural quieting, and iii) optical control.

[Scribner et al., 1993] considers instability issues when machines are mounted on flexible supporting structures. They concluded that the performance is limited by three factors:

- Passive damping of the system machine (payload) and base support
- Pole-zero pattern of the TF from actuators to sensors. It was observed that, for rigid machines, the most important parameter is the relation between the mass of the machine and the effective modal mass of the base.
- Spectral bandwidth of the disturbance. Hence resulting that VI is easy to reach for slowly time-varying quasi-periodic disturbances.

The effect of the supporting structure on the VI performance was considered in [Sciulli and Inman, 1998]. The results show that if the isolator frequency is designed such that the frequency is between two modes of the supporting structure, a coupling condition will exist between the affected modes. Also, if damping is added, three modes will damped, instead of one. Different controllers are also proposed to reduce the effect of flexible base modes. Moreover [Sciulli and Inman, 2000] considers the payload as a flexible system too. To analyse the problem, Yang's method was used [Yang, 1994] to solve complex distributed parameter systems.

Electromagnetic actuators for VI purposes considering non-rigid bases have been studied in [Huang et al., 2003], in which a flexible equipment is isolated from either a vibrating rigid or non-rigid supporting base (Figures 2.16, 2.17). The VI control law used is velocity feedback. The actuators are mounted in parallel with four passive mounts. With a rigid base, the theoretical stability of the system is guaranteed, regardless the flexibility of the equipment. The system may be non-collocated (i.e. sensor and actuator are not attached to the same degree of freedom [Preumont, 2018b]), due to the flexibility of the equipment and the base. However, robust stability is found when the base is a flexible base. Successful VI is achieved for a wide frequency range.

The use of inertial actuators for VI has been shown in multiple works: [Benassi et al., 2004], in which inner local FF and outer velocity feedback control

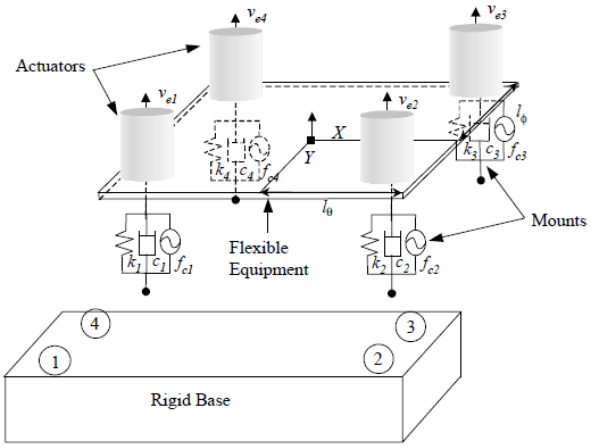


Figure 2.16: Four-mount AVI system for a rigid base [Huang et al., 2003].

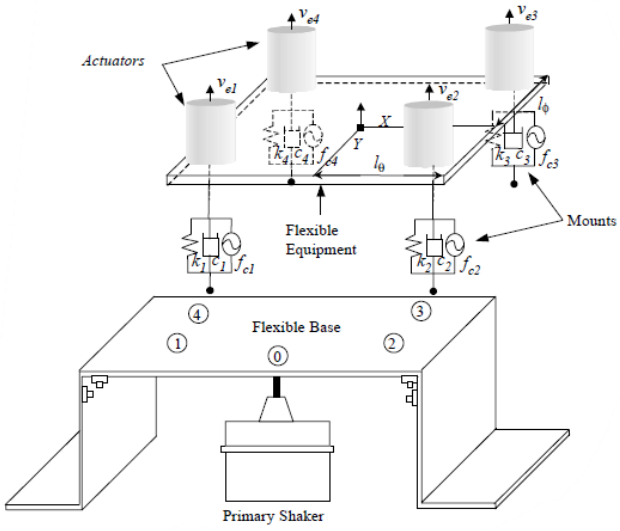


Figure 2.17: Four-mount AVI system for a flexible base [Huang et al., 2003].

strategy is used to isolate a rigid equipment from a vibrating flexible base. The results are compared with those obtained from a full state feedback optimized with a Linear Quadratic Gaussian (LQG), and very similar results are found.

A flexible base is also considered in [Brennan et al., 2006]. It shows the implementation of a local displacement feedback control in an inertial actuator. It is important to note that this technique is not the same as PF shown above, since in this case the relative displacement between the base and the platform is measured. Stability margins are guaranteed for low natural frequency of the isolator, however it may lead to static deflection. To solve this problem, a displacement sensor and a local Proportional Integral Derivative (PID) controller is used. It is shown that

natural frequency and damping of the isolator can be virtually changed virtually, hence showing the possibility of adapting the device to different applications.

It is shown in [Elliott et al., 2004] that, if the actuator and sensor dynamics are not considered, the use of FF is unconditionally stable. If the equipment and the base to be isolated are rigid, both techniques DVF and FF show similar effectiveness in isolation performance. However, if the base is rigid, but the equipment is flexible, DVF shows better results than FF. For a flexible equipment and a flexible base, the use of DVF shows again better performance.

A distributed parameter isolator using DVF is analysed in [Yan et al., 2010]. In this case, the isolator frequencies must be considered and the use of DVF is not valid to suppress them. The paper proposes a stability criterion based on the mode shapes of the system. The results compare both cases: rigid and flexible base. It is shown that the isolator resonances can cause the control system to become unstable if the isolated equipment is supported on a flexible base.

### 2.4.2 Novel vibration isolation approach

Although previous works have considered the interaction between the isolators and the supporting structure, most of them are particularised to specific devices, or present difficult governing equations. With the aim to easily consider the effect that the supporting structure has on the VI performance, and also to show how the VI task affects its response, a novel VI approach is proposed.

Figure 2.18 shows a block diagram of the supporting structure and isolator system. The model of the isolator is described in Equation (2.4). The supporting structure is modelled by considering $n$ control forces, $\boldsymbol{F}_I$, exerted by the $n$ isolators and $l$ disturbance forces, $\boldsymbol{F}_d$, which can be applied at the isolation locations and/or at other base locations, where $l \geq 1$. The outputs of the supporting structure are the accelerations measured at the $n$ locations of the isolators. The forces exerted by the $n$ isolators are obtained by multiplying the vector $\boldsymbol{Y}_I$ by the diagonal matrix $\boldsymbol{M}_p = \text{diag}\,(m_{p_1}, m_{p_2}, \ldots, m_{p_n})$.

The state-space equations of the base structure considering the first $m$ vibration

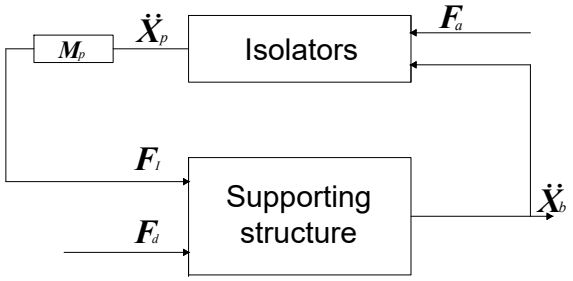


Figure 2.18: Schematic block diagram of the coupled isolator-structure system.

modes can be expressed as follows:

$$\begin{aligned} \dot{\boldsymbol{x}}_B(t) &= \boldsymbol{A}_B\boldsymbol{x}_B(t) + \boldsymbol{B}_{BD}\boldsymbol{f}_d(t) + \boldsymbol{B}_{BI}\boldsymbol{f}_I(t) \\ \boldsymbol{y}_b(t) &= \boldsymbol{C}_B\boldsymbol{x}_B(t) + \boldsymbol{D}_{BD}\boldsymbol{f}_d(t) + \boldsymbol{D}_{BI}\boldsymbol{f}_I(t), \end{aligned} \tag{2.21}$$

where the matrices $\boldsymbol{A}_B$, $\boldsymbol{B}_{BD}$, $\boldsymbol{B}_{BI}$, $\boldsymbol{C}_B$, $\boldsymbol{D}_{BD}$ and $\boldsymbol{D}_{BI}$ are defined as:

$$\boldsymbol{A}_B = \begin{bmatrix} \boldsymbol{0}_m & \boldsymbol{I}_m \\ -\boldsymbol{\Omega}^2 & -2\boldsymbol{Z}\boldsymbol{\Omega} \end{bmatrix}; \qquad \boldsymbol{B}_{BD} = \begin{bmatrix} \boldsymbol{0}_{m,l} \\ \boldsymbol{\Phi}_D \end{bmatrix}; \qquad \boldsymbol{B}_{BI} = \begin{bmatrix} \boldsymbol{0}_{m,n} \\ \boldsymbol{\Phi}_I \end{bmatrix};$$

$$\boldsymbol{C}_B = \boldsymbol{\Phi}_I^T \begin{bmatrix} -\boldsymbol{\Omega}^2 & -2\boldsymbol{Z}\boldsymbol{\Omega} \end{bmatrix}; \qquad \boldsymbol{D}_{BD} = \begin{bmatrix} \boldsymbol{\Phi}_I^T\boldsymbol{\Phi}_D, \end{bmatrix}; \qquad \boldsymbol{D}_{BI} = \begin{bmatrix} \boldsymbol{\Phi}_I^T\boldsymbol{\Phi}_I, \end{bmatrix};$$

with vectors $\boldsymbol{x}_B(t) = [x_{B_1}(t), \dot{x}_{B_1}(t), \ldots, x_{B_m}(t), \dot{x}_{B_m}(t)]^T$, $\boldsymbol{f}_d(t) = [f_{d_1}(t), \ldots, f_{d_l}(t)]^T$ and $\boldsymbol{f}_I(t) = [f_{I_1}(t), \ldots, f_{I_n}(t)]^T = \boldsymbol{M}_p\boldsymbol{y}_I(t)$ the state-space vector, the disturbance force and the forces exerted by the $n$ isolators, respectively. The output vector is $\boldsymbol{y}_b(t) = \ddot{\boldsymbol{x}}_b(t) = [\ddot{x}_{b_1}(t), \ldots, \ddot{x}_{b_n}(t)]^T$. Note that $\ddot{x}_{b_j}(t)$ is the acceleration measured at the $j^{th}$ isolation location and $x_{B_q}(t)$ is modal variable of the $q^{th}$ mode, which is used to define the state vector $\boldsymbol{x}_B(t)$ of the supporting structure. The terms $\boldsymbol{\Omega}$ =diag$(\omega_{b_1}, \ldots, \omega_{b_m})$ and $\boldsymbol{Z}$ =diag$(\zeta_{b_1}, \ldots, \zeta_{b_m})$ are $m \times m$ diagonal matrices formed by the natural frequencies of the structure and

the damping ratios, respectively. The matrices $\mathbf{0}_m$ and $\boldsymbol{I}_m$ are zero and identity matrices of dimension $m \times m$, while $\mathbf{0}_{m,l}$ and $\mathbf{0}_{m,n}$ represent $m \times l$ and $m \times n$ zero matrices, respectively. $\boldsymbol{\Phi}_D$ is an $m \times l$ matrix whose columns are the mode shapes at the disturbance locations, while $\boldsymbol{\Phi}_I$ is a $m \times n$ matrix whose columns are formed by the mode shapes of the supporting structure at the isolator locations. Note that Equations (2.21) can be used to model any $\boldsymbol{F}_I, \boldsymbol{F}_d$ and $\ddot{\boldsymbol{X}}_b$. In addition, system identification between $\ddot{\boldsymbol{X}}_b$ and $\boldsymbol{F}_I$ can be represented. This is the key to study the interaction between an isolator and a non-rigid base. Hence, it is not necessary to consider more complex models.

The model of Equation (2.21) can also be expressed in the Laplace domain as follows:

$$\boldsymbol{Y}_b(s) = s^2 \boldsymbol{X}_b(s) = \boldsymbol{G}_{BD}(s)\boldsymbol{F}_d(s) + \boldsymbol{G}_{BI}(s)\boldsymbol{Y}_I(s), \tag{2.22}$$

in which the variables $\boldsymbol{Y}_b(s)$ and $\boldsymbol{F}_d(s)$ are the Laplace transforms of $\boldsymbol{y}_b(t)$ and $\boldsymbol{f}_d(t)$, respectively, and the matrices $\boldsymbol{G}_{BD}(s)$ and $\boldsymbol{G}_{BI}(s)$ are obtained as follows:

$$\boldsymbol{G}_{BD}(s) = \boldsymbol{C}_B \left[s\boldsymbol{I}_{2m} - \boldsymbol{A}_B\right]^{-1} \boldsymbol{B}_{BD} + \boldsymbol{D}_{BD}, \tag{2.23}$$

$$\boldsymbol{G}_{BI}(s) = (\boldsymbol{C}_B \left[s\boldsymbol{I}_{2m} - \boldsymbol{A}_B\right]^{-1} \boldsymbol{B}_{BI} + \boldsymbol{D}_{BI})\boldsymbol{M}_p, \tag{2.24}$$

where $\boldsymbol{I}_{2m}$ is a $2m \times 2m$ identity matrix of the same dimensions as $\boldsymbol{A}_B$.

If Equation (2.22) is substituted into Equation (2.5), the accelerations of the isolator masses are given by:

$$\begin{aligned} \boldsymbol{Y}_I(s) = \left[\boldsymbol{I}_n - \boldsymbol{G}_{IB}(s)\boldsymbol{G}_{BI}(s)\right]^{-1} \boldsymbol{G}_{IB}(s)\boldsymbol{G}_{BD}(s)\boldsymbol{F}_d(s) + \\ \left[\boldsymbol{I}_n - \boldsymbol{G}_{IB}(s)\boldsymbol{G}_{BI}(s)\right]^{-1} \boldsymbol{G}_{IF}(s)\boldsymbol{F}_a(s), \end{aligned} \tag{2.25}$$

which depend on the disturbance forces ($\boldsymbol{F}_d$) and the active forces ($\boldsymbol{F}_a$). This equation is needed to study the influence of the platform acceleration when a non-rigid supporting structure, an AVI and disturbance forces are considered together.

### 2.4.3 Feedback control strategy for AVI

This thesis studies the influence of the interaction between the isolator system and supporting structure when a feedback AVI is considered. Firstly, the transmissibility of the isolator is obtained by substituting Equation (2.8) into Equation (2.5). Thus, the platform acceleration can be expressed as:

$$\boldsymbol{Y}_I(s) = \left[\boldsymbol{I}_n - \boldsymbol{G}_{IF}(s)\boldsymbol{G}_{AVI,F}(s)\right]^{-1}\boldsymbol{G}_{IB}(s)\boldsymbol{Y}_b(s), \tag{2.26}$$

in which $\boldsymbol{I}_n$ the $n \times n$ identity matrix. Note that this equation does not depend on the base frame. However, if a non-rigid base frame is considered, the vector $\boldsymbol{Y}_b(s)$ depends on $\boldsymbol{F}_I(s) = \boldsymbol{Y}_I(s)\boldsymbol{M}_p$ and $\boldsymbol{F}_d(s)$. Then, the isolator response $\boldsymbol{Y}_I(s)$ can be obtained by substituting Equation (2.22) into Equation (2.26), resulting in:

$$\begin{aligned}\boldsymbol{Y}_I(s) = \big[\boldsymbol{I}_n - \left[\boldsymbol{I}_n - \boldsymbol{G}_{IB}(s)\boldsymbol{G}_{BI}(s)\right]^{-1}\boldsymbol{G}_{IF}(s)\boldsymbol{G}_{AVI,F}(s)\big]^{-1} \\ \cdot \left[\boldsymbol{I}_n - \boldsymbol{G}_{IB}(s)\boldsymbol{G}_{BI}(s)\right]^{-1}\boldsymbol{G}_{IB}(s)\boldsymbol{G}_{BD}(s)\boldsymbol{F}_d(s)\end{aligned} \tag{2.27}$$

The feedback control strategy is illustrated in Figure 2.19. Considering Equation (2.8), the matrix $\boldsymbol{G}_{AVI,F}(s)$ is defined, in this thesis, as:

$$\boldsymbol{G}_{AVI,F}(s) = \boldsymbol{C}_f(s)\boldsymbol{K}_B^C = \begin{bmatrix} C_{f_{11}}(s) & \dots & C_{f_{1n}}(s) \\ \vdots & \ddots & \vdots \\ C_{f_{n1}}(s) & \dots & C_{f_{nn}}(s) \end{bmatrix}\begin{bmatrix} k_{b_{11}} & \dots & k_{b_{1n}} \\ \vdots & \ddots & \vdots \\ k_{b_{n1}} & \dots & k_{b_{nn}} \end{bmatrix}, \tag{2.28}$$

in which $\boldsymbol{C}_f(s)$ is the controller matrix and $\boldsymbol{K}_B^C$ is the control gain matrix. This thesis shows the influence of considering a non-rigid supporting structure by considering a particular controller $\boldsymbol{C}_f(s)$ and optimally designing the control gains $\boldsymbol{K}_B^C$. In order to denote the matrix $\boldsymbol{K}_B^C$ in each case, the sub-index $_B$ can be $_V$ or $_{FV}$, which means rigid or non-rigid supporting structure. The super-index $^C$ denotes if the controller is a SISO ($^S$) or a MIMO ($^M$) controller. Finally, any matrix denoted with $\hat{\boldsymbol{K}}_B^C$ is used when the optimal control gains have been found, for any case mentioned above. Then, this thesis studies the influence of considering $\hat{\boldsymbol{K}}_V^S$, $\hat{\boldsymbol{K}}_{FV}^S$

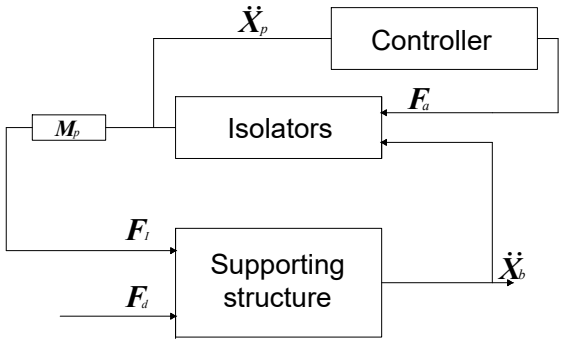


Figure 2.19: Dynamic model of a single isolator on a rigid supporting base with a feedback controller.

and $\hat{\boldsymbol{K}}_{FV}^{M}$ when the isolation and alignment performance of the isolator system is considered.

If a rigid base frame is considered, the vector $\boldsymbol{Y}_b(s)$ is independent of $\boldsymbol{Y}_I(s)$. Then, the AVI controller $\boldsymbol{G}_{AVI,F}(s)$ is tuned to improve the response with respect to the passive configuration. In this case, the matrix $\boldsymbol{G}_{AVI,F}(s)$ is considered diagonal and the transmissibility can be expressed as:

$$\frac{s^2 X_{p_j}(s)}{s^2 X_{b_j}(s)} = \frac{2\zeta_{p_j}\omega_{p_j}s + \omega_{p_j}^2}{s^2 + 2\zeta_{p_j}\omega_{p_j}s + \omega_{p_j}^2 - (C_{f_{jj}}(s)k_{b_{jj}}/m_{p_j})s^2}. \tag{2.29}$$

The optimal value for the gain matrix ($\hat{\boldsymbol{K}}_{V}^{S}$) is obtained considering the best isolation performance in terms of the transmissibility defined in Equation (2.29).

If a non-rigid base frame is considered, the vector $\boldsymbol{Y}_b(s)$ depends on $\boldsymbol{F}_I(s) = \boldsymbol{Y}_I(s)\boldsymbol{M}_p$ and $\boldsymbol{F}_d(s)$. Then, the isolator response $\boldsymbol{Y}_I(s)$ is obtained by substituting Equation (2.28) into (2.27). In this case, the variable $\boldsymbol{Y}_I(s)$ is used to define the alignment between isolator platforms. Thus, the matrix $\boldsymbol{K}_B^C$ can be optimally designed in terms of transmissibility, supporting structure vibration and/or the alignment between isolator platforms. The main objective of this thesis (Chapters 4 and 5) is to show how the response ($\boldsymbol{Y}_I(s)$) can be improved in terms of transmissibility and alignment when the dynamics of the non-rigid base are considered in Equations (2.27) and (2.29) ($\hat{\boldsymbol{K}}_{FV}^{S}$ and $\hat{\boldsymbol{K}}_{FV}^{M}$) with respect to the optimal design of Equation (2.29) for the assumption of a rigid base frame assumption ($\hat{\boldsymbol{K}}_{V}^{S}$).

# Chapter 3

# Active vibration isolation under isolator-structure interaction

This chapter is based on two conference papers published in 2019 and 2021 as well as a journal manuscript submitted for review, as listed below:

- Pérez-Aracil, J., Pereira-González, E., Muñoz-Díaz, I., and Reynolds, P. (2019). "Study of active vibration isolation systems considering isolator–structure interaction". In CMMoST 2019: 5th International Conference on Mechanical Models in Structural Engineering, pages 645–654, Alicante, Spain. Editorial Club Universitario.

- Pérez-Aracil, J., Pereira, E., Díaz, I. M. and Reynolds, P. (2021). Study on the "Isolator-Structure Interaction. Influence on the Supporting Structure". In Gonçalves, J. A., In CONTROLO 2020, pages 394–403, Cham. Springer International Publishing.

- Pérez-Aracil, J., Pereira, E., Díaz, I. M. and Reynolds, P. "Active vibration isolation under isolator-structure interaction". It has been accepted for publication in *Meccanica*.

## 3.1 Introduction

This chapter is used as a proof of concept of the theory developed in Chapter 2. It shows, with a simplified example, the importance of the interaction phenomenon, specially on the base response.

To show the effect that the VI task has on the supporting structure response, a single isolator is situated on a SDOF supporting structure. Different scenarios are analysed, such that an extensive set of dynamic properties relations between the isolator and the base are considered. Two techniques are analysed: PVI and AVI. In terms of changing the PVI performance, different damping ratios are considered, whilst for the AVI technique, the controller is designed to achieve the same H-infinity norm in all the transmissibility TFs, for every case, using Equation (2.29). It will be shown how, in terms of the transmissibilty, the use of AVI technique always improves the performance, as expected. However, the response of the base response may not follow this behaviour. Depending on the relation between the dynamic properties of the isolator and the supporting structure, and also on the isolator damping ratio, the use of AVI instead of PVI may produce different base response changes: i) reduction of the base response, ii) increment of the base response, or iii) it can produce no changes on the base response. If these changes appear on the base response behaviour, it affects the platform acceleration, hence modifying the task performance, i.e., the absolute acceleration of the payload.

With the aim of validating the theory developed in Chapter 2, particularized here for a single isolator situated on a SDOF base, an experimental test has been carried out. The test is valid not only to check the theory, but also to find issues in a real VI implementation. The experimental results fit with the theoretical ones. Then, they can be can be extrapolated to analogous systems.

The remainder of the chapter is as follows. The following Section 3.2 shows the theory developed in Chapter 2 but for a particular case in which a single isolator is situated on a SDOF structure. In Section 3.3, the influence on the base structure response of including an AVI strategy is formulated, also showing the effect, in simulations, for the particular case of a DVF. To validate the simulation carried

out, laboratory experimental measurements are conducted and presented in Section 3.4. Finally, conclusions are presented in Section 3.5.

## 3.2 Particularization of the vibration isolation framework

This section particularizes the model of a non-rigid frame when only one isolator is placed on it and when its dynamics can be modelled by only one vibration mode. In addition, a feedback AVI technique is considered.

First of all, if only a single isolator is considered, the transmissibility TF can be expressed as:

$$\frac{s^2 X_p(s)}{s^2 X_b(s)} = \frac{2\zeta_p \omega_p s + \omega_p^2}{s^2 + 2\zeta_p \omega_p s + \omega_p^2 - (C_f(s) k_b / m_p) s^2}. \tag{3.1}$$

The TFs $G_{IB}(s)$ and $G_{IF}(s)$, defined in Equations (2.6) and (2.7) for $n$ isolators, result for a single isolator as follows:

$$G_{IB}(s) = \frac{2\zeta_p \omega_p s + \omega_p^2}{s^2 + 2\zeta_p \omega_p s + \omega_p^2} \tag{3.2}$$

$$G_{IF}(s) = \frac{1}{m_p} \frac{s^2}{s^2 + 2\zeta_p \omega_p s + \omega_p^2}. \tag{3.3}$$

where the subscript $j$ has been suppressed since only one isolator is being considered.

Secondly, Equation (2.22), which models the supporting structure, is particularized for one vibration mode as follows:

$$s^2 X_b(s) = \frac{s^2/m_b}{s^2 + 2\zeta_b \omega_b s + \omega_b^2} (F_d(s) - m_p s^2 X_p(s)), \tag{3.4}$$

where the TF between the base structure acceleration and the external perturbation force without the isolator, $G_{BD}(s)$, can be expressed using Equation (2.23) for a single isolator. Thus, $G_{BD}(s)$ is now as follows:

$$G_{BD}(s) = \frac{s^2/m_b}{s^2 + 2\zeta_b \omega_b s + \omega_b^2}. \tag{3.5}$$

Note also that $G_{BI}(s) = m_p G_{BD}(s)$. Thus, considering the subsystems $G_{IB}(s)$, $G_{IF}(s)$, $G_{AVI,F}(s)$, $G_{BI}(s)$ and $G_{BD}(s)$, the Figure 2.19 can be particularized, as Figure 3.1 shows. The subsystem $G_I(s)$ in Figure 3.1 can be obtained as follows:

$$G_I(s) = \frac{2\zeta_p\omega_p s + \omega_p^2}{s^2 + 2\zeta_p\omega_p s + \omega_p^2 - \frac{1}{m_p}G_{AVI,F}(s)s^2}. \tag{3.6}$$

Note that in this case, $G_{AVI,F}(s) = C_f(s)k_b$, since only one isolator is involved in the task. In addition, Equation (3.6) is the isolator dynamic defined in Equation (2.2) particularized to a feedback AVI.

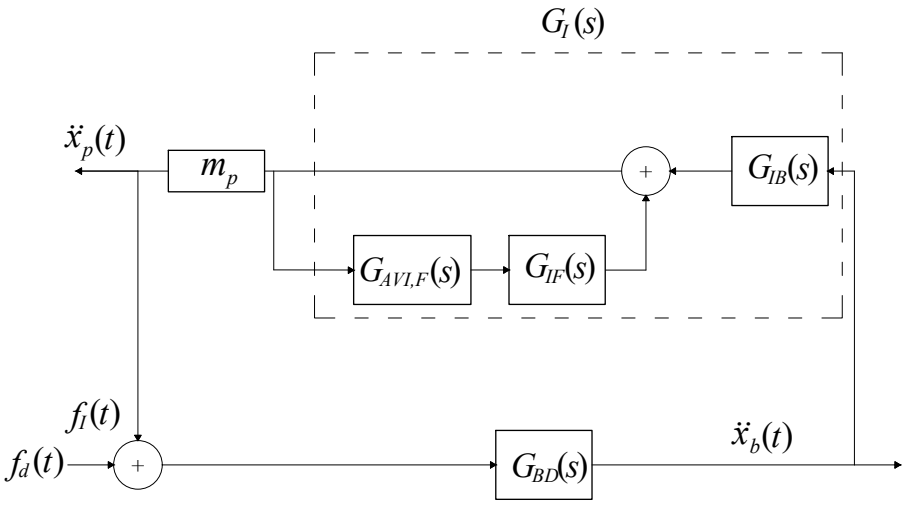


Figure 3.1: General scheme of the VI problem particularized for a non-rigid frame when only one isolator is placed on it.

This chapter studies the influence of including $G_{AVI,F}(s)$ when a non-rigid supporting structure is considered. Thus, the two following TFs are compared:

$$G_B^{PVI}(s) = \frac{G_{BD}(s)}{1 + m_p G_{BD}(s) G_{IB}(s)}, \tag{3.7}$$

$$G_B^{AVI}(s) = \frac{G_{BD}(s)}{1 + m_p G_{BD}(s) G_I(s)}, \tag{3.8}$$

where $G_B^{PVI}(s)$ and $G_B^{AVI}(s)$ are the TFs between the base acceleration $s^2X_b(s)$, and the perturbation force $F_d(s)$ when the isolation force, $f_I(t)$, is generated passively (PVI) and actively (AVI), respectively.

The effect on the base response of using an AVI control system compared with PVI control is studied using following variable:

$$\gamma = \frac{\|G_B^{AVI}(s)\|_\infty}{\|G_B^{PVI}(s)\|_\infty}, \tag{3.9}$$

in which $\gamma$ is the ratio between H-infinity norm of $G_B^{AVI}(s)$ and $G_B^{PVI}(s)$. On one hand, if the value of $\gamma$ is greater than one, the maximum value of the Frequency Response Function (FRF) of $G_B^{AVI}(s)$ is higher than that of $G_B^{PVI}(s)$, which means that the vibration level due to a disturbance force is higher when AVI is used. On the other hand, if the value of $\gamma$ is less than one, the vibration level is reduced when AVI is applied. If the value of $\gamma$ is close to one (or one) , it means that there is not a significant difference in the response of the base when the PVI or AVI are used, $\|G_B^{AVI}(s)\|_\infty \approx \|G_B^{PVI}(s)\|_\infty$.

In order to generalise the studies derived from this framework, the following ratios can be defined: mass ratio $r_m = m_p/m_b$ and frequency ratio $r_\omega = \omega_p/\omega_b$. The influence of the isolation system on the response of the base structure also depends on the damping ratios $\zeta_p$ and $\zeta_b$. The value of $\zeta_p$ is one of the main reasons of including AVI. Note that the objective of including an AVI strategy is to obtain a $G_I(s)$ with no resonance peak and a rejected band similar to a PVI with low damping ratio ($\zeta_p$). Thus, if $\zeta_p$ is increased, an attenuation of -40 dB/dec cannot be obtained because the zero placed at $-\omega_p/\zeta_p$ is close to the poles $-\zeta_p\omega_p \pm \omega_p\sqrt{1-2\zeta_p}$, which means that only a -20 dB/dec can be achieved. Therefore, a set of values of $\zeta_p$ must be considered to show that significant differences exist in the base response for values $0 \leq \zeta_p \leq 1$. Finally, small changes in the damping values of $G_B^{PVI}(s)$ and $G_B^{AVI}(s)$, which are due to $G_I(s)$, are more significant when $\zeta_b$ is smaller. Thus, a low damped base structures is of particular interest for this study.

## 3.3 Influence of AVI technique on the supporting structure. Direct velocity feedback

This study considers the base and isolator parameters defined in Table 3.1 and a DVF as the AVI control law. Ideal DVF has the form $G_{AVI,F}(s) = k_b/s$, which introduces a pure integrator to the system. This DVF damps the system $G_I(s)$ by increasing the parameter $k_b$, being the damping ratio of the AVI $k_b/(2\sqrt{k_p m_p})$, Equation (3.6). In the literature, it is said that this DVF is equivalent to a virtual sky-hook damper [Preumont, 2018b], introducing a damping force that does not depend on its relative movement with respect to the base in the bandwidth of interest. However, this pure integrator has an infinite magnitude response at zero frequency, making this controller very sensitive to low-frequency noise. Therefore, it cannot be used in practice because this ideal integrator may saturate the actuator used for imparting the force due to offsets in the acceleration signal [Díaz and Reynolds, 2010]. Thus, the following lossy integrator is considered in this case study:

$$G_{AVI,F}(s) = \frac{k_b}{s/\omega_c + 1}, \tag{3.10}$$

in which $\omega_c$ represents the low frequency cut-off frequency of the lossy-integrator and $k_b$ its control gain. If the value of $\omega_c$ is defined as $0.1\omega_p$, the ideal and real DVF has a similar behaviour in the bandwidth of interest.

High order controllers may be implemented to improve the performance of the of the VI task. This type of controller can virtually change the stiffness and mass of the isolator, hence modifying its natural frequency. However, as stated before, the main purpose of the thesis is to analyse the influence of the interaction phenomenon on both the VI and alignment performance also on the base response. For that, the use of DVF controller allows approaching the problem just modifying the damping of the isolator system and improving the rejected band of the isolator. Thus, through the set of different mass and frequency ratios, $r_m, r_\omega$, that refer to the physical parameters, the interaction problem can be studied simplifying the implementation issues, which may be derived of using more complex controllers.

| $r_m$ | $r_\omega$ | $\zeta_p$ | $\zeta_b$ |
|---|---|---|---|
| $[10^{-6}, 2]$ | $[10^{-3}, 2]$ | $\{0.001, 0.1, 0.3, 0.5, 1/\sqrt{2}, 0.9\}$ | 0.005 |

Table 3.1: Mass, frequency and damping ratio values of $r_m, r_\omega, \zeta_p, \zeta_b$,

The numerical results are organised into two subsections. The first one shows a comparative of the FRFs for two cases: i) when the a PVI is implemented $G_I^{PVI}(s)$, ii) when AVI is used $G_I^{AVI}(s)$, which is expressed as:

$$G_I^{AVI}(s) = \frac{2\zeta_p\omega_p s + \omega_p^2}{s^2 + 2\zeta_p\omega_p s + \omega_p^2 - \frac{k_b}{m_p(s/\omega_c+1)}s^2}, \tag{3.11}$$

The controller gain $k_b$ is adapted so that TF $G_I(s)$ reaches -3 dB at the damped frequency of the isolator, defined by $\omega_{p_d} = \omega_p\sqrt{1-\zeta_p^2}$. The second subsection shows some illustrative examples where the FRFs of $G_{BD}(s)$, $G_B^{PVI}(s)$ and $G_B^{AVI}(s)$ are compared. Three examples are proposed to show when AVI reduces or increases the vibration level of the base structure.

### 3.3.1 Isolation performance and influence of AVI on the base structure response

Figure 3.2 shows the comparison between $G_I^{PVI}(s)$ and $G_I^{AVI}(s)$ (top) and the value of $\gamma$ (bottom) in different analysed cases, for $\zeta_p$ equal to 0.001 and 0.1. As can be observed, for these values of $\zeta_p$ the platform response in PVI mode exhibits high amplitude response, which is reduced using the active force $f_a(t)$. In addition, the rejected band is the same for the AVI even though the damping is increased. This is the case when the beneficial effect of including AVI is better justified from an isolation point of view. If the influence into the base structure is analysed (i.e. the value of $\gamma$), AVI affects positively the base response when $\zeta_p = 0.001$ and high values of $r_m$ are considered. In other words, AVI introducing damping to the base structure more than PVI. For remaining values of $r_m$ and $r_\omega$, the differences between AVI and PVI are not significant. However, when $\zeta_p = 0.1$ the response of the base structure for AVI can be up to three times higher than the response with PVI. The critical region is observed for similar frequency values ($r_\omega \to 1$) and mass ratios between

$[10^{-4}, 0.20]$, approximately. The base response is reduced for AVI control for the region $[r_m > 10^{-3}, r_\omega > 1]$, compared with the PVI control.

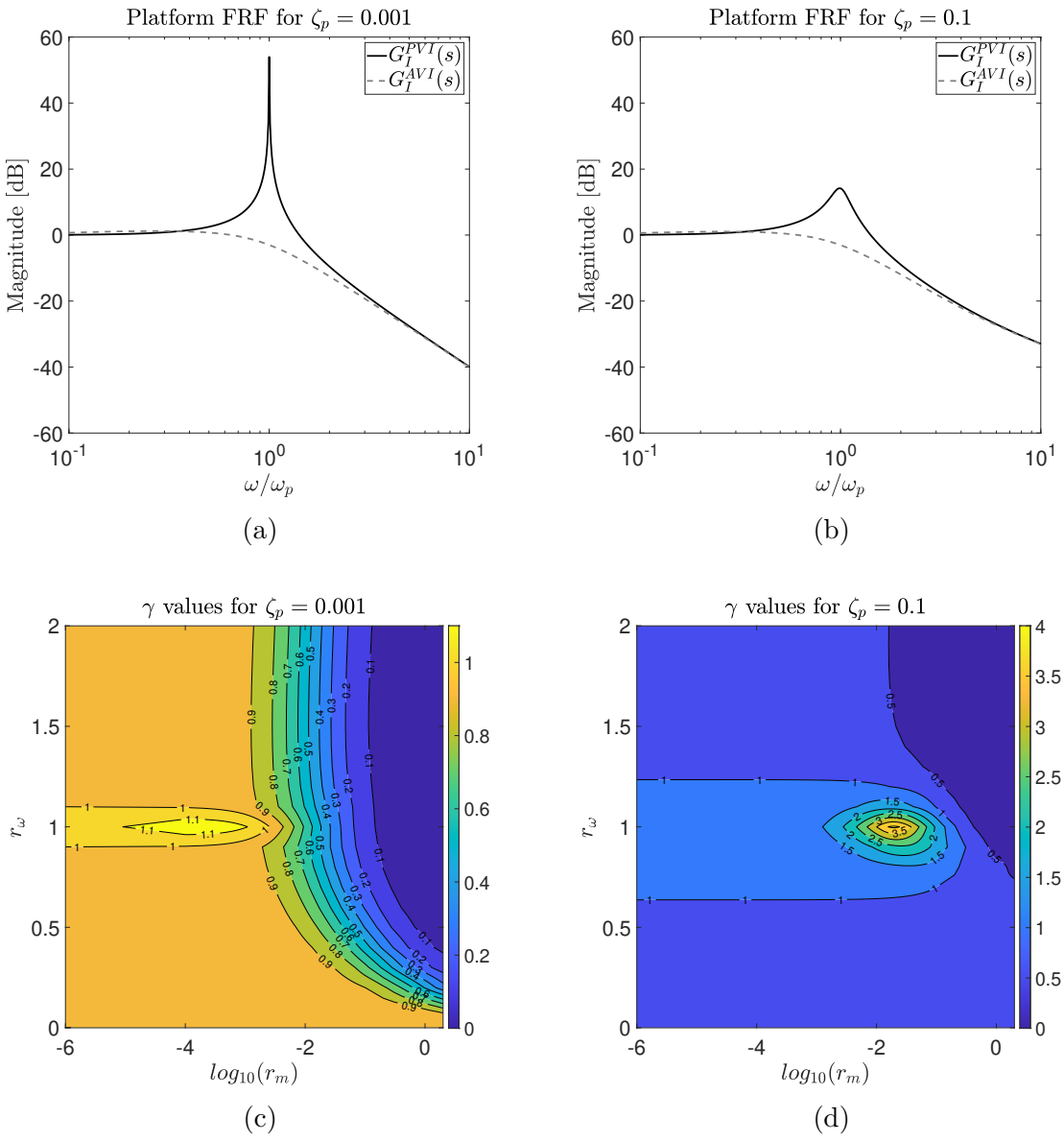


Figure 3.2: (a) and (b) isolator FRFs. (c) and (d) influence ratio $\gamma$ for $\zeta_p = 0.001$ and $\zeta_p = 0.1$.

Figure 3.3 represents the FRFs of $G_I^{PVI}(s)$ and $G_I^{AVI}(s)$, and $\gamma$ values, but for values of $\zeta_p$ equal to 0.3 and 0.5. The platform response is better for AVI control technique. However, it should be noted that this improvement is not so significant as compared with low values $\zeta_p$ (Figure 3.2). In addition, an increment of almost two times the base response with AVI control, $G_B^{AVI}(s)$ is observed compared that with PVI control, $G_B^{PVI}(s)$. In case of $\zeta_p = 0.3$, the region for which the base response is critically increased is observed for base frequency values slightly higher

than the isolator frequency ($r_\omega \to 0.9$ and $0.9 < r_m < 10^{-4}$). However, for high frequency and mass ratios, the use of AVI control provides a huge reduction in the base response compared with PVI control. The same behaviour is presented in the case of $\zeta_p = 0.5$, but this region is softer and the critical region is situated at lower frequency ratios.

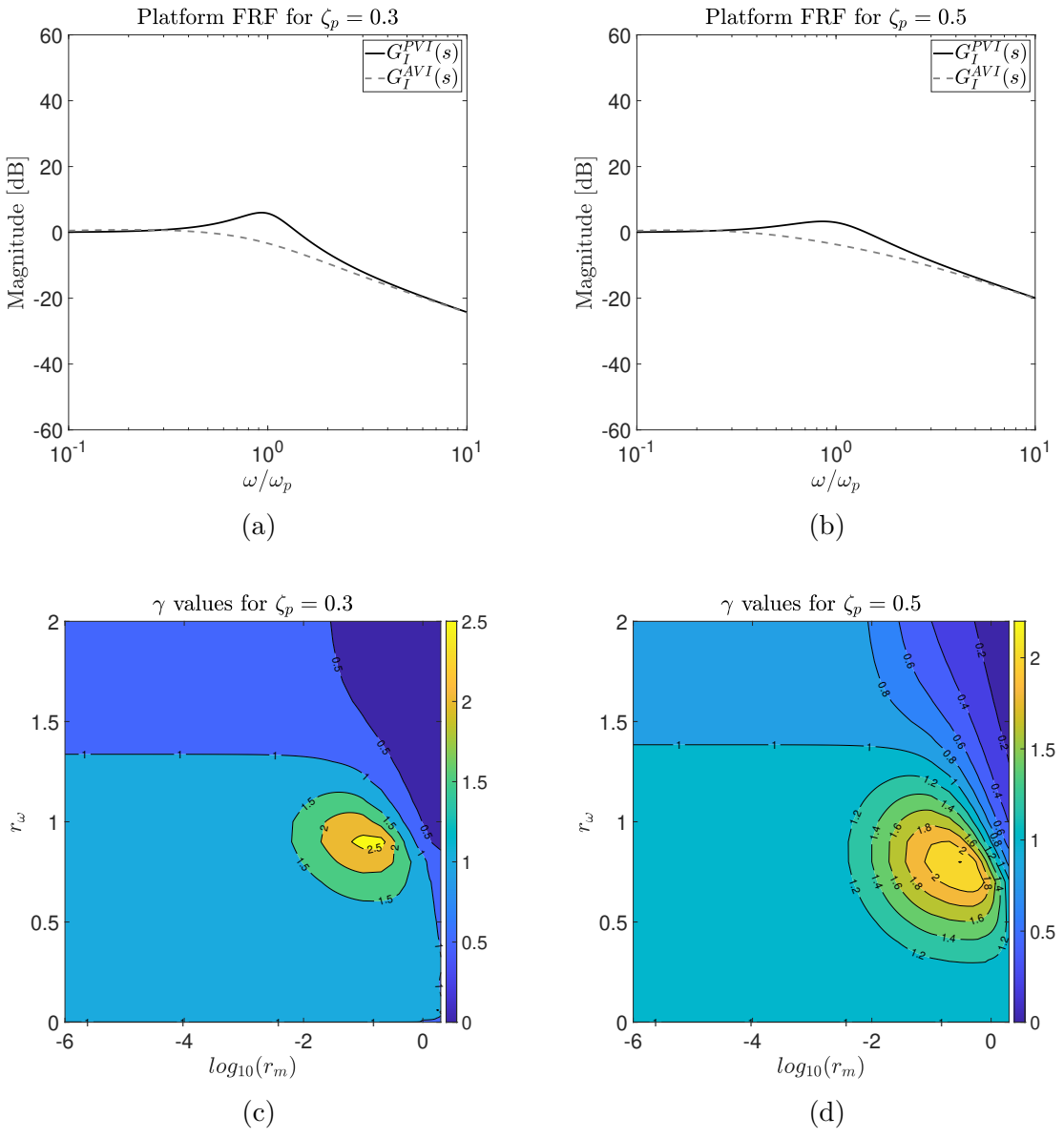


Figure 3.3: (a) and (b) isolator FRFs. (c) and (d) influence ratio $\gamma$ for $\zeta_p = 0.3$ and $\zeta_p = 0.5$.

Finally, in Figure 3.4, the isolation performance is quite similar when PVI and AVI are compared. In addition, the rejected band is -20 dB/dec since the poles and zeros are quite close. In these cases an AVI to increase the damping value is not well justified. Moreover, for $\zeta_p = 1/\sqrt{2}$, $\gamma$ reaches its maximum value when the frequency

of the base structures tends to be the double the isolator frequency, $r_\omega \rightarrow 0.5$ (approximately two times). In terms of mass ratio, its influence is important for high frequency ratios, for which the base response is reduced. However, if the damping of the isolator is almost critical $\zeta_p = 0.9$, the response is only slightly different. The maximum values of $\gamma$ are located in a lower frequency ratio region than for the rest of the cases. Also, the value increases respect to the case of $\zeta_p = 1/\sqrt{2}$. Therefore, for high mass ratios and high values of $\zeta_p$, the use of AVI depends on the ratio between the natural frequencies of the base and the isolator ($r_\omega$).

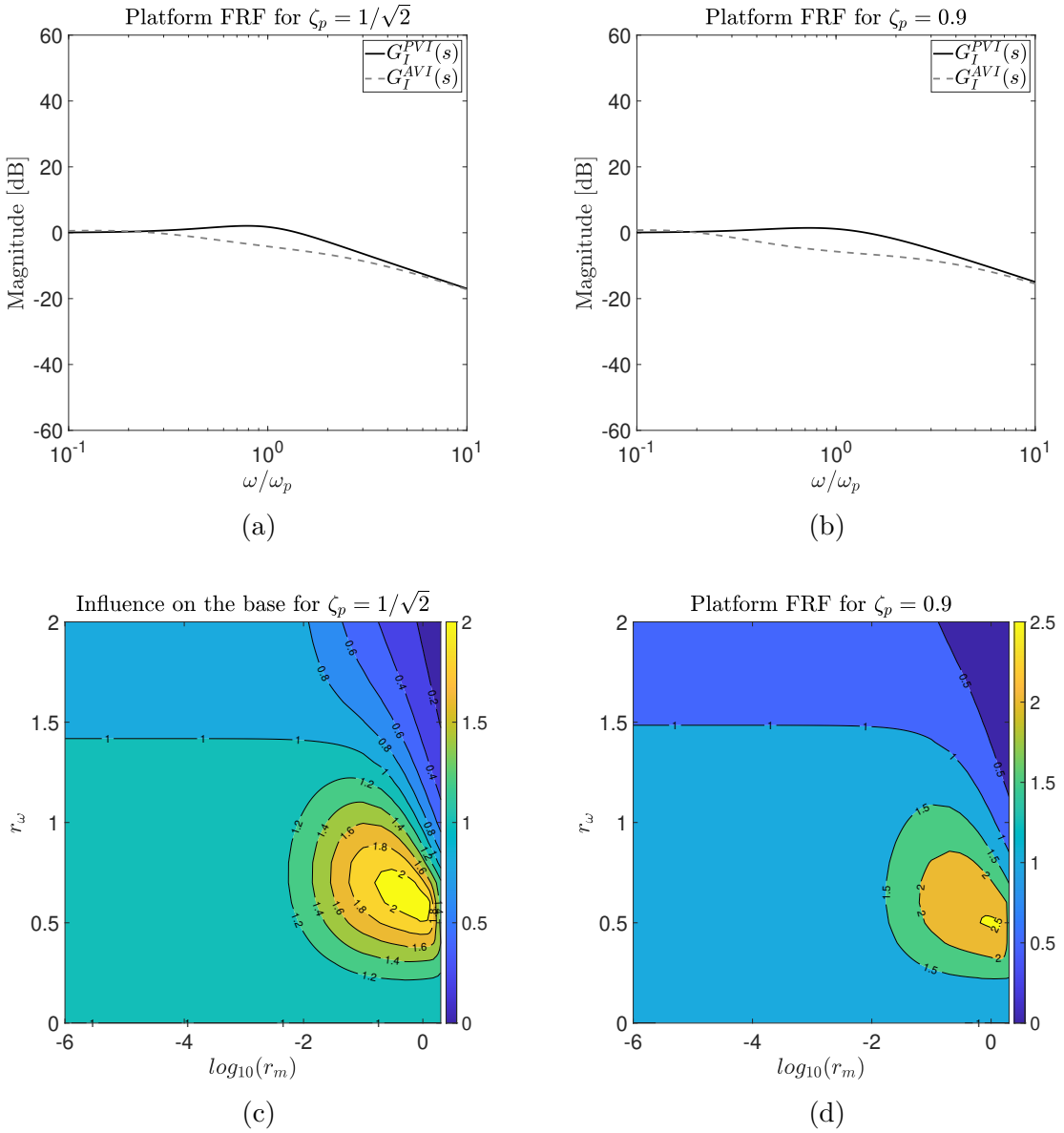


Figure 3.4: (a) and (b) isolator FRFs. (c) and (d) influence ratio $\gamma$ for $\zeta_p = 1/sqrt(2)$ and $\zeta_p = 0.9$.

### 3.3.2 Influence of PVI and AVI on the base structure

To show the effect that PVI and AVI have on the base response, three different cases of $r_m$ and $r_\omega$ are studied for damping values $\zeta_p = \{0.1, 0.5, 0.9\}$. This phenomenon is not well shown in the above figures, since $G_{BD}(s)$ was not plotted and the parameter $\gamma$ considers only the difference between PVI and AVI. It is important to note that these cases are extracted from the data shown above, so the same isolation performance is achieved in all the cases studied here. The figures show the effect of using both techniques, PVI and AVI, on the supporting structure. The FRFs are normalised with respect the peak base response when no isolator device is situated on it, which can be expressed as $\|G_{BD}(s)\|_\infty$.

**Case** $r_m = 0.0889$ **and** $r_\omega = 0.8$

This case shows an example for which the collocation of the isolator implies a reduction of the base response, but the use of AVI control in the isolator increases the response in the supporting structure compared with the passive mode. Figure 3.5 shows that the maximum reduction in PVI mode is achieved for $\zeta_p = 0.5$. When the AVI control is activated in the isolator, there is an increase in the base response for all three cases compared with the PVI case. Also, the resonance frequency of supporting structure is moved sightly.

In this scenario, the accomplishment of the VI requirement affects negatively the dynamic response of the base structure. This may be very important in different scenarios, such as in civil structures, in which the vibration serviceability can be affected. Moreover, in applications in which multiple isolators are situated in the same supporting structure, since their response is coupled. This case is analysed in Chapters 4 and 5.

**Case** $r_m = 0.048$ **and** $r_\omega = 1.6$

In this scenario, the use of AVI control induces a reduction in the base response compared with PVI control. Figure 3.6 shows that the supporting structure is more damped with AVI than with PVI. Thus, the use of PVI implies basically the same

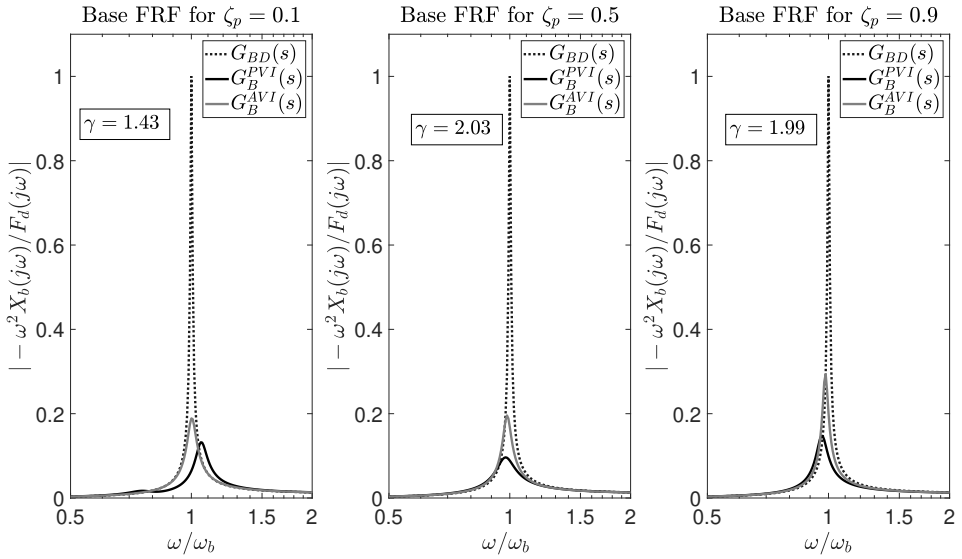


Figure 3.5: Case $r_m = 0.0889$ and $r_\omega. = 0.8$. Normalised FRFs of the base with no isolator situated on the structure (dashed line), with an isolator collocated but no control activated (black line), with the isolator collocated and DVF working (grey line).

base response for $\zeta_p = 0.1$. However, the damping imparted by the AVI control is greater. This effect, although less significant in terms of $\gamma$ reduction, can be seen for $\zeta_p$ equal to 0.5 and 0.9. For this combination of dynamic parameters, the use of AVI does not compromise the base structure response. However, it is important to note that only a SDOF system is considered for the base, and only one isolator is studied. This effect may be different when multiple modes and multiple isolators are considered.

**Case $r_m = 0.0794$ and $r_\omega = 1.3$**

This case presents a scenario in which the damping ratio of the isolator determines if the base response for AVI control increases or not with respect to PVI control. The following mass and frequency ratio values considered here are $r_m = 0.0794$ and $r_\omega = 1.3$ (Figure 3.7). If AVI control is used, $\|G_B^{AVI}(s)\|_\infty > \|G_B^{PVI}(s)\|_\infty$ for $\zeta_p = 0.1$. A different phenomenon occurs for $\zeta_p = 0.5$, for which $\|G_B^{AVI}(s)\|_\infty \approx \|G_B^{PVI}(s)\|_\infty$. If the damping of the isolator is 0.9, $\|G_B^{AVI}(s)\|_\infty < \|G_B^{PVI}(s)\|_\infty$. This shows the importance of the isolator damping in terms of its influence in the base. According to this fact, different control strategies must be considered to accomplish possible

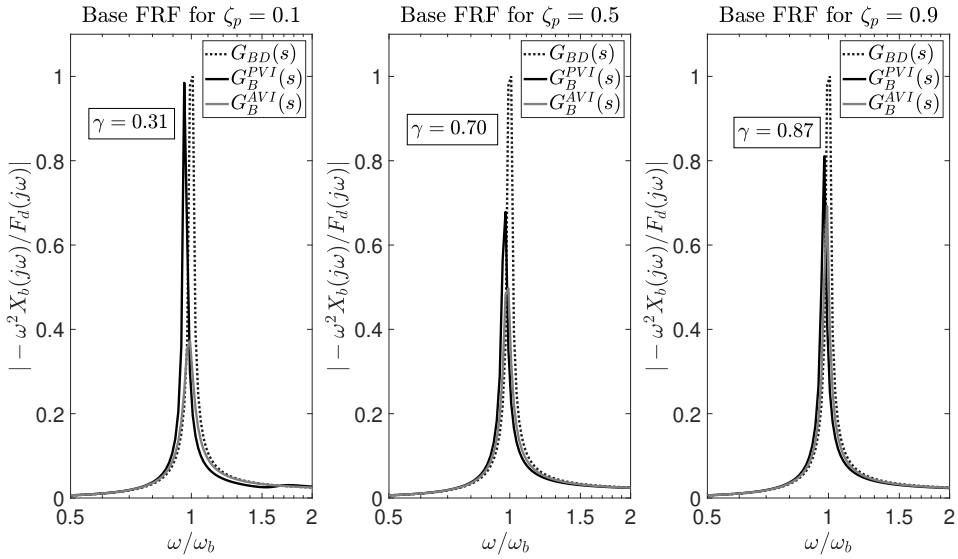


Figure 3.6: Case $r_m = 0.048$ and $r_\omega = 1.6$. Normalised FRFs of the base with no isolator situated on the structure (dashed line), with an isolator collocated but no control activated (black line), with the isolator collocated and DVF working (grey line).

base acceleration requirements.

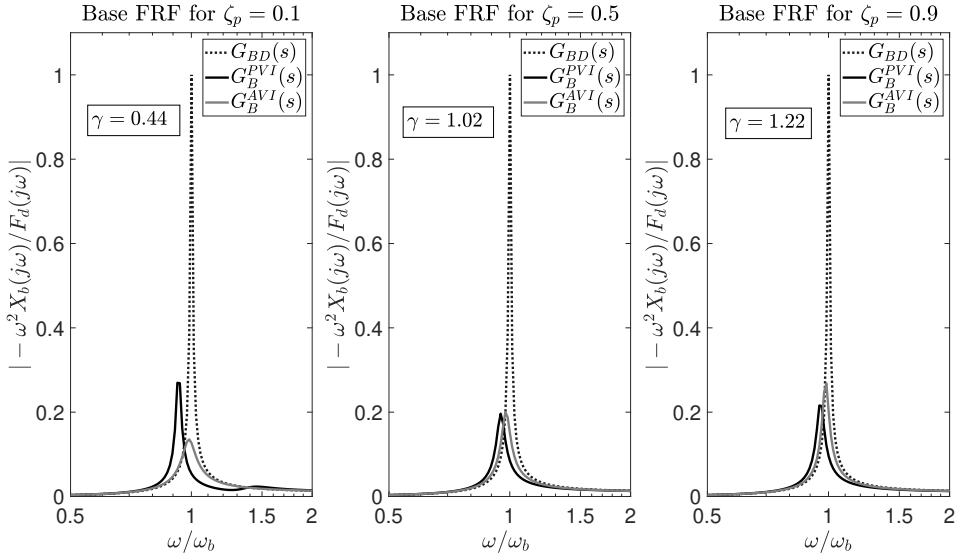


Figure 3.7: Case $r_m = 0.0794$ and $r_\omega = 1.3$. Normalised FRFs of the base with no isolator situated on the structure (dashed line), with an isolator collocated but no control activated (black line), with the isolator collocated and DVF working (grey line).

## 3.4 Experimental test

In this section, the application of VI on a full-scale beam structure is described. The experimental results are compared with numerical simulations to illustrate the theoretical framework presented in the chapter. The application example presented here shows a case in which the use of AVI control implies the improvement of both the VI performance and the response of the base structure.

### 3.4.1 Experimental set-up and system dynamics

An isolator was situated at mid-span of a simply supported beam (knife edge supports at both ends) of length 5.0 m (Figure 3.8). The beam was excited by a perturbation force $f_d(t)$, generated by an exciter situated on the ground and linked to the supporting structure by a stinger. An accelerometer was attached to the platform to measure the payload acceleration, $\ddot{x}_p(t)$, and another one to the beam, close to the isolator, to measure the base acceleration, $\ddot{x}_b(t)$.

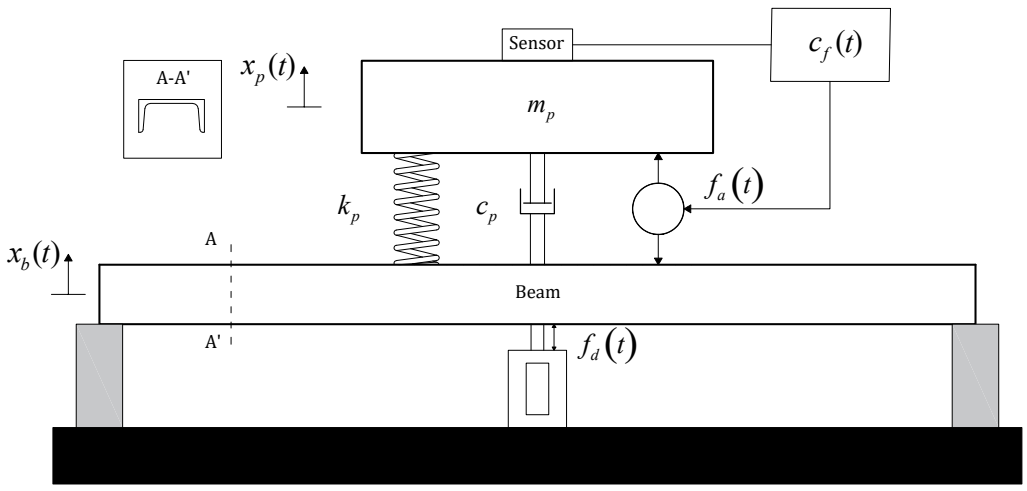


Figure 3.8: Illustration of the experimental set-up.

A general view of the experimental setup is shown in Figure 3.9. The device used for isolation was an APS Dynamics Model 400 electrodynamic actuator. A platform

was attached to the top of the armature. The acceleration of both platform and base were measured with PCB® model 393A03 accelerometers. The isolator device has mass 82 kg when $m_p$ is unattached. The mass of the beam without the isolator is approximately 126 kg. The total mass of the isolation platform $m_p$ is 31 kg. The perturbation force was generated by another electrodynamic actuator of the same model. This was driven in current mode, so the applied force may be considered proportional to the supplied current [Preumont, 2018b]. The experimental setup is completed by a data acquisition device National Instruments compactRIO 9066 equipped with an IEPE acquisition module for accelerometers and an output module to generate both the excitation signals and the control law for the AVI.


Figure 3.9: General view of the experimental setup.

The FRF of the TF, $G_{BD}(s)$, between the acceleration of the base $\ddot{x}_b(t)$ and the perturbation force $f_p(t)$ is shown in Figure 3.10. It shows only the first flexural mode of the beam, which was used for analysis of the results. To identify this TF, the isolator device was collocated on the beam without the moving mass $m_p$. Thus, the weight of the device was included in the identification but not the effect of the

force $f_I(t)$ due to platform movement. The identified TF from the experimental FRF is as follows:

$$G_{BD}(s) = \frac{0.0078s^2}{s^2 + 0.25s + 738.46} \tag{3.12}$$

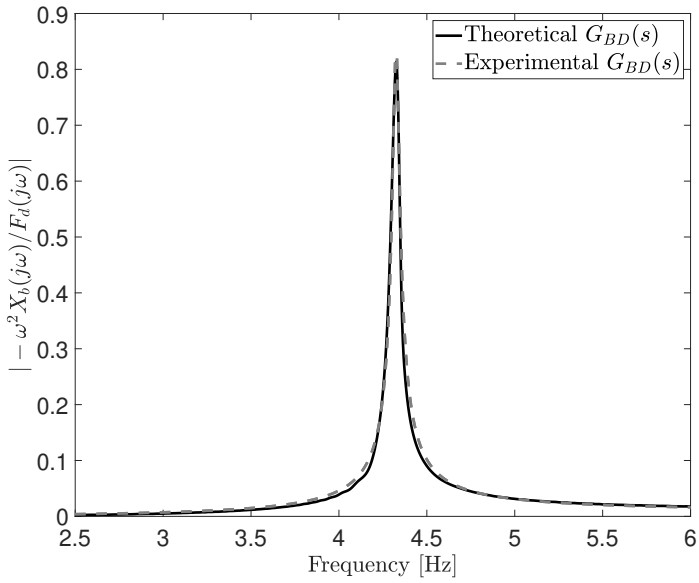


Figure 3.10: Experimental and theoretical FRFs of the TF $G_{BD}(s)$.

Thus, from the identified TF, according to the form of Equation (3.5), the natural frequency of the first mode of the beam was therefore identified at $\omega_b = 27.64$ rads$^{-1}$ (4.4 Hz). The damping ratio, extracted by the half power bandwidth method [Bendat and Piersol, 1993] was $\zeta_b = 0.0046$.

To obtain the dynamic parameters of the isolator, it was situated at mid-span of the beam, which was excited by a random perturbation. The TF $G_{IB}(s)$ was obtained from the beam and platform accelerations, which allows identification of the dynamic parameters $(\omega_p, \zeta_p)$. This was given by:

$$G_{IB}(s) = \frac{1.32s + 77.37}{s^2 + 1.32s + 77.37}, \tag{3.13}$$

where the identified natural frequency and damping ratio are $\omega_p = 8.79$ rads$^{-1}$ (1.4 Hz) and $\zeta_p = 0.075$, respectively (Equation 3.2). Using these parameters it is possible to obtain the TF that relates the force applied in $m_p$ and its acceleration

$\ddot{x}_p(t)$ (Equation 3.3) which was identified to be:

$$G_{IF}(s) = \frac{0.032s^2}{s^2 + 1.32s + 77.37}. \tag{3.14}$$

### 3.4.2 Vibration isolation effect on the supporting structure

The control strategy chosen for this experiment is DVF as defined in Equation (3.10). According to that, and using the natural frequency of the isolator (1.4 Hz), the following controller, for unitary static gain, results:

$$C_f(s) = \frac{0.8796}{s + 0.8796}. \tag{3.15}$$

It should be highlighted that the imparted damping with $G_{AVI,F}(s)$ would be improved theoretically if the TF $G_{IF}(s)$ is considered (i.e. the mechanical dynamic part of the isolator). However, there are further dynamics (e.g. the amplifier driving the shaker, the accelerometers, the signal conditioning electronics) that have not been considered in Equation (3.14). Therefore, the isolation reduction around the resonant frequency is worse in practice since these non-considered dynamics tend to make the AVI unstable at high gains. It should also be highlighted that the damping achieved with the active force is enough to demonstrate the influence that AVI has in the supporting structure compared with PVI.

The influence that an isolator with various dynamic properties has on different structures is shown in Figure 3.11. As can be observed, the surface shape is very similar to those showed in Figure 3.2 for $\zeta_p = 0.1$. According to Equation 3.5, the equivalent mass of the first mode of the base structure $m_b$ can be extracted from the identified TF of the beam (Figure 3.10). Thus, if the beam is simplified to a SDOF system, the equivalent mass is 128 kg. The resulting mass and frequency ratios are $r_m = 0.24$ and $r_\omega = 0.31$, respectively. The value of $\gamma$ for the numerical simulations is 0.80. This implies that the use of an AVI system provides an improvement with respect to the PVI system.

The identified transmissibility for both PVI and AVI systems and their influence on the beam TFs are shown in Figure 3.12. At the top, the passive (black line) and

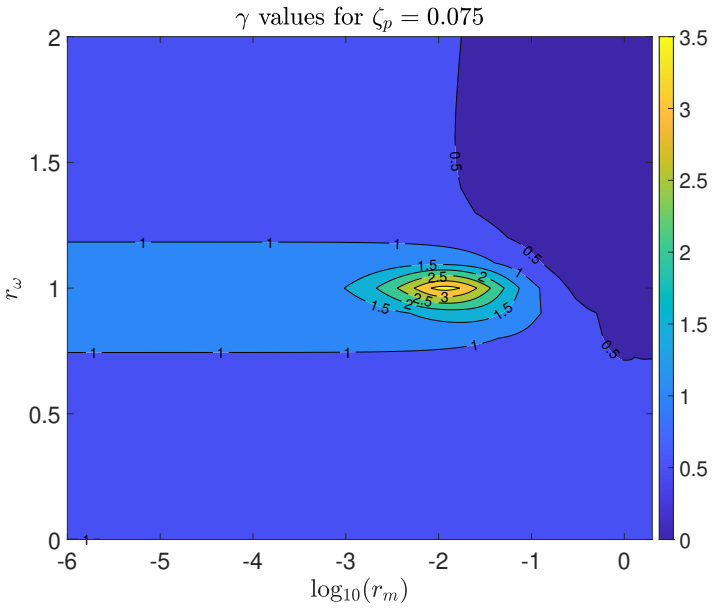


Figure 3.11: Influence map for the isolator used in the experimental test on different supporting structures.

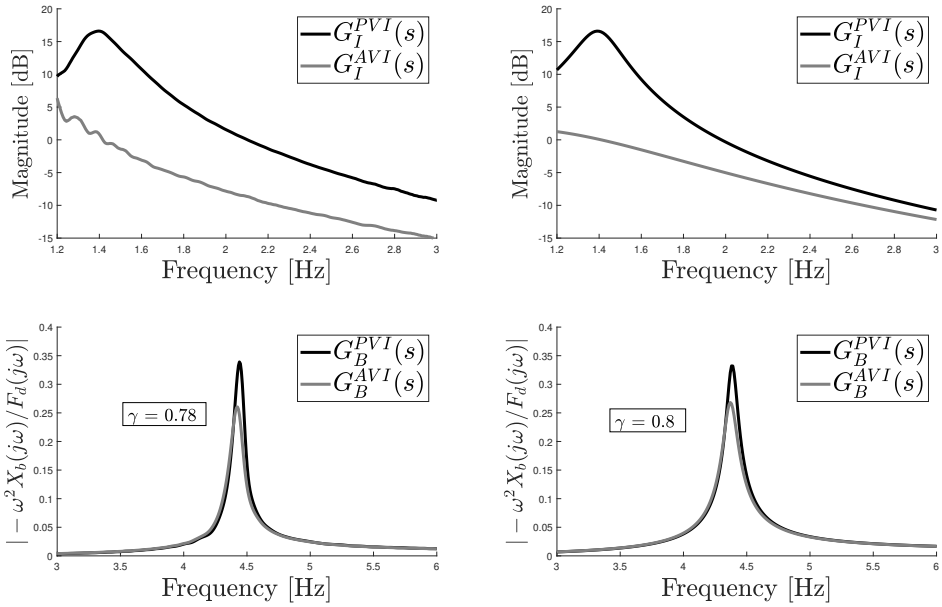


Figure 3.12: Experimental (left) and theoretical (right) results for the transmissibility functions (top row) and the FRFs of the beam TFs (bottom row) for PVI $G_{BD}^{PVI}$ and AVI $G_{BD}^{AVI}$.

active (grey line) transmissibility functions ($G_I^{PVI}(s)$, $G_I^{AVI}(s)$) are shown for both experimental (left) and numerical (right) cases. The response of the base for both strategies is shown at the bottom of the figure. For AVI control, the response in the base is reduced with respect to PVI control. This implies that, for these dynamic

parameters, the use of AVI provides improvement in terms of VI and also reduces the base acceleration. For the experimental test, the value of $\gamma$ is 0.78, whereas for the numerical simulation it is 0.80.

## 3.5 Conclusions

The problem of VI has been studied extensively in the past without considering its effect on the supporting structure. When it has been considered, the previous studies have only dealt with the effect in the VI performance. In this work, a theoretical development of the complete interaction problem has been developed.

The transmitted vibration from the isolator to light-weight, and usually lively, base structures might not always be negligible and should be carefully considered in some cases. This study has provided understanding of how the VI system might affect the base response for an active controller. This perspective grants to the problem the possibility to analyse the effect of an isolator for a range of different supporting structures. The controller used for this study is DVF. Its implementation on a generic isolator has been studied and its influence on different base structures has been illustrated using influence contour plots. Different particular cases have been analysed to show the effect in the supporting structure. Thus, the parameter $\gamma$, which shows how the base response changes with AVI control with respect to PVI control, has been chosen to determine whether the base response improves or worsens for AVI respect the PVI and by how much. The formulation has been validated against an experimental test, which was developed on a full-scale structure with appropriate sensor, controller and actuator hardware.

# Chapter 4

# Vibration isolation and alignment of multiple platforms on a non-rigid supporting structure

This chapter is based on the following published journal paper:

- Pérez-Aracil, J., Pereira, E., Aphale, S. A. and Reynolds, P. "Vibration Isolation and Alignment of Multiple Platforms on a Non-Rigid Supporting Structure". *Actuators* 9, no. 4, 2020.

## 4.1 Introduction

Many industrial and research applications require the use of multiple devices for the same task. The control objective is not just the vibration reduction of every platform, but also to maintain the alignment between the different devices. The hypothesis of a rigid base in the alignment problem of multiple isolators leads to consider the best solution, in terms of the control gains, the same as that obtained for the best vibration isolation performance: decrease of the platform movement with respect to the supporting structure. This implies that no isolator interacts with the supporting structure. As was aforementioned, this hypothesis is not valid when the supporting structure is a non-rigid system. The design of the controller

must deal with the base dynamic, in order to consider the interaction phenomenon effect on both systems: isolators and base structure.

This chapter studies how the control forces exerted by the isolation system may improve performance according to the isolation and alignment control objectives. Thus, under the hypothesis of perturbation forces exerted at the supporting structure, which lead to the mentioned above scenario 2, two designs are compared. The first one considers a rigid supporting structure with no dynamic interaction with the isolator system. In this case, the best transmissibility between the accelerations of supporting structure and sensitive equipment is always the best overall solution. The second case considers a flexible supporting structure with dynamic interaction with the isolator systems. The objective of this chapter is to highlight when the best AVI design does not correspond with the best transmissibility, showing the importance of considering this interaction.

The remainder of the chapter is as follows: it continues with the definition of the functional value used to evaluate the performance of the of the controller proposed. Section 4.3 includes illustrative results obtained with a large set of optimal AVI multiple SISO controllers designed for a large set of supporting structures and isolator systems. This large set of examples are normalised in terms of mass and frequency ratios of both systems. Finally, the main conclusions derived are presented.

## 4.2 Formulation of the vibration isolation and alignment problem

The VI framework was formulated in Chapter 2. The scenario studied here considers $n$ isolators situated on a flexible supporting structure. Thus, the acceleration of the $j^{th}$ isolator is the output of the system formulated in Equation (2.2), expressed as $Y_{I_j}(s)$ in Laplace domain. The base acceleration at the $j^{th}$ isolator location is expressed as $Y_{b_j}(s)$. The supporting structure is modelled using Equation (2.21).

To evaluate the reduction of the platform vibration and the alignment between different devices, when multiple isolators are situated on a flexible sup-

porting structure, the H-infinity norm of the FRFs, defined by $Y_{I_j}(s)/Y_{b_j}(s)$ and $(Y_{I_j}(s) - Y_{I_{j+1}}(s))/F_{d_k}(s)$ are considered. Thus, the following variables are defined: i) the transmissibility between the platform and supporting structure acceleration, defined in this work as:

$$\Lambda_T = \frac{1}{n}\sum_{j=1}^{n}\left\|\frac{Y_{I_j}(s)}{Y_{b_j}(s)}\right\|_\infty, \tag{4.1}$$

and ii) the alignment of the isolators located on the supporting structure, which is illustrated in Figure 4.1 and defined as follows:

$$\Lambda_A = \frac{1}{l(n-1)}\sum_{j=1}^{n-1}\frac{\sum_{k=1}^{l}\left\|\frac{Y_{I_j}(s)-Y_{I_{j+1}}(s)}{F_{d_k}(s)}\right\|_\infty}{L_{j,j+1}}. \tag{4.2}$$

The expression of Equation (4.2) is based on the tangent of the angle between adjacent platforms, $\tan\theta_{j,j+1}$. The angle has been considered to be small enough such that $\tan(\theta_{j,j+1}) \approx \theta_{j,j+1}$.

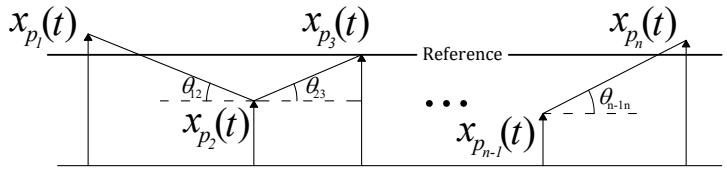


Figure 4.1: Illustration of the alignment problem.

As can be observed, both expressions are divided by the number of addends, thus the functional values can be compared independently of the number of isolators and disturbance forces applied on the supporting structure.

The design criterion based on a rigid supporting structure hypothesis considers the AVI that minimises $\Lambda_T$ defined by Equation (4.1). The design criterion based on a flexible supporting structure considers the AVI objectives defined by the combination of $\Lambda_T$ and $\Lambda_A$.

### 4.2.1 AVI control law for a SISO control system

The matrix control matrix $\boldsymbol{G}_{AVI,F}(s)$, defined for a general case in Equation (2.28), is particularised here for the SISO control system in which multiple isolators are

involved in the same task. It results:

$$\boldsymbol{G}_{AVI,F}(s) = \begin{bmatrix} C_{f_{11}}(s) & \dots & 0 \\ \vdots & \ddots & \vdots \\ 0 & \dots & C_{f_{nn}}(s) \end{bmatrix} \begin{bmatrix} k_{b_{11}} & \dots & 0 \\ \vdots & \ddots & \vdots \\ 0 & \dots & k_{b_{nn}} \end{bmatrix} = \frac{1}{s}\boldsymbol{K}_B^S, \tag{4.3}$$

where $C_{f_{jj}}(s)$ is considered in this work as a pure integrator, with the aim to emulate the behaviour of a sky-hook damper [Preumont, 2018b], in which each force $f_{a_j}(t)$ only depends on the movement of the platform. The active damping added to the isolator by the DVF increases with the absolute value of the gain $k_{b_{jj}}$. As was aforementioned, the matrix $\boldsymbol{K}_B^S$ is the control gains matrix for a SISO control technique, for either a rigid ($\boldsymbol{K}_V^S$) or a flexible ($\boldsymbol{K}_{FV}^S$) supporting structure. The DVF controller of the $j^{\text{th}}$ isolator can be expressed as:

$$\boldsymbol{G}_{AVI,F}(s)[j,j] = k_{b_{jj}}/s. \tag{4.4}$$

The matrix of the isolator system of Equation (4.3) is given by $\boldsymbol{K}_B^S = diag(k_{b_{11}}, \dots, k_{b_{nn}})$. This matrix is diagonal since a SISO control technique is used. The TF between the platform acceleration ($\ddot{x}_{p_j}$) and the base acceleration ($\ddot{x}_{b_j}$) for the $j^{\text{th}}$ isolator, and the DVF of Equation (4.4) is as follows:

$$\frac{s^2 X_{p_j}(s)}{s^2 X_{b_j}(s)} = \frac{2\zeta_{p_j}\omega_{p_j}s + \omega_{p_j}^2}{s^2 + 2\zeta_{p_j}\omega_{p_j}s + \omega_{p_j}^2 - (k_{b_{jj}}/m_{p_j})s}. \tag{4.5}$$

Note that the value of $\zeta_{p_j}$ should be small enough to guarantee a -40 dB/dec attenuation in first part of the rejected band. For example, if the value of $\zeta_{p_j}$ is equal to 0.01, there is a -40 dB/dec attenuation between $\omega_{p_j}$ and $50\omega_{p_j}$ (i.e., the zero is placed at $-50\omega_{p_j}$). The objective of Equation (4.5) is to increase the damping of the poles, reducing the peak response. The value of this closed-loop damping, denoted in this work as $\zeta_{p_j}^{AVI}$, is obtained with following equation:

$$\zeta_{p_j}^{AVI} = \zeta_{p_j} - \frac{k_{b_{jj}}}{2m_{p_j}\omega_{p_j}}. \tag{4.6}$$

## 4.3 Application example

In this section, the analysis of the VI and the alignment problem is particularised to the case of three isolators placed on a simply supported beam. The numerical results illustrate when the dynamics of the supporting structure must be considered in the alignment problem (i.e. the combination of $\Lambda_T$ and $\Lambda_A$). This section is divided into: i) system dynamics, ii) design criterion and iii) numerical examples for symmetrical and non-symmetrical configurations of the three isolators.

### 4.3.1 System dynamics

The system can be divided into two parts: the supporting structure and the three isolators (Figure 4.2). The first is chosen to be a pinned-pinned supported beam. The material of the beam is defined by its Young's modulus ($E_x$) and its density ($\rho$). The geometrical properties of the beam are defined such that the inertia of the cross-section with respect to the horizontal axis is $I_x$, and the length between the supports is $L_b$.

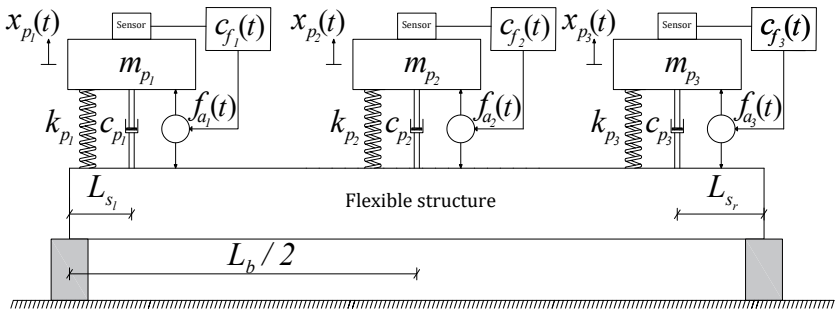


Figure 4.2: Illustration of three isolators situated on a flexible beam support.

The $q^{\text{th}}$ mode shape of the beam can be expressed as [Chopra, 2011]:

$$\phi_{b_q}(x) = C_1 \sin \frac{q\pi x}{L_b} \tag{4.7}$$

in which $C_1$ is a constant that has been chosen to be unity. The frequency of the

$q^{\text{th}}$ mode can be expressed as:

$$\omega_{b_q} = \left(\frac{q\pi}{L_b}\right)^2 \sqrt{\frac{E_x I_x}{M_l}} \tag{4.8}$$

in which $M_l$ is the mass per unit length of the beam. The relationship between the vibration modal frequencies can be defined by considering Equation (4.8) as: $\omega_{b_q} = \omega_{b_1} \cdot q^2$, in which $1 \leq q \leq m$.

The variables $L_{s_l}$ and $L_{s_r}$ are the distances from the end isolators with respect to the left and right supports, respectively, and they correspond with the location of the isolators $j = 1$ and $j = 3$, respectively. The isolator $j = 2$ has been considered to be at the mid-span of the beam structure for the symmetrical and non-symmetrical cases. The distances used for the functional are $L_{12} = L_b/2 - L_{s_l}$ and $L_{23} = L_b/2 - L_{s_r}$.

The state-space representation proposed in Equation (2.21) is used to model the supporting structure, in which: i) the number of modes considered is $m = 3$, ii) the number of inputs of the isolator system (i.e. the number of outputs of the supporting structure) is $n = 3$, iii) the disturbance forces are considered to be at the isolator locations ($l = 3$) or one force located at $L_b/4$ from the left support, which can excite all the considered vibration modes ($l = 1$) and iv) the damping is assumed to be constant for all modes, with a value of $\zeta_{b_q} = 0.005$, in which $1 \leq q \leq 3$.

The three isolators are considered to have the same dynamic properties (i.e. the values of $m_{p_j}$, $\omega_{p_j}$ and $\zeta_{p_j}$ are the same for $j = 1, 2, 3$). The values of the masses and natural frequencies are defined with respect to the supporting structure model as follows:

$$m_{p_j} = r_m M_m, \tag{4.9}$$

$$\omega_{p_j} = r_\omega \omega_{b_1}, \tag{4.10}$$

where $r_m$ is the ratio between the isolator mass and the beam modal mass, which is defined as $M_m = M_l L_b/2$, and $r_\omega$ is the ratio between natural frequency of the isolator and the first vibration mode of the beam. The simulations have been developed

considering $\zeta_{p_1} = \zeta_{p_2} = \zeta_{p_3} = 0.01$.

### 4.3.2 Design criterion

The design criterion is based on finding the optimal gains values $k_{v_{11}}$, $k_{v_{22}}$ and $k_{v_{33}}$ for each pair of values $r_m$ and $r_\omega$ in order to minimise the following functional:

$$f_{fv}(\boldsymbol{K}_B^C, r_m, r_\omega) = \alpha\Lambda_T(\boldsymbol{K}_B^C, r_m, r_\omega) + \beta M_m L_b \Lambda_A(\boldsymbol{K}_B^C, r_m, r_\omega), \tag{4.11}$$

In this case, $\boldsymbol{K}_B^C = \boldsymbol{K}_B^S$. The parameters $\alpha$ and $\beta$ balance the importance of vibration level reduction for every platform, which is defined by $\Lambda_T$, and the relative alignment between the isolators, which is defined by $\Lambda_A$. In this particular example, these parameters are considered as $\alpha = \beta = 0.5$. Note that: i) the function $\Lambda_T$ depends on $\boldsymbol{K}_B^S$, $r_m$, and $r_\omega$ and ii) the function $\Lambda_A$ is scaled by $M_m L_b$ in order to make $f_{fv}$ independent of the flexible beam, depending only on $\boldsymbol{K}_B^S$, $r_m$ and $r_\omega$. Thus, the conclusions can be generalised to any simply supported beam where such configurations of isolator systems are used, simplifying a future experimental validation.

Firstly, if the rigid case is considered, the minimisation of the functional value $f_{fv}$ is simplified to the minimisation of $\Lambda_T$. Thus, the optimal value of $\boldsymbol{K}_V^S$ must be as large as possible. In order to limit this value, this work considers that the maximum damping in this numerical example is one. Thus, the gain $k_{b_{jj}}$ obtained for this damping value, which is denoted as $\hat{k}_{v_{jj}}$, is calculated as follows:

$$\hat{k}_{v_{jj}} = -2(1 - \zeta_{p_j}) m_{p_j} \omega_{p_j}, \tag{4.12}$$

where the optimal matrix for the rigid case is defined as $\hat{\boldsymbol{K}}_V^S$. Secondly, the flexible supporting structure is also considered in order to minimise Equation (4.11). The optimal value of $\boldsymbol{K}_B^S$ is denoted as $\hat{\boldsymbol{K}}_{FV}^S$. Thus, the differences in $f_{f_v}(\hat{\boldsymbol{K}}_V^S)/f_{f_v}(\hat{\boldsymbol{K}}_{FV}^S)$, which must be greater or equal to one, and $\hat{\boldsymbol{K}}_V^S/\hat{\boldsymbol{K}}_{FV}^S$, where each component must be also be greater than or equal to one, are useful to illustrate and quantify the in-

teraction between the supporting structure and isolator system in terms of isolation and alignment objectives. Note that the damping of the transmissibility for $\hat{\boldsymbol{K}}^S_{FV}$ will be always less than or equal to that obtained with $\hat{\boldsymbol{K}}^S_V$, showing that a worse transmissibility may improve the alignment objective.

### 4.3.3 Numerical results

Since the functional $f_{fv}(\boldsymbol{K}^S_B, r_m, r_\omega)$ does not depend on $M_m$ and $L_b$, the values of $M_m$ and $L_b$ can be assumed as unity for the pinned-pinned supported beam. The interval ratios for $r_m$ and $r_\omega$ are defined in the Table 3.1. The value of each $k_{v_{jj}}$ (i.e., the control gain considering a rigid supporting structure) must be between zero and $\hat{k}_{v_{jj}}$.

| $r_m$ | $r_\omega$ |
|---|---|
| $[1 \cdot 10^{-4}, 1.5]$ | $[0.1, 1.5]$ |

Table 4.1: Mass ratios $r_m$ and frequency ratios $r_\omega$ used in the numerical experiment.

Two examples are presented: i) a symmetrical case with $L_{s_l} = L_{s_r} = L_b/4$ ($L_{12} = L_{23} = L_b/4$) and ii) a non-symmetrical case with $L_{s_l} = L_b/4$ and $L_{s_r} = L_b/6$ ($L_{12} = L_b/4$ and $L_{23} = L_b/3$). In addition, two scenarios are independently studied in order to compare the effect of disturbance force location. The first one considers a single disturbance force applied at $L_b/4$. The second considers three disturbances forces applied at the isolator locations. The optimal control gains for each case have been obtained using the Nelder-Mead simplex algorithm [Lagarias et al., 1998] with boundary conditions [D'Errico, 2020]. The maximum number of iterations has been chosen to be 2000, and a tolerance on convergence of $10^{-6}$. Additionally, the stability of the overall system defined in Equations (2.5), (2.22) and (2.25) is verified. Thus, if there are positive real poles, the functional defined in Equation (4.11) is penalised and all unstable solutions are discarded.

With the aim of showcasing the effect of uncertainty in isolator dynamics on the VI and alignment performance, a robustness analysis has been conducted. The single force disturbance input case is analysed for symmetrical and non-symmetrical

scenarios, considering variations of 5% and 10% in the dynamic properties $\zeta_{p_2}, \omega_{p_2}$, of the mid-span isolator.

**Symmetrical case:** $L_{12} = L_{23} = L_b/4$

A comparison of the functional $f_{fv}(\boldsymbol{K}_B^S)$ for both optimal control gains $\hat{\boldsymbol{K}}_V^S, \hat{\boldsymbol{K}}_{FV}^S$ is shown in Figure 4.3. Figure 4.3a shows the case of a single disturbance force, which is applied at $L_b/4$ from the left support, and Figure 4.3b show the three disturbance forces applied at the isolator locations.

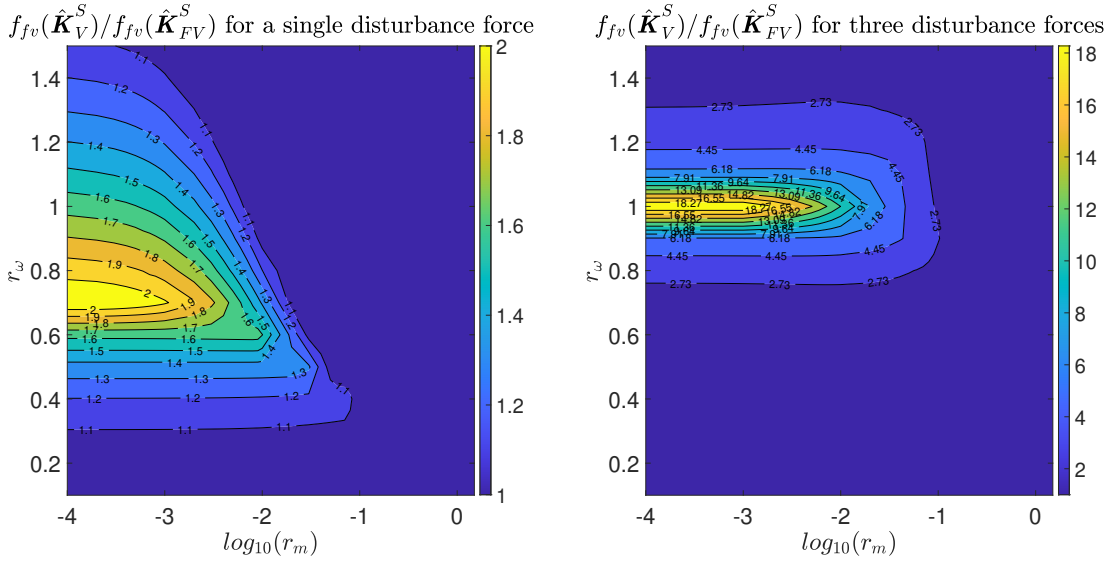


(a) (b)

Figure 4.3: Ratio $f_{fv}(\hat{\boldsymbol{K}}_V^S)/f_{fv}(\hat{\boldsymbol{K}}_{FV}^S)$ for (a) a single disturbance force and (b) three disturbance forces for the symmetrical case.

The influence of the frequency ratio $r_\omega$ is much higher than the influence of the mass ratio $r_m$ for the scenario of a single disturbance force. The highest influence region is located in the are defined by $r_\omega \to 0.8$ and low mass ratios. The use of $\hat{\boldsymbol{K}}_V^S$ may imply an increment of two times the value of $f_{fv}(\hat{\boldsymbol{K}}_V^S)$ with respect to the use of $\hat{\boldsymbol{K}}_{FV}^S$. It is important to note that, for most of the domain analysed here, the influence of the dynamics of the supporting structure on the functional value is high. This influence starts to be significant from $r_m \leq 0.1$. In addition, the interval for $r_\omega$ is between 0.3 and 1.5, when $r_m = 10^{-4}$, where the functional varies from 9 % to 200 %

Before analysing the case of three disturbance forces applied at the isolator

locations, it should be noted that the total effect of the force applied at isolators 1 and 3 is null and the force applied at isolator 2 does not excite the second mode. Thus, the second mode of the flexible support does not affect to Equation (4.11). Therefore, the three gains of the isolators must be tuned to find a trade-off between the transmissibility and the cancellation of the first and third mode. Thus, the improvement must be more important than for a single disturbance force, which excites the three vibration modes. This is evidenced in Figure 4.3b, where the ratio $f_{fv}(\hat{\boldsymbol{K}}_V^S)/f_{fv}(\hat{\boldsymbol{K}}_{FV}^S)$ is shown. For most of the region, the use of $\hat{\boldsymbol{K}}_V^S$ implies an increment of the functional value two times higher than the use of $\hat{\boldsymbol{K}}_{FV}^S$. Also, if the frequency of the isolators are similar to the first natural frequency of the supporting structure, the influence of the base dynamic on the functional value is higher, reaching an increment of nineteen times higher if $\hat{\boldsymbol{K}}_V^S$ is used. Note that this increment shows that the isolators are working as tuned mass dampers tuned to the resonant frequency of the first vibration mode of the base supporting structure. The difference between an isolator system optimally tuned to damp the first vibration mode respect to other tuned to minimise $\Lambda_T$, with $\zeta_{p_j}^{AVI} = 1$, is more significant for low values of $r_m$. This justifies that the maximum difference occurs for $r_m = 10^{-4}$.

The functional value $f_{fv}(\boldsymbol{K}_B^S)$ is determined by the control gains. It must be highlighted that, for most of the domain analysed in this work, the optimal control gain found is not the one that implies maximum damping ($\zeta_{p_j}^{AVI} = 1$). Figure 4.4a shows the ratio $\hat{k}_{v_{11}}/\hat{k}_{fv_{11}}$ when a single disturbance force is applied, while Figure 4.4b shows the same ratio when three disturbance forces are applied. In both scenarios, the highest gain reduction region is almost coincident with the highest influence region of $f_{f_v}(\hat{\boldsymbol{K}}_V^S)/f_{f_v}(\hat{\boldsymbol{K}}_{FV}^S)$. Hence, the compromise between alignment and VI is shown, since considerable reductions in $\Lambda_A$ are achieved with values of $\zeta_{p_j}^{AVI}$ less than one.

Next, the impulse responses of $(y_{I_1}(t) - y_{I_2}(t))$ are compared for three particular cases of $r_\omega$ and $r_m$, to illustrate the importance of considering the supporting structure dynamics in the control design problem.

For the cases $r_m = 0.01$, $r_\omega = 0.3$, which are shown in Figures 4.5a and 4.5d,

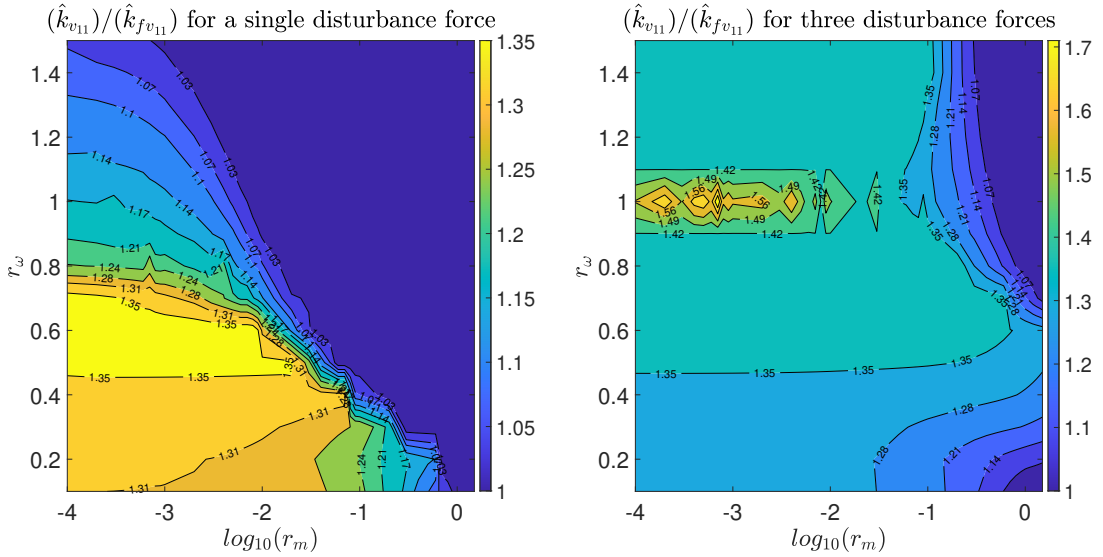


Figure 4.4: Ratio $\hat{k}_{v_{11}}/\hat{k}_{fv_{11}}$ for (a) a single disturbance force and (b) three disturbance forces for the symmetrical case.

the ratios $f_{fv}(\hat{\boldsymbol{K}}_V^S)/f_{fv}(\hat{\boldsymbol{K}}_{FV}^S)$ are 1.08 and 1.09 for a single and three disturbance inputs, respectively. A small improvement in the temporal responses can be seen in these figures.

For the cases $r_m = 0.001$, $r_\omega = 0.5$, which are shown in Figures 4.5b and 4.5e (middle), the ratios $f_{fv}(\hat{\boldsymbol{K}}_V^S)/f_{fv}(\hat{\boldsymbol{K}}_{FV}^S)$ are 1.34 and 1.37 for a single and three disturbance inputs, respectively. An appreciable change in the time response can be observed in these temporal responses.

For the cases $r_m = 0.0001$, $r_\omega = 0.9$, which are shown in Figures 4.5c and 4.5f (right), the ratios $f_{fv}(\hat{\boldsymbol{K}}_V^S)/f_{fv}(\hat{\boldsymbol{K}}_{FV}^S)$ are 1.78 and 6.34 for a single and three disturbance inputs, respectively. A high influence of the supporting structure dynamic into the time response can be seen. Note the considerable reduction for the scenario with three disturbance inputs.

Finally, it should be noted that there are two effects. The first one is associated with the level of vibration, which depends mainly on the synchronisation of isolators 1 and 2 and their transmissibility. In this case, the response of $(y_{I_1}(t) - y_{I_2}(t))$ is reduced in amplitude but its settling time is not significantly changed (i.e. the damping imparted to the vibration modes is not significant). For example, in Figure 4.5 (mid-column) the setting time is slightly increased but the amplitude is reduced.

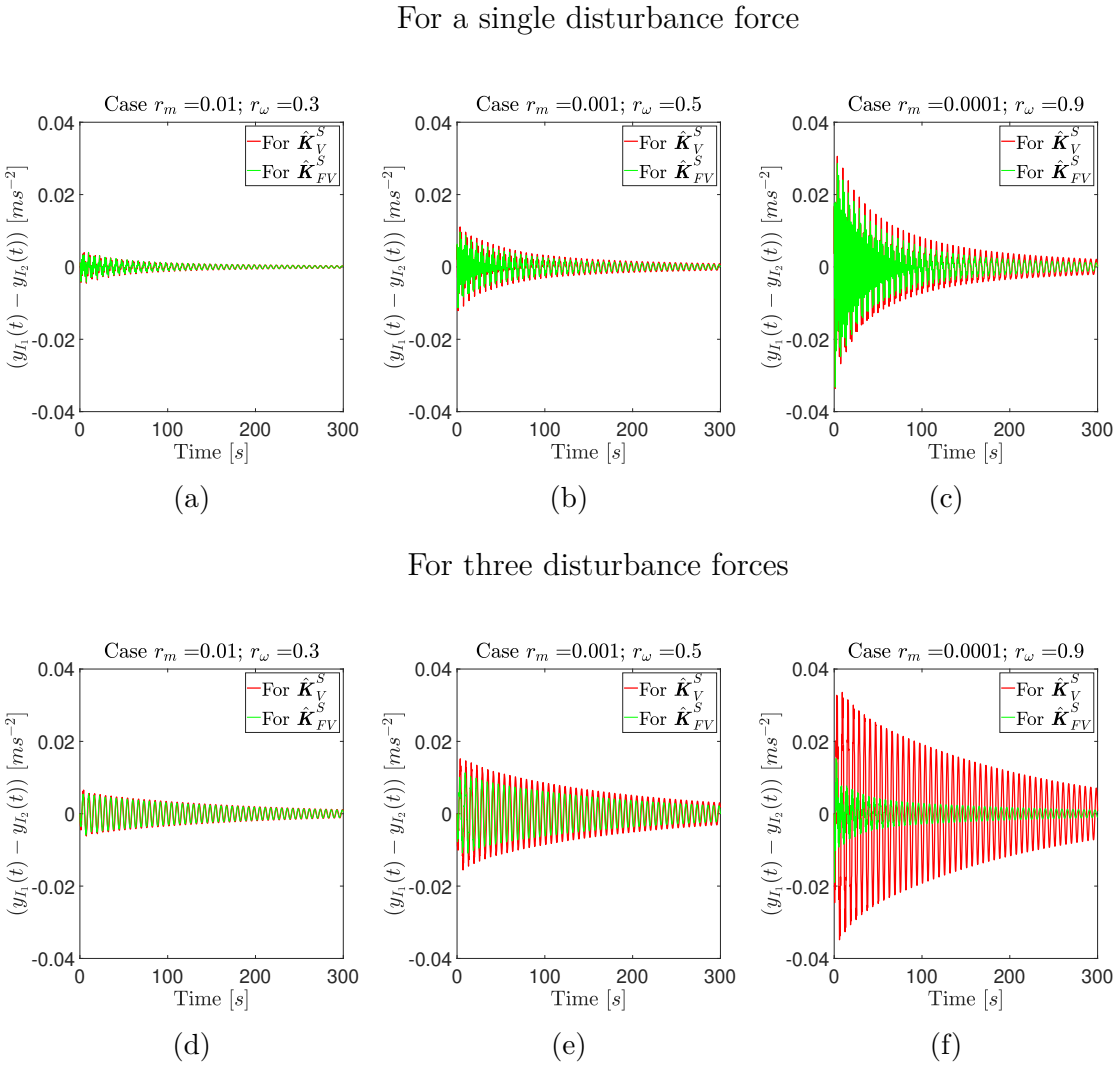


Figure 4.5: Impulse responses for three particular cases: (a) and (d) ($r_m = 0.01, r_\omega = 0.3$) (b) and (e) ($r_m = 0.001, r_\omega = 0.5$) (middle) (c) and (f) ($r_m = 0.0001, r_\omega = 0.9$) (right), for (top row) a single disturbance input and (bottom row) three disturbance inputs for the symmetrical case.

The second one is associated with the damping imparted to the supporting structure, which reduces the settling time of the response $(y_{I_1}(t) - y_{I_2}(t))$. This can be clearly seen in 4.5 (right-column), as was explained in Figure 4.3b comments. Therefore, these behaviours, which depend on the interaction between the isolator system and the supporting structure, are not obvious and must be considered when a dual VI and alignment problem is being examined.

**Non-symmetrical case: $L_{12} = L_b/4$ and $L_{23} = L_b/3$**

In this subsection, the case in which the end isolators are located asymmetrically with respect to the mid-span isolator is studied. The distances have been defined to be at the maximum amplitude location for the three first vibration modes, i.e. $L_{s_l} = L_b/4$, $L_{s_r} = L_b/6$. The objective of including this case is to show how the position of the isolators in the supporting structure can also affect the task performance. Note that the contribution of the disturbance forces and the isolators to the vibration modes of the base supporting structure are different respect to the symmetrical case.

The influence of the supporting structure dynamics on the functional $f_{fv}(\boldsymbol{K}_B^S)$ is analysed for a single disturbance force applied at $L_b/4$ (Figure 4.6a). In this case, the first difference observed with respect to the symmetric all case is the change in the highest influence region, which is observed for $r_\omega \to 0.9$. The influence of mass ratios seems to be slightly higher than for the symmetrical case. Also, the maximum value of the functional ratio $f_{fv}(\hat{\boldsymbol{K}}_V^S)/f_{fv}(\hat{\boldsymbol{K}}_{FV}^S)$ is greater than in the symmetrical case.

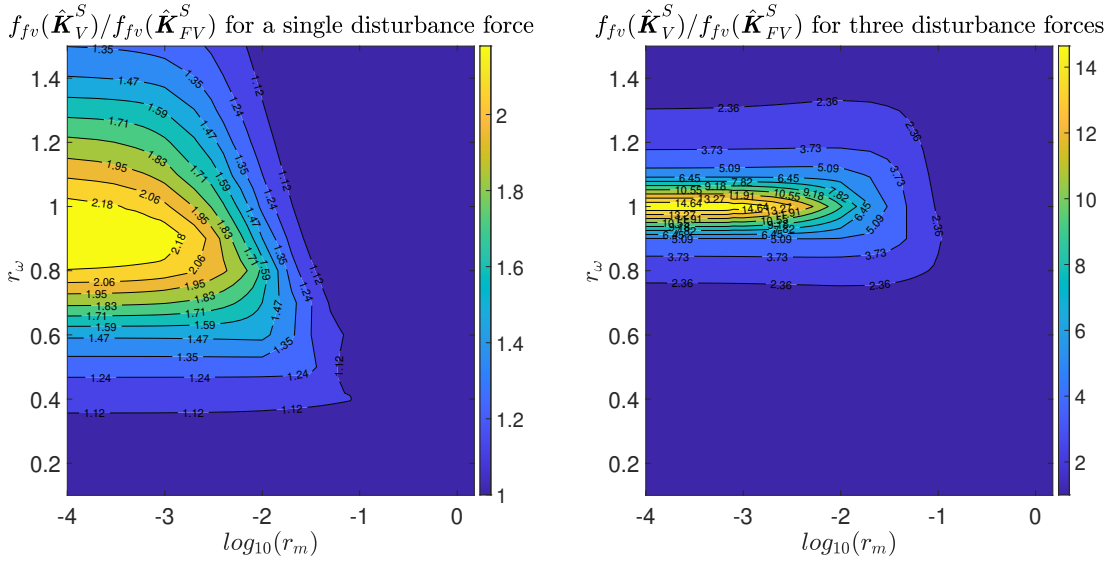


Figure 4.6: Ratio $f_{fv}(\hat{\boldsymbol{K}}_V^S)/f_{fv}(\hat{\boldsymbol{K}}_{FV}^S)$ for (a) a single disturbance force and (b) three disturbance forces for the non-symmetrical case.

In this case, the three disturbance forces can excite the three vibration modes. However, the forces applied to $L_{s_l}$ and $L_{s_r}$ do not excite the second vibration mode

significantly in comparison with the first and the third vibration modes. Thus, its contribution is not significant in Equation (4.11). In addition the contribution to the third vibration mode is more significant in Equation (4.11), with respect to the symmetrical case. Thus, the improvement in the ratio $f_{fv}(\hat{\boldsymbol{K}}_V^S)/f_{fv}(\hat{\boldsymbol{K}}_{FV}^S)$ is less important in this example, as shown in Figure 4.6b. Note also that the maximum influence region is similar to that of the symmetrical case. The highest ratio values of $f_{fv}(\hat{\boldsymbol{K}}_V^S)/f_{fv}(\hat{\boldsymbol{K}}_{FV}^S)$ are lower than for the symmetrical case.

Another difference with respect to symmetrical case is that both end isolators ($j = 1$ and $j = 3$) have different optimal control gains, since their locations with respect to the mid-span isolator are different. The comparisons between $\hat{k}_{fv_{11}}$ and $\hat{k}_{v_{11}}$ and between $\hat{k}_{fv_{33}}$ and $\hat{k}_{v_{33}}$ are shown in Figures 4.7a and 4.7b for one disturbance force scenario. For the left isolator, ($j = 1$), the optimal gain value $\hat{k}_{fv_{11}}$ can be reduced more than 1.40 times the gain value $\hat{k}_{v_{11}}$. For the right isolator, the optimal control gain considering the supporting structure dynamic $\hat{k}_{fv_{33}}$ may be reduced more than 1.90 times the gain value $\hat{k}_{v_{33}}$. In both cases, a considerably reduction of the damping ratio is achieved. The same comparisons for the three disturbance forces scenario is shown in Figures 4.7c and 4.7d. It is observed that the influence of the mass ratio is much higher than for a single disturbance force. For the left isolator, the optimal control gain $\hat{k}_{fv_{11}}$ can be even 1.60 lower than $\hat{k}_{v_{11}}$. For the right isolator, the ratio $\hat{k}_{fv_{33}}/\hat{k}_{v_{33}}$ can be higher than 2.

The same strategy of examining impulse response functions of the tangent is followed here to demonstrate the beneficial effect of using the optimal control gain $\hat{\boldsymbol{K}}_{FV}^S$ for the alignment problem. The same pairs $(r_m, r_\omega)$ were used in the symmetrical case are analysed here.

For the case $r_m = 0.01$, $r_\omega = 0.3$, the relative alignment between left and mid-span isolators is observed in an impulse response in Figure 4.8. For this case, the influence of the supporting structure is not very high, with $f_{fv}(\hat{\boldsymbol{K}}_V)/f_{fv}(\hat{\boldsymbol{K}}_{FV}^S) = 1.06$ for one disturbance input and $f_{fv}(\hat{\boldsymbol{K}}_V^S)/f_{fv}(\hat{\boldsymbol{K}}_{FV}) = 1.07$ when three disturbances inputs are applied. However, it is observed in both temporal responses (Figures 4.8a and 4.8d ) that the use of $\hat{\boldsymbol{K}}_{FV}^S$ slightly improves the alignment.

For a single disturbance force

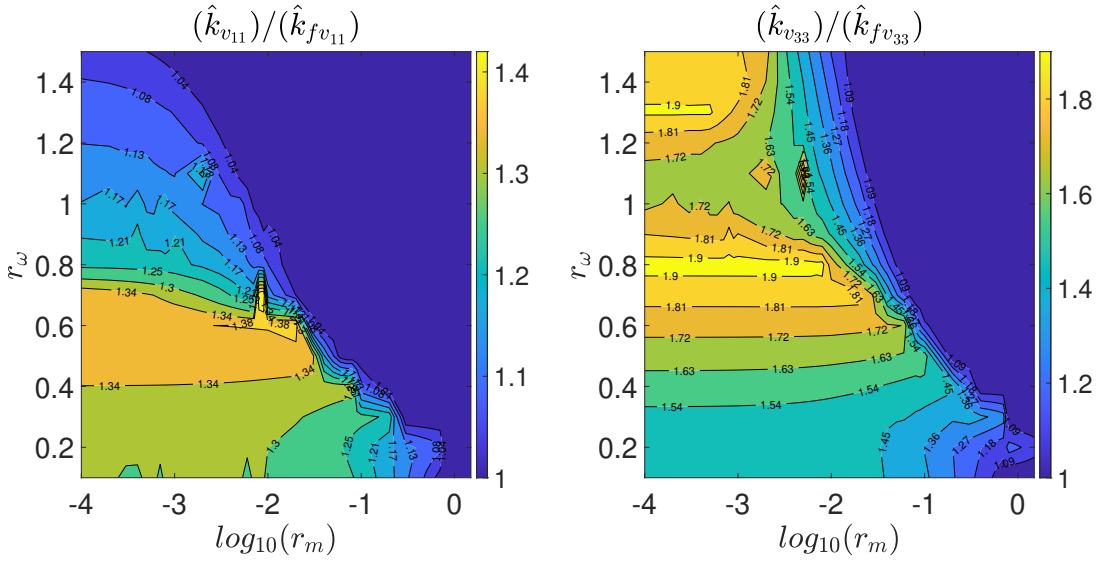


(a) (b)

For a three disturbance forces

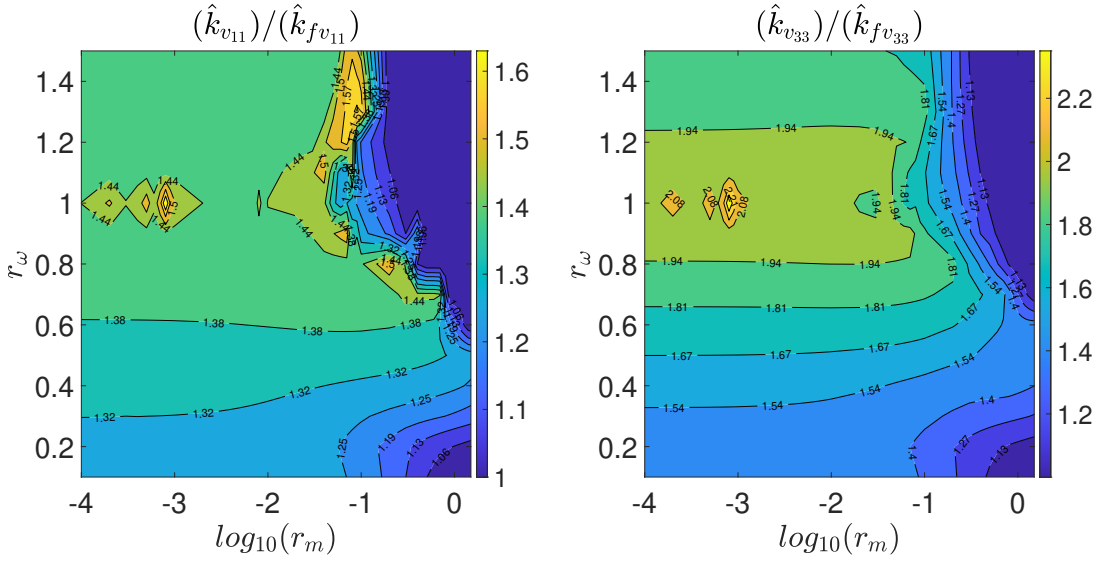


(c) (d)

Figure 4.7: Impulse responses for three particular cases: (a) and (d) ($r_m = 0.01, r_\omega = 0.3$) (b) and (e) ($r_m = 0.001, r_\omega = 0.5$) (middle) (c) and (f) ($r_m = 0.0001, r_\omega = 0.9$) (right), for (top row) a single disturbance input and (bottom row) three disturbance inputs for the symmetrical case.

For the pair $r_m = 0.001, r_\omega = 0.5$, the difference of considering $\hat{\boldsymbol{K}}_V^S$ or $\hat{\boldsymbol{K}}_{FV}^S$ is clearly highlighted in Figure 4.8b for a single disturbance force, in which the functional ratio $f_{fv}(\hat{\boldsymbol{K}}_V^S)/f_{fv}(\hat{\boldsymbol{K}}_{FV}^S)$ is equal to 1.27. If three disturbance forces are considered, this ratio is equal to 1.29, and the effect in the alignment problem is

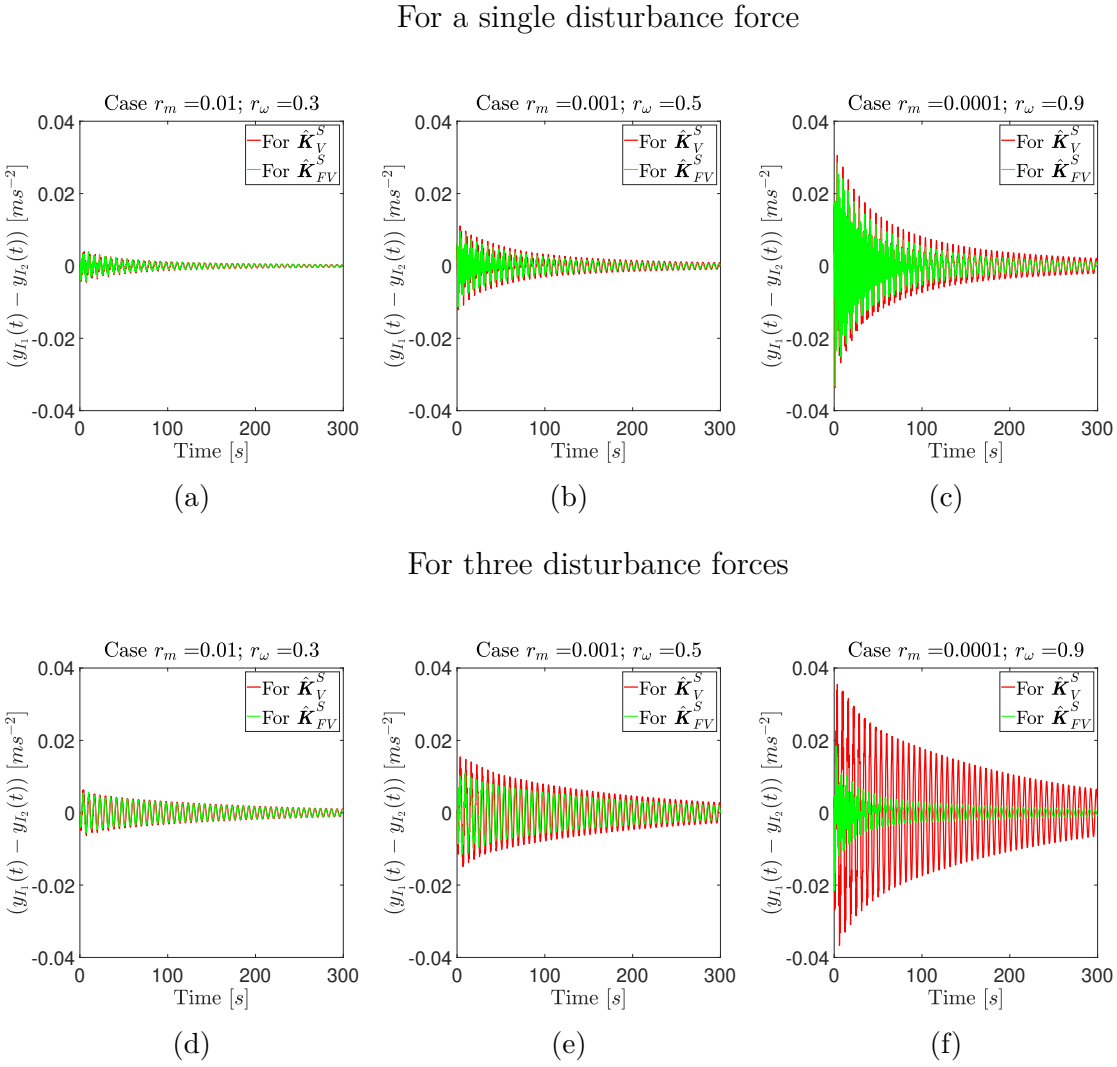


Figure 4.8: Impulse responses for three particular cases: (a) and (d) ($r_m = 0.01, r_\omega = 0.3$) (b) and (e) ($r_m = 0.001, r_\omega = 0.5$) (middle) (c) and (f) ($r_m = 0.0001, r_\omega = 0.9$) (right), for (top row) a single disturbance input and (bottom row) three disturbance inputs for the non-symmetrical case.

shown in Figure 4.8e. Note that the settling time for the three disturbances forces is higher than for the single disturbance force case.

For the pair $r_m = 0.0001, r_\omega = 0.9$, the value of $f_{fv}(\hat{\boldsymbol{K}}_V^S)/f_{fv}(\hat{\boldsymbol{K}}_{FV}^S)$ is equal to 2.38 for a single disturbance force and 5.28 for three disturbance forces. In Figure 4.8c, the alignment problem is improved for $\hat{\boldsymbol{K}}_{FV}^S$. In Figure 4.8f, the settling time is also reduced, and the consideration of the supporting structure dynamics clearly improves the functional value.

## 4.4 Conclusions

This chapter has considered the particular problem of isolation and alignment of multiple devices placed on a single flexible supporting structure. The objective is to show when the dynamic interaction between the isolators and the supporting structure is significant, with respect to this particular problem. A general formulation of the alignment and VI problem of multiple isolators has been made, where the transmissibility (i.e., VI) and the alignment are integrated in a design functional.

A particularisation of this problem, which consists of three isolators placed on a pinned-pinned supported beam, has been analysed in depth. Symmetrical and a non-symmetrical configurations of the isolators have been considered. These simple examples have highlighted the importance of considering the dynamics of the supporting structure in the control design. The main conclusions of these numerical examples are: i) the best isolator in terms of transmissibility is not the optimum when the alignment is considered, ii) the influence of the designs when the supporting structure is considered or not is more important for low mass ratios, iii) there is a trade-off between the transmissibility and the vibration cancellation of the supporting structure, iv) this trade-off also depends on how the vibration modes are excited (by the disturbance forces) and are cancelled (by the isolators), and v) the contribution of the vibration modes may produce large differences between the rigid and non-rigid hypotheses, as illustrated in the three disturbance forces cases.

Therefore, this chapter has shown that the interaction between isolators and supporting structure must be considered when the problems of transmissibility and alignment need to be solved. This interaction depends on the frequency and mass ratios and location of the isolators and disturbance forces.

# Chapter 5

# Optimal vibration isolation and alignment over non-rigid bases with the CRO-SL ensemble

This chapter is based on the following journal manuscript, which was submitted for review in December 2020:

- Pérez-Aracil, J., Camacho-Gómez, C., Reynolds, P., Pereira, E. and Salcedo-Sanz, S. "Optimal vibration isolation and alignment over non-rigid bases with the CRO-SL ensemble". *Engineering Applications and Artificial Intelligence.*

## 5.1 Introduction

This chapter discusses a similar scenario to Chapter 4. However, in this case, a MIMO control strategy is proposed. This arises from the fact that the use of MIMO control strategies leads to better solutions in AVI problems than SISO strategies [Chanan et al., 2004, Beijen et al., 2018, Song et al., 2018, Xie et al., 2018]. It is important to note that the implementation of the MIMO controller may be difficult, mainly due to the following issues: i) there must be a trade off between the objectives of VI and alignment, ii) the stability of the intrinsic feedback loop must be guaranteed and iii) the number of controller parameters should be optimally tuned.

In this chapter, the optimal control design of the MIMO active vibration controllers subjected to stability restrictions is analysed. It results in a very complex problem, which may not be solved by traditional optimization approaches. Instead of using the Nelder-Mead simplex algorithm [Lagarias et al., 1998] as in Chapter 4, in this chapter the control design parameters are obtained with the recently proposed multi-method ensemble meta-heuristic algorithm, the Coral Reefs Optimization algorithm with Substrate Layer (CRO-SL) [Salcedo-Sanz et al., 2017b, Salcedo-Sanz et al., 2016]. This has been motivated not only by the good results CRO-SL has obtained in different problems but also the difficulty in finding good solutions in the MIMO case by using Nelder-Mead simplex algorithm. The use of CRO-SL allows AVI to obtain considerable and not obvious improvements when the interaction between the isolator system and the base frame is considered. This motivates the use of this type of algorithm in this control problem. This algorithm may combine different traditional optimization algorithms. Its potential lies in that combination, which leads to better results than the individual algorithms when the work separately. This has been demonstrated in different works, such as in the design of optimal submerged arch structures [Perez-Aracil et al., 2020] or in vibration control problems. For example, in the optimal design and location of tuned mass dampers (TMDs) in structures of subjected to earthquakes excitations [Salcedo-Sanz et al., 2017a]. Another example in which CRO-SL has been satisfactorily implemented is in the design of a MIMO active vibration control (AVC) system oriented to reduce vibrations in floor structures. [Camacho-Gómez et al., 2018].

The rest of the chapter has been structured as follows: Section 5.2 shows the AVI for a MIMO controller. Section 5.3 presents an application example in which the controllers, both SISO and MIMO, and the functionals are particularized for the case of three isolators situated on pinned-pinned supported beam. Section 5.4 presents the CRO-SL algorithm, its most important characteristics and a description of the search procedures implemented in the algorithm. Section 5.5 shows an illustrative set of experiments, in which the effect of the dynamic of the supporting structure on the task performance is shown for a set of scenarios. In addition,

the improvements of considering MIMO controllers optimally tuned by CRO-SL are explained in detail. Section 5.6 shows a real experimental application. A set of verified practical guidelines, based on the experimental test shown in Chapter 4 are proposed. It is shown that considering real data, the use of the MIMO controller improves the performance of the VI and alignment problem. Finally, in Section 5.7, the conclusions derived in this chapter are presented.

## 5.2 Active vibration isolation for MIMO control

The general control matrix defined in Equation (2.28), can be expressed for this particular case as follows:

$$\boldsymbol{G}_{AVI,F}(s) = \frac{1}{s}\begin{bmatrix} k_{b_{11}} & k_{b_{12}} & k_{b_{13}} \\ k_{b_{21}} & k_{b_{22}} & k_{b_{23}} \\ k_{b_{31}} & k_{b_{32}} & k_{b_{33}} \end{bmatrix} = \frac{1}{s}\boldsymbol{K}_B^M, \tag{5.1}$$

since $C_{f_{jj}}(s) = 1/s$. The control gain $k_{b_{jr}}$ relates the active force of the $j^{th}$ actuator with the acceleration measured on $r^{th}$ isolation platform.

Three different designs are studied, which are shown in Table 5.1.

| Supporting structure type | Control technique type | Control gain matrix (Optimal) |
|---|---|---|
| Rigid | SISO | $\boldsymbol{K}_V^S$ ($\hat{\boldsymbol{K}}_V^S$) |
| Flexible | SISO | $\boldsymbol{K}_{FV}^S$ ($\hat{\boldsymbol{K}}_{FV}^S$) |
| Flexible | MIMO | $\boldsymbol{K}_{FV}^M$ ($\hat{\boldsymbol{K}}_{FV}^M$) |

Table 5.1: Relation of supporting structure and controller types, with their control gain matrices.

As it occurred in the case analysed in Chapter 4, for the rigid case, the control gains will be coincident with those which lead to the maximum damping ratio. When the dynamic of the supporting structure is considered in the analysis, it is observed how optimal control gains do not reach this value.

## 5.3 Case Study

To analyse how the MIMO control strategy can improve the response for the VI and alignment problem respect to SISO control strategy, the example of Section 4.3 is studied. The same system is considered, in which three isolators are situated on a flexible pined-pined supported beam, Figure 5.1.

The design criteria is those proposed in Equation (4.11). The functional values that will be analysed are then: i) rigid base with SISO control, $f_{fv}(\boldsymbol{K}_V^S, r_m, r_\omega)$, ii) flexible blase with SISO control, $f_{fv}(\boldsymbol{K}_{FV}^S, r_m, r_\omega)$ and iii) flexible base with MIMO control $f_{fv}(\boldsymbol{K}_{FV}^M, r_m, r_\omega)$. The weights $\alpha$ and $\beta$ have been chosen as the example of Section 4.3.3, ($\alpha = \beta = 0.5$).

The VI framework and the alignment problem have been presented in Sections 2.3 and 4.2. The case of three isolators situated on pinned-pinned supported beam is studied in detail.

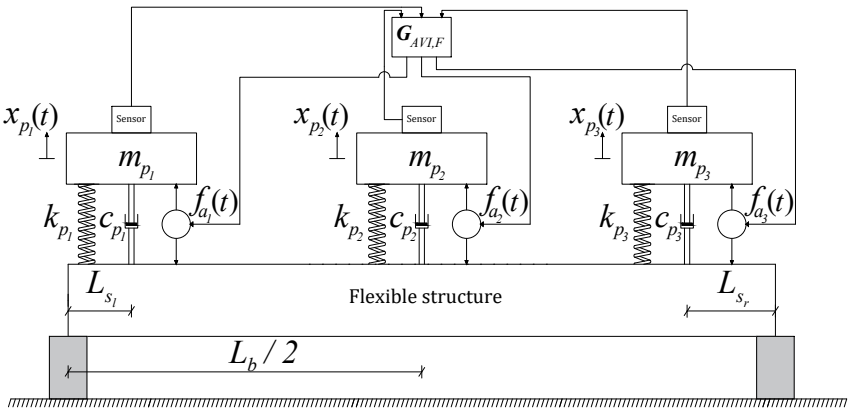


Figure 5.1: Schematic illustration of three isolators situated on a flexible supporting structure, with a MIMO controller.

## 5.4 The CRO-SL: an ensemble multi-method evolutionary algorithm

In optimization, an *ensemble* method refers to an algorithm which combines different types of other algorithms, search strategies or operators, in order to obtain high quality solutions in optimization problems [Wu et al., 2019]. In the last years, the application of ensemble approaches has increased, due to the good results obtained by these combinations of techniques, mainly in hard optimization problems. Following [Wu et al., 2019], there are different types of ensemble algorithms, but basically the literature distinguishes two main class of combinations: High-level ensembles, which are focused on selecting the best optimization algorithm for a given problem, and low-level ensembles, which refers to the optimal combination of different types of search strategies or operators within a single approach.

The Coral Reefs Optimization Algorithm with Substrate Layers (CRO-SL) is a low-level ensemble for optimization, based on evolutionary computation. The CRO-SL has been recently proposed as an advanced version of a basic original version of the CRO [Salcedo-Sanz et al., 2014a]. The CRO-SL, in turn, was first introduced in [Salcedo-Sanz et al., 2017b] to tackle a problem of total energy demand estimation. It was further developed in [Camacho-Gómez et al., 2019] for large-scale optimization problems. Since then, the CRO-SL has been successfully applied to a large number of optimization problems, including problems related to structural design and vibration cancellation [Salcedo-Sanz et al., 2017a, Camacho-Gómez et al., 2018].

In order to fully describe the CRO-SL algorithm, the basic CRO approach is first detailed. Then, the concept of *substrate*, which in this case is related to different search procedures defined within a single evolutionary population, will be described.

### 5.4.1 Basic CRO

The Coral Reef Optimization Algorithm [Salcedo-Sanz et al., 2014a, Salcedo-Sanz, 2017] is an evolutionary-type meta-heuristic, which was proposed as a kind of hybrid between Evolutionary Algorithms [Eiben and Smith, 2003]

and Simulated Annealing [Kirpatrick et al., 1983]. The CRO uses a model of a rectangular-shaped reef of size $M_\Lambda \times N_\Lambda$, ($\Lambda$), where the possible solutions to the problem at hand (corals) are set. Each space $\Lambda(i, j)$, where $i$ and $j$ are the space's coordinates, can be empty or contain a coral $\mathbf{x}_k$. The algorithm carries out a reef evolution, as follows:

1. **Initialization**: A fraction $\rho_0$ of the total reef capacity is occupied with randomly generated corals. The reef position that each coral occupies is also randomly selected.

2. **Evolution**: Once the reef has been populated the evolution process begins. This process is divided in five phases per generation:

   (a) **Sexual reproduction**: In this phase new solutions (larvae set) are created from the ones belonging to the reef in order to compete for a place in the reef. Sexual reproduction can be performed in two ways: external and internal. A percentage $F_b$ of the corals settled in the reef performs external reproduction (Broadcast spawning) and the rest of them $(1-F_b)$ reproduce themselves through internal sexual reproduction (Brooding). Both reproduction processes are performed as follows:

      i. **Broadcast spawning**: from the set of corals selected for external sexual reproduction ($F_b$), couples are set randomly so a coral can become a parent only one time per generation. Each couple generates a child (larva) which is released to the water to be placed in future stages.

      ii. **Brooding**: each one of the remaining corals $(1-F_b)$ produce a larva by means of a small perturbation and release it.

   (b) **Larvae setting**: In this step, all the larvae produced try to find a spot in the reef to grow up. A reef position is randomly chosen, and the larva will settle in that spot only in one of the following scenarios:

      i. The spot is empty.

ii. The larva has a better health function value (fitness) than the coral currently occupying that spot.

Each larva can try to settle in the reef a maximum of three times. If the larva has not been able to settle down in the reef after that number of attempts, it is discarded.

(c) **Asexual reproduction**: In this phase (also called budding) a fraction $F_{ad}$ of the corals with better fitness present in the reef duplicate themselves and, after a small mutation, are released. They will try to settle in the reef as in the previously described step.

(d) **Depredation**: Finally, each coral belonging to the $F_{dep}$ worst fraction can be predated (erased from the reef) with a low probability $P_d$.

Note that evolution process is a kind of hybrid between evolutionary algorithms and Simulated Annealing, where the empty places in the reef introduce a probability that worse solutions still count on the search. This way the algorithm secures an increasing selective pressure per generation, which makes for a more extensive search in the first generations and gradually intensifies the exploitation of certain regions of the search space. The CRO has been applied to different optimization problems with very good results [Salcedo-Sanz et al., 2014b, Yang et al., 2016, Yang et al., 2018, Yan et al., 2019].

### 5.4.2 CRO with Substrate Layers (CRO-SL)

The CRO-SL algorithm [Salcedo-Sanz et al., 2017b, Salcedo-Sanz et al., 2016] is a further evolution of the CRO approach. It proceeds basically as the basic CRO, but with a significant difference: it considers several *substrate layers* ($n_s$) of the approximately same size in the reef Figure 5.2. Each substrate, in turn, represents a particular evolution strategy or searching procedure. Thus, the CRO-SL is a multi-method ensemble algorithm [Wu et al., 2019], where several searching strategies are carried out within a single population.

According to what has been previously stated, this new approach adds a dimension to the reef $\Lambda$, so a reef position is now given by three coordinates $\Lambda(t, i, j)$,

where $t$ is the substrate index, and $i$ and $j$ have the same meaning as in basic CRO. The evolutionary process is the same as in basic CRO at a general level, but there are some substantial differences produced by the new layered reef disposition in both sexual reproduction processes and larvae placement change. The reproduction phase is performed at substrate level, although all produced larvae are released to a common reservoir. From there, at larvae placement time, each larva searches for a space to settle down in the whole reef, regardless of its original substrate, enhancing diversity in the reef and in the search process. The CRO-SL has been successfully applied to a large number of very hard optimization problems [Camacho-Gómez et al., 2019, Tsai et al., 2019, Sánchez-Montero et al., 2018, Salcedo-Sanz et al., 2019].

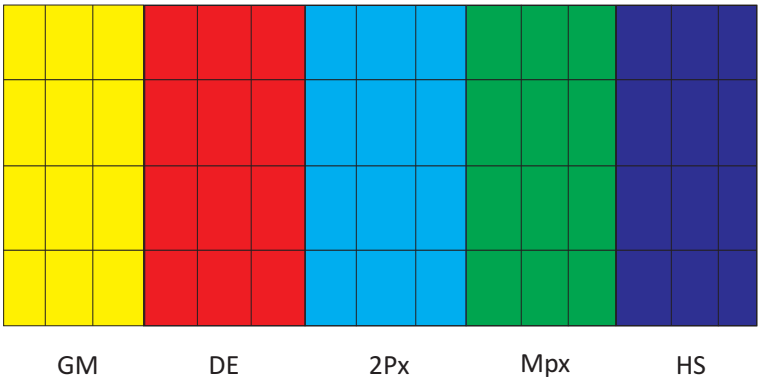


Figure 5.2: Reef in the CRO-SL example. An example where 5 different substrates stand for different search procedures applied to the problem: Gaussian Mutation (GM) (yellow); Differential Evolution (DE) (red); Two-points crossover (light blue); Multi-point crossover (green) and Harmony Search (HS) (dark blue).

### 5.4.3 Substrate layers defined in the CRO-SL

Note that very different search strategies can be defined in the CRO-SL as part of the multi-method approach. They are usually defined at the practitioner's discretion. Some of the most used traditional operators in previous applications of the CRO-SL are HS, DE, classical two-points crossover (2Px), classical multi-points crossover (MPx) and Gaussian-based mutation (GM). There have been previous works in which specific operators have been applied, such as operators based on chaotic or strange attractors [Salcedo-Sanz, 2016], or tailor-made operators for the specific problem at hand [Garcia-Hernandez et al., 2020, Bermejo et al., 2018]. In this chapter, the combination of the traditional search strategies with two operators for search

and optimization are combined. These new operators are the Firefly algorithm (FA) and the Water Wave Optimization (WWo) approach, which have been implemented satisfactorily in other optimization problems [Perez-Aracil et al., 2020]. This novel approach improves the results of the optimization in terms of the best solution can be achieved.

Then, a short definition of all the substrates considered in this chapter in the CRO-SL ensemble is provided.

1. HS: Mutation from the HS algorithm. HS [Geem et al., 2001] is a population based meta-heuristic that mimics the improvisation of a music orchestra while its composing a melody. HS controls how new larvae are generated in one of the following ways: i) with a probability HMCR$\in [0, 1]$ (Harmony Memory Considering Rate), the value of a component of the new larva is drawn uniformly from the same values of the component in the other corals. ii) with a probability PAR$\in [0, 1]$ (Pitch Adjusting Rate), subtle adjustments are applied to the values of the current larva, replaced by any of its neighbouring values (upper or lower, with equal probability).

2. DE: Mutation from DE algorithm. This operator is based on the evolutionary algorithm with the same name [Storn and Price, 1997], a method with powerful global search capabilities. DE introduces a differential mechanism for exploring the search space. Hence, new larvae are generated by perturbing the population members using vector differences of individuals. Perturbations are introduced by applying $\mathbf{x}'_i = \mathbf{x}^1_i + F(\mathbf{x}^2_i - \mathbf{x}^3_i)$ (where $F = 0.6$ determines the evolution factor weighting the perturbation amplitude) for each encoded parameter on a random basis. After this perturbation, final perturbed vector $\mathbf{x}'$ is combined with an alternative coral in the reef following a classical 2-points crossover, as defined next.

3. 2Px: Classical 2-points crossover. The crossover operator is the most classical exploration mechanism in genetic and evolutionary algorithms [Eiben and Smith, 2003]. It consists of coupling to individuals at random,

choosing two points for the crossover, and interchanging the genetic material in-between both points. In the CRO-SL, one individual to be crossed is from the 2Px substrate, whereas the couple can be chosen from any part of the reef.

4. MPx: Multi-points crossover. Similar to the 2-points crossover, but in this case a number $k$ of crossover points are selected, and a binary template decides whether parts of the individuals are interchanged.

5. GM: with a $\sigma$ value linearly decreasing during the run, from $0.2 \cdot (A_{GM} - B_{GM})$ to $0.02 \cdot (A_{GM} - B_{GM})$, where $[B_{GM}, A_{GM}]$ is the domain search. Specifically, the Gaussian probability density function is:

$$f_{G(0,\sigma^2)}(x) = \frac{1}{\sigma\sqrt{2\pi}} e^{-\frac{x^2}{2\sigma^2}}.$$

   The reason of adapting the value of $\sigma$ along the generations is to provide a stronger mutation in the beginning of the optimization, while fine tuning with smaller displacements nearing the end. The mutated larva is thus calculated as: $x'_i = x_i + \delta N_i(0,1)$, where $N_i(0,1)$ is a random number following the Gaussian distribution.

6. FA: The FA is a kind of swarm intelligence algorithm, first introduced by Yang in [Yang, 2008]. The FA is based on the flashing patterns and behaviour of fireflies in nature. The pattern movement of a firefly $i$ attracted to another (brighter) firefly $j$ is calculated as follows:

$$\mathbf{x}_i^{t+1} = \mathbf{x}_i^t + \beta_0 e^{-\gamma r_{ij}^2} (\mathbf{x}_j^t - \mathbf{x}_i^t) + \alpha_c \boldsymbol{\epsilon}_i^t \tag{5.2}$$

   where $\beta_0$ stands for the attractiveness at distance $r = 0$. The specific FA mutation implemented in the CRO-SL is a modified version of the algorithm known as Neighbourhood Attraction Firefly Algorithm (NaFa) [Wang et al., 2017]. It has been implemented as follows: when a coral (solution) in the reef belongs to the NaFa substrate, it is updated by following Equation (5.2). All the parameters of the equation are tuned during the CRO-SL evolution. The corals in the

NaFa substrate consider as swarm a neighbourhood among all the other corals in the reef (not only the NaFa substrate). Thus, the corals in the NaFa substrate are updated taking into account some solutions from other substrates, since all the corals in the reef share the same objective function (brightness for the NaFa substrate).

7. WWo: The WWo [Zheng, 2015] is a recently proposed meta-heuristic based on the phenomena of water waves, such as propagation, refraction, and breaking. Three different procedures are then defined in this algorithm: Wave propagation: at each generation of the algorithm, each wave $\mathbf{x}$ in the population is propagated, to generate another wave $\mathbf{x}'$ in the following way:

$$x'(d) = x(d) + \mathcal{U}(-1, 1) \cdot \Lambda L(d) \tag{5.3}$$

where $\mathcal{U}(-1, 1)$ is a uniformly distributed random number within the range $[-1, 1]$, $\Lambda$ stands for a wavelength associated to each wave, which will be updated in each iteration of the algorithm and $L(d)$ is the length of the $d^{th}$ dimension of the search space [Zheng, 2015] for details on these parameters. Then, wave refraction is simulated as

$$x'(d) = N\left(\frac{x^*(d) + x(d)}{2}, \frac{|x^*(d) - x(d)|}{2}\right) \tag{5.4}$$

where $x^*(d)$ is the best solution found so far, and $N(\cdot)$ is a Gaussian random number with mean $\mu$ and standard deviation $\sigma$. Finally, a wave breaking process is also simulated as

$$x'(d) = x(d) + N(0, 1) \cdot \beta_w L(d) \tag{5.5}$$

where $\beta_w$ is the breaking coefficient.

The implementation of the WWo algorithm as CRO-SL is straightforward, as any solution within the substrate is just applied the set of operators described above, with the algorithm's parameters described in [Zheng, 2015].

## 5.5 Application examples

In this section, the search of nearly-optimal control gains in a particular problem is made by using the CRO-SL.

### 5.5.1 General description

Two different scenarios are analyzed in this subsection. In the first one, the end isolators are situated at the same distance respect to the mid-span isolator, while in the second one, the distances are different. Both scenarios are analyzed using both SISO and MIMO control strategies. The functional values for the two cases are compared for the VI and alignment problem. The disturbance forces $F_{d_k}(s)$ are considered to be applied at the isolator locations.

The control gain matrix $\hat{\boldsymbol{K}}_B^C$ is found for every scenario using the CRO-SL algorithm. The parameters used in the experiments are shown in Table 5.2. These parameters have been chosen by trial and error methodology. They are based on many different experiments, which arise from vibration control and different field problems [Salcedo-Sanz et al., 2017a, Camacho-Gómez et al., 2018, Perez-Aracil et al., 2020].

In addition, the stability of the overall system defined into Equations (2.27) is checked in every step. Thus, if there are positive real poles, the functional defined into Equation (4.11) is penalised, then the result is discarded. Thus, that solution cannot be considered if the stability is not achieved. The linear time-invariant system presented in this thesis is absolutely stable if all the poles of the state matrix are in the stability region [Ogata, 2010].

The computational time to calculate the optimal control gains for each pair $(r_m, r_\omega)$ is about 8 minutes in the symmetrical and non-symmetrical cases (note that vector operations do not imply a high computational effort) considering 30 iterations. This time may differ for different value pairs $(r_m, r_\omega)$. It has been calculated using a HP® desktop computer: Intel® Core™ i3-9100 CPU, 3.60 GHz with 8.00 GB of RAM. This time can be reduced to 6 minutes for the same computer by using parallel fitness calculation. The computer has four workers (processors).

To analyse the effect that the supporting structure dynamic has on the VI and

Table 5.2: Parameters values used in the CRO-SL.

| Parameter | Description | value |
|---|---|---|
| Reef | Reef size | 100 |
| $\rho_0$ | Fraction of reef capacity initially occupied | 80% |
| $F_b$ | Frequency of broadcast spawning | 97% |
| Substrates | HS, DE, 2Px, GM, MPx, NaFa, WWo | 7 |
| $F_{ad}$ | Percentage of asexual reproduction | 5% |
| $F_{dep}$ | Fraction of corals for depredation | 5% |
| $P_d$ | Probability of depredation | 10% |
| $\alpha_c$ | Maximum number of iterations | 30 |

alignment problem, different scenarios have been studied. The different mass and frequency ratios analysed in this work are shown in Table 4.1. The process followed to calculate the optimal control gain for every scenario is shown in Figure 5.3.

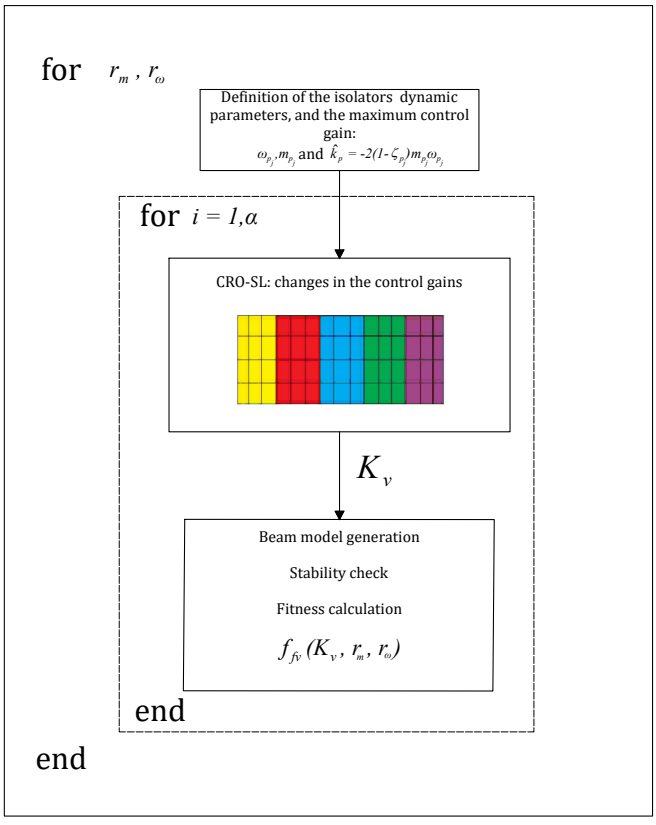


Figure 5.3: Illustrative example of the fitness calculation.

It is important to note that, for the SISO problem, the CRO-SL changes three variables in both cases, symmetrical and non-symmetrical. However, for the MIMO control strategy, the variables to be changed are five if the symmetrical case is analysed, since the gain matrix of Equation (5.1) is considered symmetrical, and for

non-symmetrical case, the number of variables is nine.

### 5.5.2 Symmetrical case

In this scenario, the end isolators are situated from the same distance respect to the mid-span isolator. This implies that $L_{12} = L_{23}$. The symmetrical conditions allows applying the next equivalences in the problem: $\hat{k}_{v_{11}} = \hat{k}_{v_{33}}$, $\hat{k}_{v_{12}} = \hat{k}_{v_{32}}$, $\hat{k}_{v_{13}} = \hat{k}_{v_{31}}$ and $\hat{k}_{v_{21}} = \hat{k}_{v_{23}}$. Thus, only five variables are changed.

It was aforementioned that, if the base is considered as a infinitely rigid system, the best control gain for the VI and alignment problem is the higher one, for the chosen controller in this work, since it leads to the higher damping ratio. However, if the base is not a rigid system, the dynamic of the platforms are coupled, and the best control gain matrix solution is not a trivial, especially if a MIMO controller is used. It can observed in Figure 5.4 a comparison of the functional values are shown. The comparison between the best solution for a rigid case ($\hat{\boldsymbol{K}}_V^S$) and the best MIMO solution for the non-rigid base ($\hat{\boldsymbol{K}}_{FV}^M$) is shown in Figure 5.4(a). In this figure can be observed the improvements obtained by considering the dynamic of the supporting structure, which can be close to 19 times around when $r_\omega$ is around one. This solution could be obvious since the isolator system can imparted damping to the base structure working as a TMD. When the value of $r_\omega$ is not close to one, the improvement is also significant. Figure 5.4(b) shows the comparison between SISO and MIMO for the non-rigid base. Note that in this figure the largest improvements are achieved when $r_\omega$ is not close to one, which means that the MIMO can considerably improves the alignment objective. This is a not obvious solution, which is the main conclusion of this numerical experiment.

In order to better illustrate the above results, system time responses are also included. The alignment objective is analyzed for three individual cases. The first one considers a high mass ratio $r_m = 0.01$, and low frequency ratio $r_\omega = 0.3$. The second scenario considers a medium mass ratio $r_m = 0.001$, and medium frequency ratio $r_\omega = 0.5$. While in the third scenario, a low mass ration and high frequency ratio are considered: $r_m = 0.0001$, $r_\omega = 0.8$. Figure 5.5 shows the three impulse

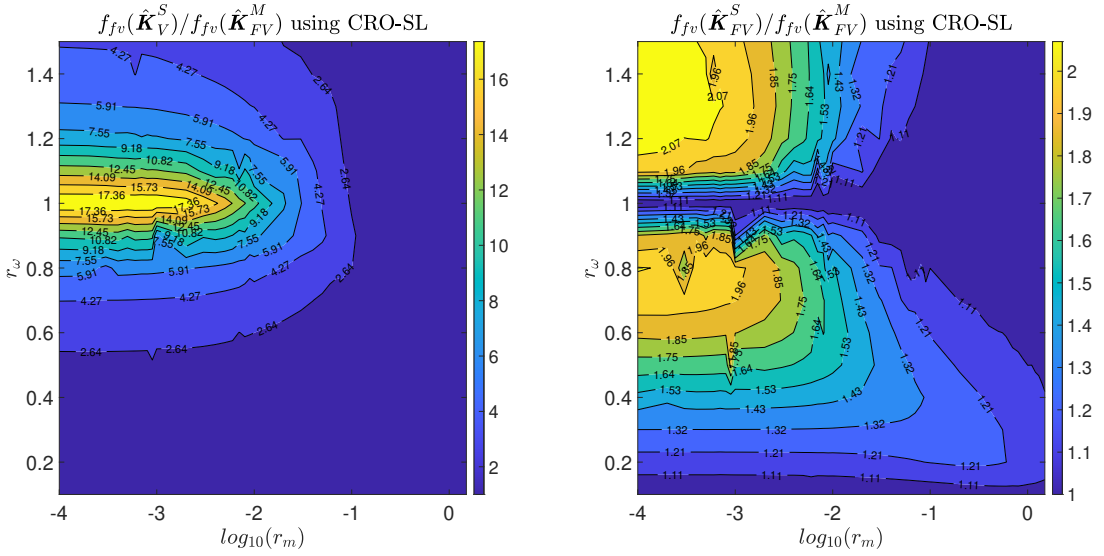


Figure 5.4: Functional ratio (a) $f_{fv}(\hat{\boldsymbol{K}}_V^S)/f_{fv}(\hat{\boldsymbol{K}}_{FV}^M)$, (b) $f_{fv}(\hat{\boldsymbol{K}}_{FV}^S)/f_{fv}(\hat{\boldsymbol{K}}_{FV}^M)$ in the symmetrical case.

responses, for the difference $(y_{I_1}(t) - y_{I_2}(t))$, when the disturbance forces are applied at the isolator locations.

For the first case, Figure 5.5a, the use of the diagonal control gain matrix $\hat{\boldsymbol{K}}_V^S$, which leads to the maximum damping ratio in every isolator, implies the worst alignment response. It can be observed that the use of the SISO control gain matrix obtained considering the supporting structure dynamics $\hat{\boldsymbol{K}}_{FV}^S$, considerably improves the response, also reducing the settle time. This improvement is even higher if the MIMO control strategy is considered, which implies to use $\hat{\boldsymbol{K}}_{FV}^M$. As was shown in Figure 5.4, the improvement of considering the dynamic of the supporting structure in the control design is even higher as the mass ration is reduced. This is shown for the second case, Figure 5.5b. In this case, the improvement of the MIMO control strategy is clearly shown. For the third case Figure 5.5c, as it occurs in the above cases, to choose the control gain matrix which leads to the highest damping ratio in every isolator $\hat{\boldsymbol{K}}_V^S$ is clearly the worst solution. However, the improvement reached for this case when $\hat{\boldsymbol{K}}_{FV}^S$ is particularly high, but even more if the MIMO control strategy is used.

Regarding the computational performance of the CRO-SL in the problem, Figure 5.6 shows the fitness evolution for the three specific scenarios considered ($r_m$ =

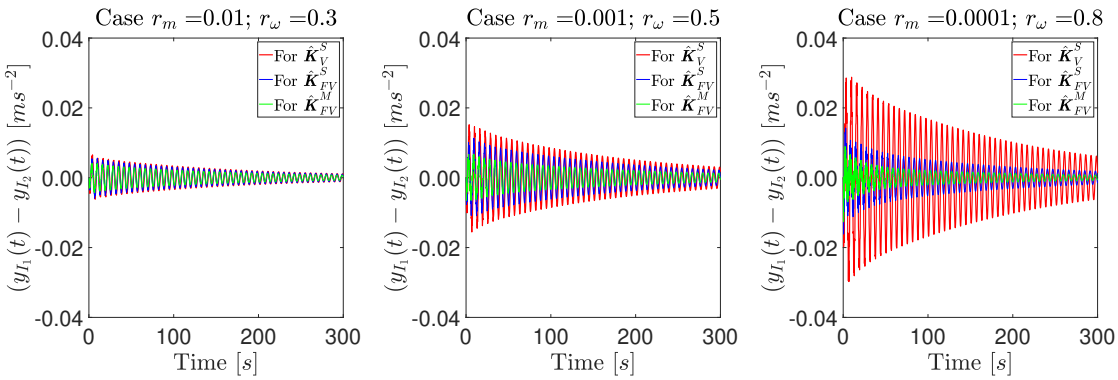


(a) (b) (c)

Figure 5.5: Impulse responses for the acceleration difference between platforms for three cases: (a) $r_m = 0.01$, $r_\omega = 0.3$ , (b) $r_m = 0.001$, $r_\omega = 0.5$ (middle) (c) $r_m = 0.0001$, $r_\omega = 0.8$ (right).

0.01, $r_\omega = 0.3$ (continuous line), $r_m = 0.001$, $r_\omega = 0.5$ (dashed line) and $r_m = 0.0001$, $r_\omega = 0.8$ (dotted line)) for MIMO, which is the most complex problem from the computational point of view. As can be seen, the CRO-SL has a similar convergence for the three scenarios, around 10 to 15 generations, with the best values of objective function (Equation (4.11)) obtained for the first one, close to the solution for the third scenario, and far way from the second scenario, which seems to be more difficult to optimize.

Figure 5.7 illustrates the importance of combining different strategies or operators (i.e., substrates). Figures 5.7 (a), (c) and (e) show the ratio of times that each substrate generates the best larva. Note that, in each iteration, only one substrate can increase this ratio and the sum of all ration must be 100%. It is interesting that the algorithm's behaviour is quite similar in all the scenarios, with slight variations on the substrate that contributes the most to the search. In the first scenario, it seem that the best substrate is the DE, but the contribution of other substrates seems significant until the end of the CRO-SL evolution, specially the FA substrate, which seems to dominate the search in the first stages of the algorithm, and the WWo which also seems to contribute in an important manner to the algorithm's evolution. In the second and third scenarios, the contribution of the DE and FA substrates is also clear, but the contribution to the search of the rest of substrates

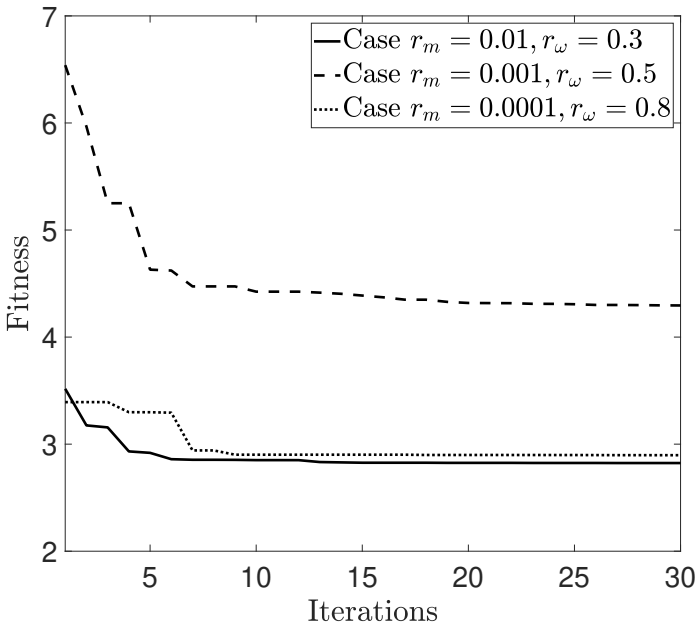


Figure 5.6: Fitness evolution in the CRO-SL for three cases: $r_m = 0.01,\ r_\omega = 0.3$ (continuous line), $r_m = 0.001,\ r_\omega = 0.5$ (dashed line) and $r_m = 0.0001,\ r_\omega = 0.8$ (dotted line), in the symmetrical case.

seems to be smaller, at least in terms of best larvae production (best solutions), though it seems that all the substrates put larvae into the reef until the end of the evolution.

Figures 5.7 (b), (d) and (f) show the number of larvae settling in the reef per substrate for the different scenarios considered. These Figures complement the information given by Figures 5.7 (a), (c) and (e). Note that when a larvae settling occurs means that the solution in this substrate is improved. Thus, the substrates with large number of larvae settling usually achieve the best larva (i.e. solution) in each iteration.

In general, this analysis shows that DE and FA substrates are the predominant ones in the CRO-SL evolution for this problem, with important contributions of other substrates which depend on the scenario considered.

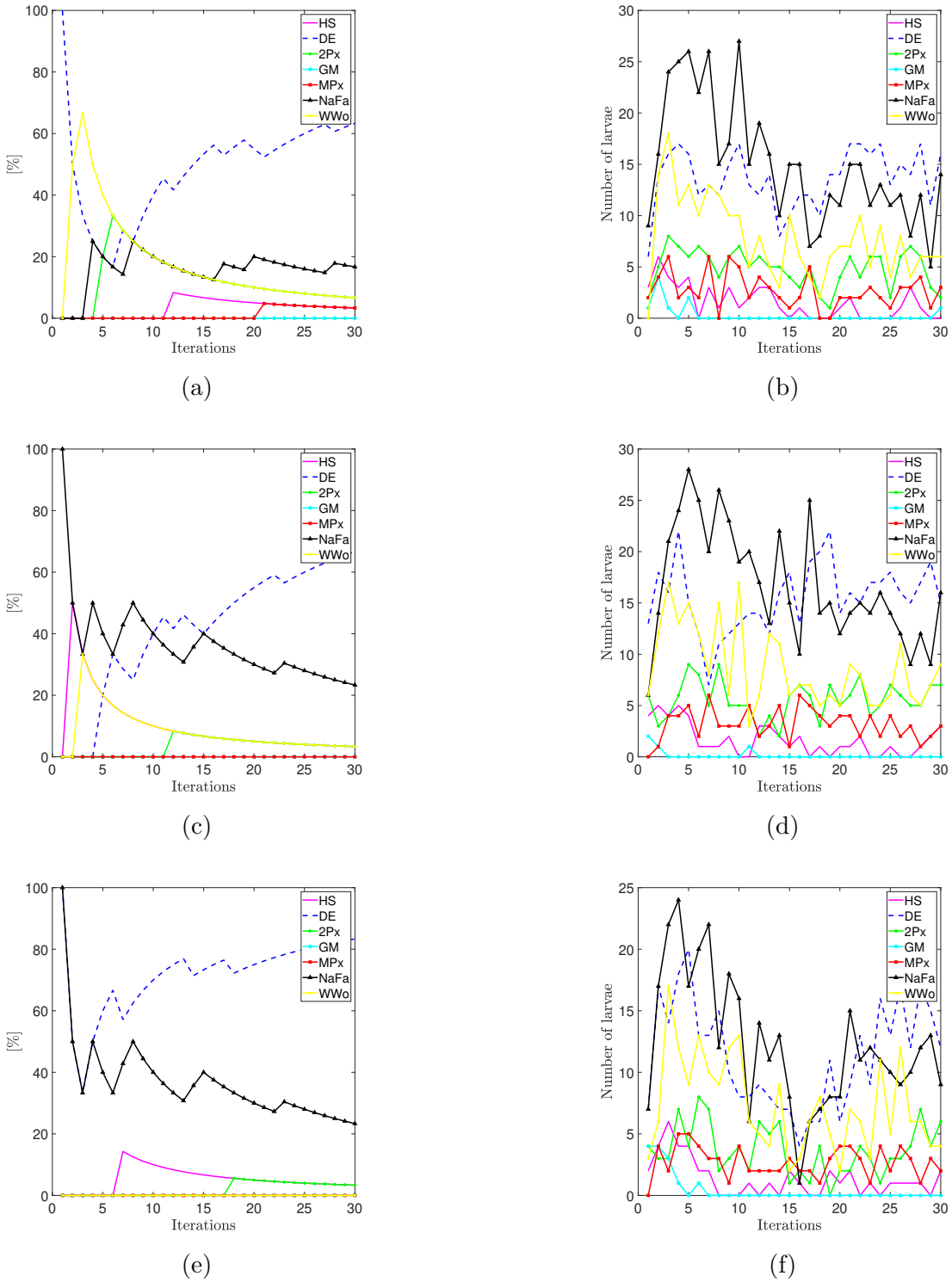


Figure 5.7: Ratio of times that each substrate generates the best larva and number of larvae settling in the reef per substrate for the different scenarios considered, in the symmetrical case; (a) Ratio of times for the best larva, Scenario 1; (b) Number of larvae into the reef, Scenario 1; (c) Ratio of times for the best larva, Scenario 2; (d) Number of larvae into the reef, Scenario 2; (e) Ratio of times for the best larva, Scenario 3; (f) Number of larvae into the reef, Scenario 3.

### 5.5.3 Non-symmetrical case

In this case, the distances between the end isolators and the mid-span isolator are different. The distances have been chosen to be $L_{12} = L_b/2 - L_b/4$, and $L_{23} = L_b/2 - L_b/6$. Hence, it is pretended to show the importance of the relative distance between the isolators, also the importance of their locations on the beam. It is important to note that the locations are coincident with the maximum modal displacement of the first, second and third modes of the beam.

As was made for the last scenario, a comparative of the functional value $f_{fv}(\boldsymbol{K}_V)$ for different control gains matrices is made. Figure 5.8a shows the ratio $f_{fv}(\boldsymbol{K}_V^S)/f_{fv}(\hat{\boldsymbol{K}}_{FV}^M)$, and the ratio $f_{fv}(\boldsymbol{K}_{FV}^S)/f_{fv}(\hat{\boldsymbol{K}}_{FV}^M)$ is shown in Figure 5.8b. An improvement of the response in the VI and relative alignment problem is reached for the whole domain compared in this work, when the MIMO control gain matrix $\hat{\boldsymbol{K}}_{FV}^M$ is used instead the matrix which leads to the maximum damping ratio for every isolator $\hat{\boldsymbol{K}}_V^S$. It can be observed, that the maximum improvement is reached for low mass ratios $r_m$ and $r_\omega$ to 1, where the use of the MIMO control strategy leads to functional values more than fourteen times lower than for the use of $\hat{\boldsymbol{K}}_V^S$. If the dynamic of the supporting structure is considered in the control design, but a MIMO control strategy is used instead of the SISO control strategy, an improvement of the response is reached for the whole domain considered in this work. Thus, although the use of a MIMO controller may imply a more difficult implementation, its use leads to better task performance. It should be highlighted that the influence of using MIMO compared with SISO in this non-symmetrical case if more significant than in the symmetrical one. Note that the maximum improvement in the non-symmetrical case is higher (close to 3.5) and the region is not uniform. This denotes that this problem is more complex from the computational point of view and the solution is less obvious.

In order to better illustrate the influence of using SISO and MIMO, considering the interaction between the base and the isolators, the same three cases that in above scenario are studied here: i) $r_m = 0.01,\ r_\omega = 0.3$, ii) $r_m = 0.001,\ r_\omega = 0.5$ and iii) $r_m = 0.0001,\ r_\omega = 0.8$. The impulse responses of the differences $(y_{I_1}(t) - y_{I_2}(t))$

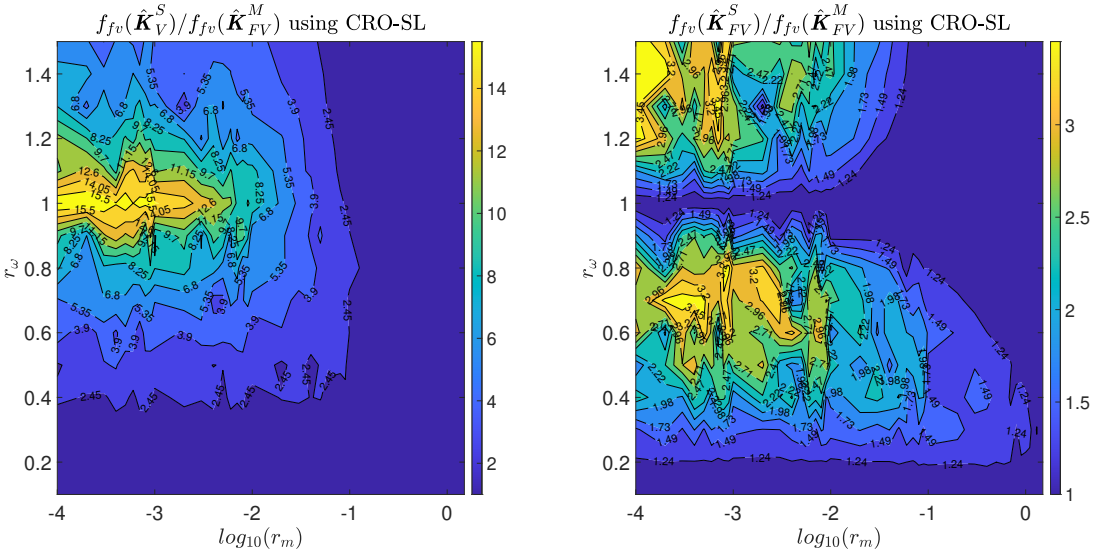


Figure 5.8: Functional ratios (a) $f_{fv}(\hat{\boldsymbol{K}}_V^S)/f_{fv}(\hat{\boldsymbol{K}}_{FV}^M)$, (b) $f_{fv}(\hat{\boldsymbol{K}}_{FV}^S)/f_{fv}(\hat{\boldsymbol{K}}_{FV}^M)$ in the non-symmetrical case.

(top row) and $(y_{I_2}(t) - y_{I_3}(t))$ (bottom row) are shown in Figure 5.9. For the first case Figures 5.9a and 5.9d it can be observed that the settle time is considerably reduced. The response for the mid-span and right-end isolators is clearly improved when the MIMO control strategy is used. w

For the second scenario Figures 5.9b and 5.9e, The alignment between the mid-span and right-end isolators is also improved for the MIMO control strategy. The same occurs for the third case Figures 5.9c and 5.9f, in which the relative alignment improved for the MIMO control strategy respect to the other solutions.

Note that a better alignment between the left and mid-span isolators are achieved. This is particularly significant when MIMO is used. This shows the importance of the isolator location in this complex problem, which must be considered when the base and the isolator are holistically designed.

As in the previous case, the discussion of results with an analysis of the computational performance of the CRO-SL in this problem is included. Figure 5.10 shows the fitness evolution for the three specific scenarios considered ($r_m = 0.01,\ r_\omega = 0.3$ (continuous line), $r_m = 0.001,\ r_\omega = 0.5$ (dashed line) and $r_m = 0.0001,\ r_\omega = 0.8$ (dotted line)) in this Non-symmetrical case. Note that in this case the best evolution in terms of objective function is obtained in the third scenario, though the

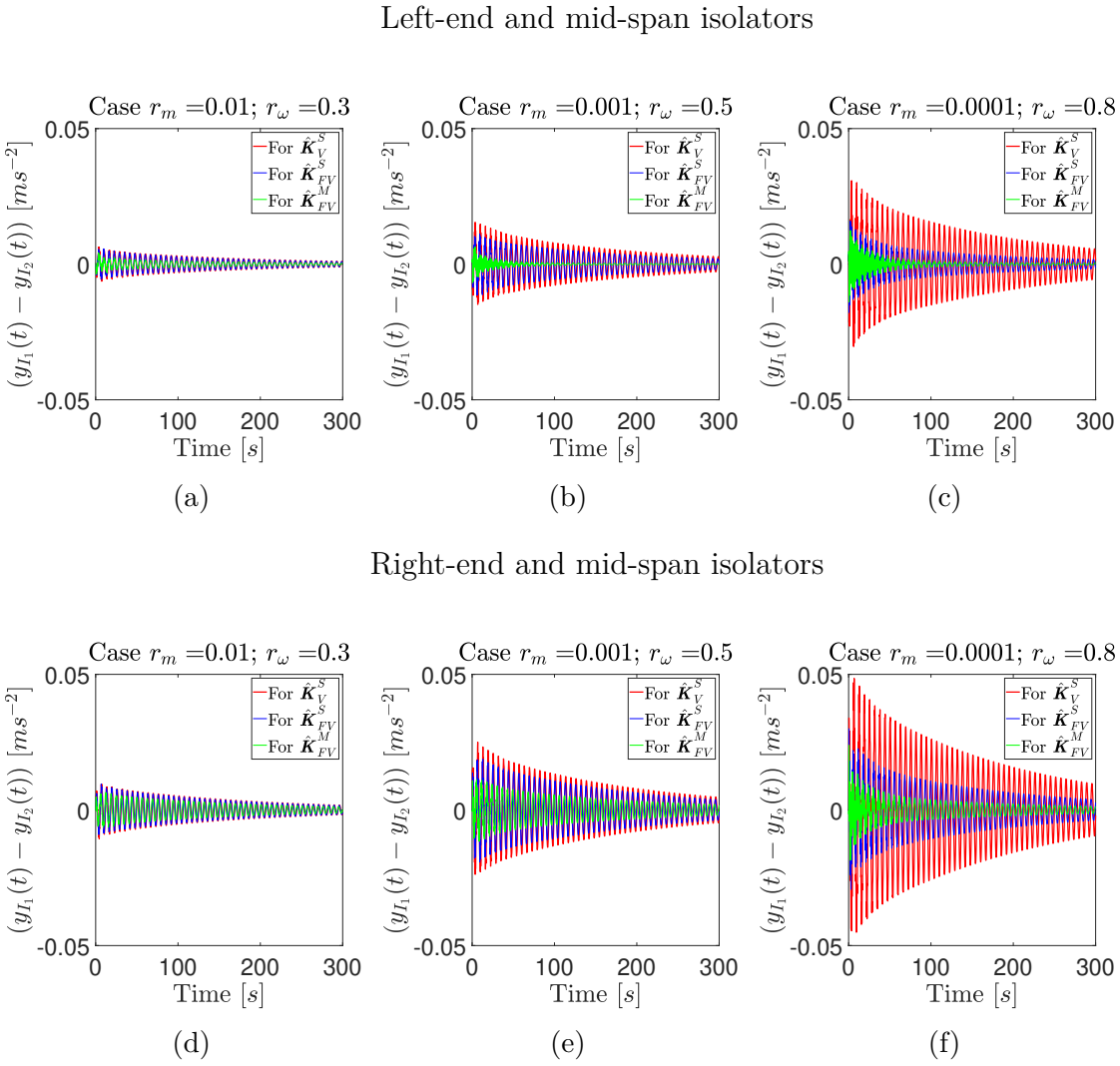


Figure 5.9: Impulse responses in the non-symmetrical case for the acceleration difference between platforms for (a), (b) and (c) the left and mid-span isolators (d), (e) and (f) right and mid-span isolators. The three different cases are: $r_m = 0.01$, $r_\omega = 0.3$ (left), $r_m = 0.001$, $r_\omega = 0.5$ (middle) and $r_m = 0.0001$, $r_\omega = 0.8$ (right).

first scenario is close, and again, the objective function of the second scenario is the worst among the three considered. The evolution of the curves shows that the improvement in the second and third scenarios is larger than for the first scenario, in which the CRO-SL obtains a small improvement over the starting solution. As in the previous experiment, in this case the most difficult problem to optimize seems to be the non-symmetrical case. The convergence of the algorithm is again obtained at around generation 15 of the CRO-SL in all the cases.

Figure 5.11 shows the analysis of the performance of each substrate in this case. In this examples, the DE and FA substrates seem to be key for the search capability of the CRO-SL, but in this case the WWo substrate seems to have less important

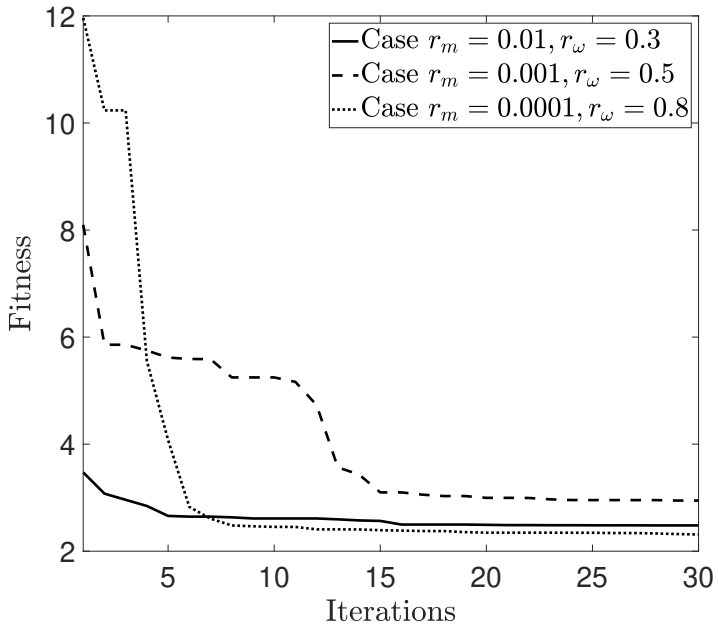


Figure 5.10: Fitness evolution in the CRO-SL for three cases: $r_m = 0.01,\ r_\omega = 0.3$ (continuous line), $r_m = 0.001,\ r_\omega = 0.5$ (dashed line) and $r_m = 0.0001,\ r_\omega = 0.8$ (dotted line), in the non-symmetrical case.

than, for example the 2Px or the MPx operators in the first and second scenarios, and only 2Px in the third scenario. In terms of solutions seeded into the reef in the evolution, it is clear that the DE and FA substrates are the most important for the search, and the contribution of other substrates also help the algorithm to search, but depending on the scenario, this contribution is small for example for HS or GM operators, whereas WWo, 2Px or MPx seem to have a relative importance in the search cabilities of the CRO-SL.

## 5.6 Practical implementation guidelines

The application examples illustrated in Section 5.5 show that the interaction between the isolator system and the non-rigid base must be considered for a large and not obvious range of parameters. However, these examples consider ideal models, which may hinder the practical application of the theory presented.

This section proposes detailed practical guidelines, which ccan be applied to a real experimental setup. These guidelines have been verified in

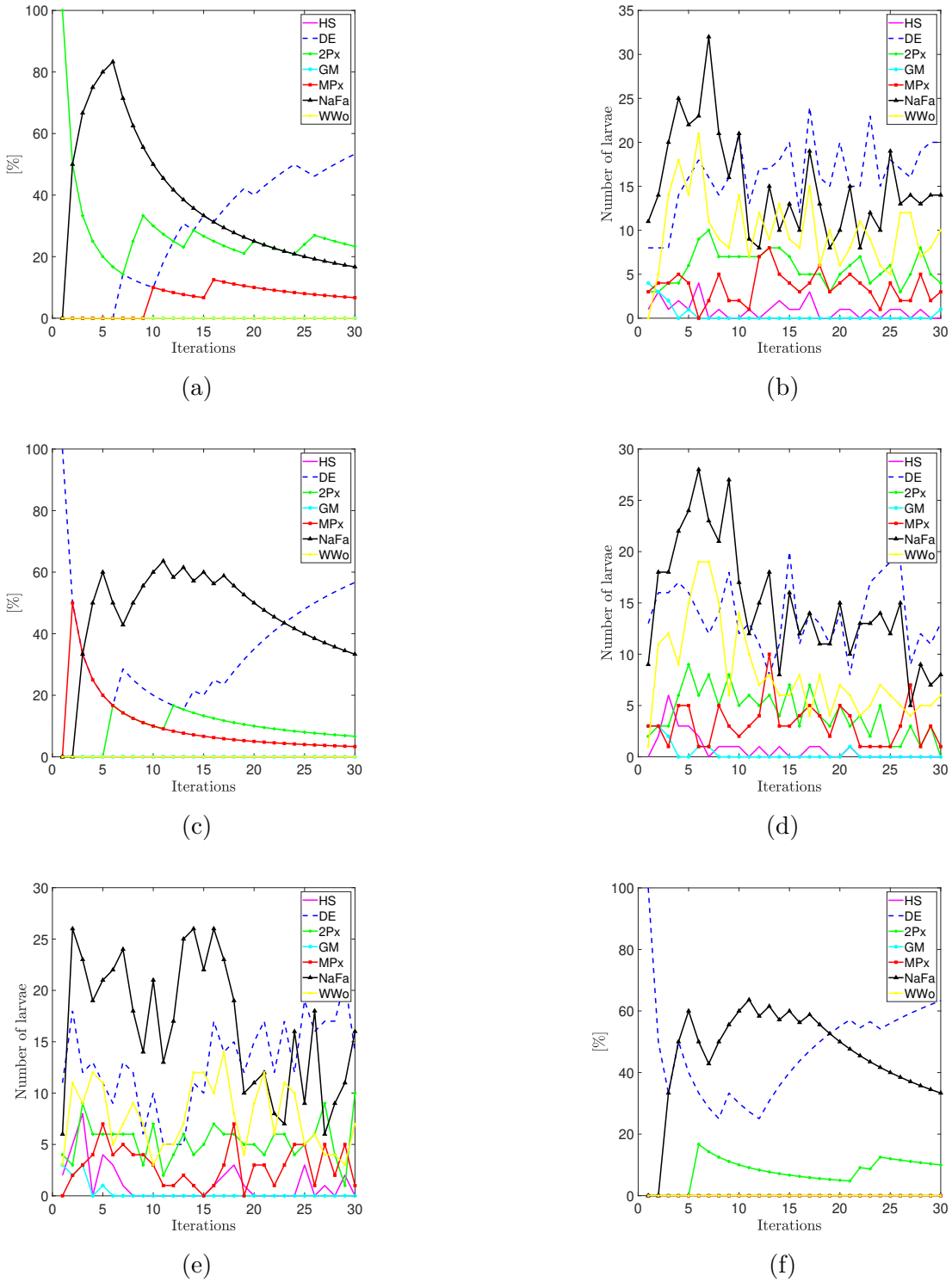


Figure 5.11: Ratio of times that each substrate generates the best larva and number of larvae settled in the reef per substrate for the different scenarios considered, in the Non-symmetrical case; (a) Ratio of times for the best larva, Scenario 1; (b) Number of larvae set into the reef, Scenario 1; (c) Ratio of times for the best larva, Scenario 2; (d) Number of larvae set into the reef, Scenario 2; (e) Ratio of times for the best larva, Scenario 3; (f) Number of larvae set into the reef, Scenario 3.

[Pérez-Aracil et al., 2021], from which the data is based on. In that work, the supporting structure was a standard UPN200 profile of 5 m length and mass 126 kg.

The isolator device was an APS Dynamics Model 400 electrodynamic actuator (see Figure 5.12a). The mass of the isolator device is 82 kg when $m_p$ is unattached and the total mass of the isolation platform $m_p$ is 31 kg.

This work considers the same supporting structure, and the isolator model extracted from the experimental verification shown in [Pérez-Aracil et al., 2021], but instead of studying a single isolator situated at the mid-span of the beam, three isolators are considered, which are assumed to be symmetrically placed at $L_{s_l} = L_{s_r} = L_b/4$. The next verified practical guidelines are proposed:

i The model of the beam with three lumped masses is obtained.

ii This model can be experimentally validated as was done in [Pérez-Aracil et al., 2021].

iii Each isolator is placed on a rigid ground and is excited by a random perturbation in order to obtain transmissibility of each isolator.

iv The transmissibility is used to identify the natural frequency and damping ratio which are $\omega_p = 8.79$ rads$^{-1}$ (1.4 Hz) and $\zeta_p = 0.075$ (see Figure 5.12b). The value of $m_p$ is equal to the moving mass (32 kg).

v The controller $\boldsymbol{G}_{AVI,F}(s)$ is optimally designed by CRO-SL (SISO and MIMO).

vi Simulation results are obtained.

vii Experimental results to be acquired.

### 5.6.1 Results

Following the above practical guidelines, a finite element model of the beam is obtained Figure 5.13. The natural frequencies and mode shapes of the non-rigid base are obtained by considering the effect of the added masses. The software used for the model is Autodesk Robot Structural Analysis Professional software

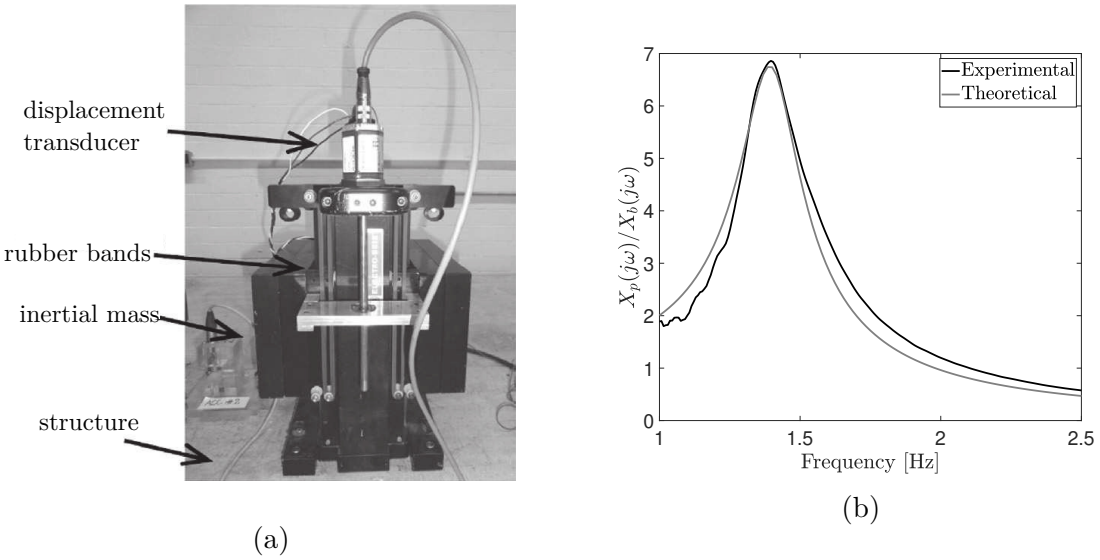


(a) (b)

Figure 5.12: (a) Real isolator device used for the experiment. (b) Comparison of the experimental and theoretical transmissibility TFs.

[Autodesk, 2020]. Thus, the model of Equation (2.21) can be developed as follows:

$$\Phi_I = \Phi_D = \begin{bmatrix} 0.046 & 0.066 & -0.046 \\ 0.066 & 0 & 0.066 \\ -0.046 & 0.066 & -0.046 \end{bmatrix}, \tag{5.6}$$

which represents the mode shapes at the isolator locations. The damping ratio $\zeta_b = 0.0047$ is the same for all modes, which was determined from measurements [Pérez-Aracil et al., 2021]. The natural frequencies are $\omega_{b_1} = 22.80$ rad $\cdot\, s^{-1}; \omega_{b_2} = 90.60$ rad $\cdot\, s^{-1}; \omega_{b_3} = 192.32$ rad $\cdot\, s^{-1}$.

The controller of Equation (5.1) has a pure integration with infinite magnitude response at zero frequency, making this controller very sensitive to low-frequency noise. Therefore, it is not suitable for being used in practice because it may saturate the actuator used for imparting the force due to offsets in the acceleration signal [Díaz and Reynolds, 2010]. Thus, the following lossy integrator is considered in this case study:

$$\boldsymbol{G}_{AVI,F}(s) = \boldsymbol{K}_B^M \frac{\omega_c}{s + \omega_c}, \tag{5.7}$$

in which $\omega_c$ represents the low frequency cut-off frequency of the lossy-integrator and $\boldsymbol{K}_B^M$ is the control gain. If the value of $\omega_c$ is defined as $0.1\omega_p$, the ideal and real

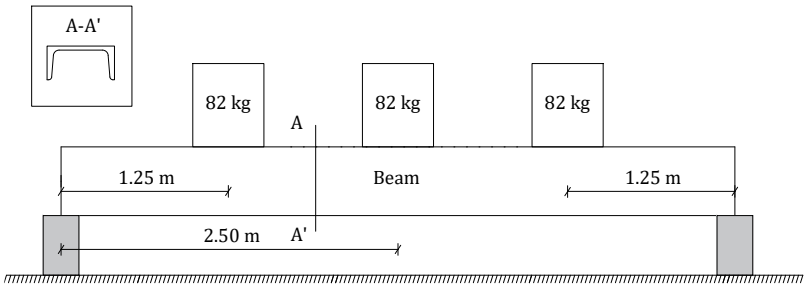


Figure 5.13: Schematic of the beam supporting structure with three isolators symmetrically situated with unattached payloads.

DVF has a similar behaviour in the bandwidth of interest. The value of $\omega_c$ is then 0.8796 rad/s. Then, the $\boldsymbol{K}_B^M$ is obtained by minimizing $f_{fv}$. The optimal value in the rigid base design is not obtained by Equation (4.12). In this case, the gain $\hat{k}_{v_{jj}}$ achieves a value of -3 dB in the FRF of the transmissibility TF at the oscillating frequency, given by $\omega_{p_{d_j}} = \omega_{p_j}\sqrt{1-\zeta_{p_j}^2}$. Thus, the best control gain for the SISO control strategy considering a rigid base is $\hat{k}_{v_{jj}} = -399.89$.

The values of the optimization are shown in Table 5.3. Note that the best solution is achieved with MIMO. In addition, it should be highlighted that SISO can improve the alignment respect to the rigid hypothesis. Analogous to the case study of Section 5.5, the time response of $(y_1(t) - y_2(t))$ is plotted. Figure 5.14 shows the comparison of Impulse responses for the acceleration difference between left-end and mid-span platforms. Note that the amplitude of the signal is reduced when the non-rigid base is considered. In addition, the settling time is also reduced for the MIMO case.

Table 5.3: Comparison between classic algorithm and CRO-SL.

| **Algorithm** | $\Lambda_T$ | $\Lambda_A$ | **Functional** |
|---|---|---|---|
| SISO with Rigid base | 1.13 | 3.54 | 2.34 |
| SISO with Non-rigid base | 1.16 | 3.21 | 2.18 |
| MIMO with Non-rigid base | 1.12 | 2.00 | 1.56 |

Then, the $\boldsymbol{K}_B^M$ is obtained by minimizing $f_{fv}$. The values of the optimization are shown in Table 5.3. Note that the best solution is achieved with MIMO. In addition, it should be highlighted that SISO can improve the alignment respect to the rigid hypothesis. Analogous to the case study of Section 5.5, the time response of $(y_1(t) - y_2(t))$ is plotted. Figure 5.14 shows the comparison of Impulse responses for the acceleration difference between left-end and mid-span platforms. Note that the amplitude of the signal is reduced when the non-rigid base is considered. In addition, the settling time is also reduced for the MIMO case.

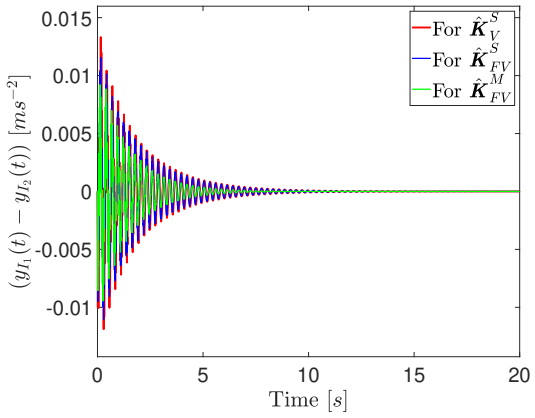


Figure 5.14: Comparison of Impulse responses for the acceleration difference between left-end and mid-span platforms for different control strategies.

## 5.7 Conclusions

A case in which three isolators situated on pinned-pinned supported beam and actively controlled by a MIMO control strategy using DVF has been studied in detail. For that, an ideal integrator has been chosen as controller. A set of numerical experiments was undertaken to show the influence of non-rigid bases into the performance of SISO and MIMO controllers. These controllers have been optimally tuned by a recently proposed ensemble multi-method meta-heuristic algorithm, the CRO-SL. The main conclusions of these numerical results are: i) the best DVF control, when a rigid base is considered, is not the best solution for a large (and not obvious) range of frequency and mass ratios when the base is flexible, ii) significant improvements

in alignment are achieved with SISO if the base structure dynamics are considered, iii) the problem of tuning the nine control parameters of the MIMO subjected to stability conditions is a hard optimisation problem, iv) the recently proposed Coral Reefs Optimisation with Substrate Layer algorithm has been successfully applied to this problem, v) the use of CRO-SL has indicated that the use of MIMO significantly extends the range of frequency and mass ratios whose alignment is considerably improved respect to the rigid assumption and vi) if MIMO control is used, the effects of the flexible base must be considered when the design criteria combines vibration level reduction and alignment objectives. Practical guidelines are also defined in this work. In addition, a final numerical example, which considers practical implementation issues, is included in order to better illustrate the these conclusions.

Finally, since the use of MIMO optimally design by CRO-SL is the best option, more complex control laws and design criteria can be explored and implemented in the future. This chapter can be used as a reference for these futures approaches.

# Chapter 6

# Conclusions and recommendations for further works

The main aim of this thesis has been to analyse the effects of the dynamics of the supporting structure on the vibration isolation (VI) and alignment problem. Also, to study how the VI task affects the response of the supporting structure. A number of conclusions can be derived from the works that have been presented, and it will be summarised in the next section. Moreover, areas of recommended future work are outlined.

## 6.1 Conclusions

In this thesis, the effect of the interaction phenomenon between the isolator and its supporting structure on the VI and alignment performance has been analysed. In addition, the effect that this phenomenon has on the supporting structure response for different VI techniques has been evaluated. Although past works have analysed some particular cases in which the VI is affected by the dynamics of the supporting structure, this work has presented a novel VI approach that allows analysing a general case, in which any number of isolators are situated on any type of flexible supporting structure. The VI approach proposed in this work also allows the definition of the control objectives, which can vary according to the task requirements.

A proof of concept has been developed considering a single axis isolator situated

on a single degree of freedom (SDOF) supporting structure. The necessary formulation to analyse the effect of the VI task on the supporting structure response has been developed. Also, it has been shown how the interaction phenomenon affects the platform response. The analysis has been made for different scenarios, in which different mass and frequency ratios between the isolator and the supporting structure have been set. In addition, the effect of the passive damping ratio of the isolator, $\zeta_p$, on the base response, when passive VI (PVI) and active VI (AVI) techniques are used, has been shown. The same design criteria has been set for all the cases, which must be accomplished by the AVI control strategy. Different damping ratios have been studied, and the effect that every case has on the base response has been analysed for different scenarios. This effect is studied through the H-infinity norm of the TF from the disturbance force, $f_d$ to the base response $\ddot{x}_b$. Also, to compare the effect that PVI and AVI have on the base response, the parameter $\gamma$ has been used, which relates relates both H-infinity norms of the base structure when PVI and AVI are used. $\gamma > 1$ implies that the use of AVI technique increases the base response with respect to the use of PVI, whereas for $\gamma < 1$, the use of AVI reduces the base response with respect to PVI. It can observed that for low damping ratios $\zeta_p < 0.1$, the influence on the supporting structure response, when considering AVI control strategy instead of PVI control is very high. The peak magnitude for AVI can be increased as much as four times compared with PVI. Also, for most of the damping ratios considered, it can be observed that for most of the domain considered (defined by mass and frequency ratios), the AVI control strategy increases the base response. However, there are some regions, which are different for each scenario, for which AVI control reduces the base response. Some particular cases of damping ratio have been analysed, showing three scenarios: i) the base response is worsened (its response increases) when AVI is used instead PVI control, ii) the base response is improved for AVI compared with PVI and iii) the response of the base depends on the damping ratio. The importance of the damping ratio of the isolator on the base response is shown, independently of the control criteria.

To validate the theory developed, an experimental test was carried out. It was

done on a pinned-pinned beam, with an isolator at the mid-span of the structure. The beam was excited by another actuator, and the effects of PVI and AVI has on beam were analysed. The experimental results fit very well with the theoretical results, hence validating the approach to the problem.

A general case was analysed, in which $n$ isolators were involved in the same task. This represents a more complex case, in which the objective is not only focused on reducing the vibration of the platform, but also to maintain the alignment between the different platforms. It was shown that the solution of this problem is trivial when the supporting structure is considered as an infinitely rigid system. It leads to find the solution for which the peak response of the transmissibility transfer function (TF) is reduced. In this case, there is not difference between the VI and alignment problem. However, it was shown that, if the dynamics of the supporting structure are considered, the solution is not trivial. A functional value to evaluate the VI and the alignment performance was proposed, which was particularised for a case in which the isolators are situated on a pinned-pinned supported beam. The dynamic properties of all isolators were considered to be the same, but different scenarios were analysed, to examine different mass and frequency ratios between the isolators and the beam structure. Three isolators were assumed to be located on the beam and the VI and alignment performance were compared under two assumptions: i) the base is rigid, ii) the dynamics of the supporting structure are considered. The results of both cases were compared, deriving very interesting results. It was shown that, for both scenarios (symmetrical and non-symmetrical), the functional values are lower (which implies better for the set criteria) if the base dynamics are considered compared with if they are not considered. For most of the cases analysed in this work, the control gains of the end isolators, for best VI and alignment performance, do not coincide with those which lead to the maximum damping ratio. Also, the effect of the supporting structure dynamics on the alignment was examined via temporal responses, hence showing that considering the base dynamics never worsen the alignment performance, improving it in most of the cases.

As the platform responses are coupled by the supporting structure dynamics,

a Multi-Inut-Multi-Output (MIMO) control strategy was studied instead of Single-Input-Single-Output (SISO). The problem used to analyse this control strategy was the same, namely three isolators located on a pinned-pinned supported beam. Also, the same functional was considered. Similar to the above scenario, the stability of both systems; isolators and base structure, have been checked. The analysis of this case allows understanding of the effect that the MIMO controller has on the functional value. It represents a very complicated optimisation problem, since it considers five variables (control gains) for the symmetrical case, and nine variables for the non-symmetrical case. To solve that, the use of the Coral Reefs Optimization algorithm with Substrate Layer (CRO-SL) was implemented, which facilitated better solution estimates than traditional algorithms with low numbers of iterations. It was demonstrated to be a very useful algorithm for this type of application. The results of the MIMO controller shows a great improvement with respect to the SISO control strategy in which the dynamics of the supporting structure are considered. In addition, the improvement is even higher compared to the case in which the base is considered as a rigid system. The analysis of temporal responses shows the effect of the MIMO controller on the alignment problem. It can be observed that for mainly the whole domain analysed in this thesis, the performance is improved when the MIMO controller is utilised. It has been observed that when verified experimental data is used for the simulations, the MIMO controller also improves the response with respect to the SISO control strategy. The implementation of the proposed practical guidelines would allow develop a real application.

## 6.2 Recommendations for further works

One of the key areas in which further research is required is the implementation of the developed VI controllers in real isolator devices. It is important to note that there are multiple isolator hardware types that can be used to develop vibration isolation task. The isolator device must be chosen according to the specific task conditions. The inherent dynamics of each device must be individually analysed. In some cases, as occurs with electrodynamic actuators, the VI task can be very

challenging. Non-linear behaviour inherent to the devices has to be considered in the controller design. The implementation of inner controllers to compensate for the dynamics of the isolators may be required. Additional research should be made in experimental implementation of VI strategies in different devices.

Additionally, future research should focus on the alignment task between isolators. Relative position sensors could be implemented at the isolator platforms. The alignment then can be approached not only by considering the original position, but also the platforms can follow trajectories, which must be followed by adjacent isolator(s). Moreover, the alignment problem should be studied with respect to fixed references independent of the supporting structure. Indeed, in some applications the relative alignment between isolators is not the unique task to be accomplished, but also some of the platforms must point to external references, as can occur in research centres or space applications. It is also important to consider the a multi-dimensional problem, instead of a single-dimension alignment. In many applications, the isolators can be distributed in the same plane, but also with different heights.

Further research is also needed in the use of more sophisticated isolator devices, such as Stewart platforms, that allow to accomplish VI, alignment and pointing tasks. Although extensive literature can be found in this field, there is a need of studying the task performance of these devices when the base is non-rigid. In addition, the implementation of popular control schemes combining damping and tracking actions considering the interaction phenomenon must be accomplished.

The payloads considered in this work are rigid. In some applications, it would be necessary to consider the flexible modes of the payload in order to better isolate it and also for alignment purposes. The interaction phenomenon between a flexible payload and supporting structure may be a very challenging problem, which has generally not been approached. A general formulation which allows to consider the whole system should be developed.

# Bibliography

[A. Chamseddine et al., 2006] A. Chamseddine, H. Noura, and T. Raharijaona (2006). Control of linear full vehicle active suspension system using Sliding Mode techniques. In *2006 IEEE Conference on Computer Aided Control System Design, 2006 IEEE International Conference on Control Applications, 2006 IEEE International Symposium on Intelligent Control*, pages 1306–1311.

[Abbott et al., 2009] Abbott, B. P., Abbott, R., Adhikari, R., Ajith, P., Allen, B., Allen, G., Amin, R. S., Anderson, S. B., Anderson, W. G., Arain, M. A., Araya, M., Armandula, H., Armor, P., Aso, Y., Aston, S., Aufmuth, P., Aulbert, C., Babak, S., Baker, P., Ballmer, S., Barker, C., Barker, D., Barr, B., Barriga, P., Barsotti, L., Barton, M. A., Bartos, I., Bassiri, R., Bastarrika, M., Behnke, B., Benacquista, M., Betzwieser, J., Beyersdorf, P. T., Bilenko, I. A., Billingsley, G., Biswas, R., Black, E., Blackburn, J. K., Blackburn, L., Blair, D., Bland, B., Bodiya, T. P., Bogue, L., Bork, R., Boschi, V., Bose, S., Brady, P. R., Braginsky, V. B., Brau, J. E., Bridges, D. O., Brinkmann, M., Brooks, A. F., Brown, D. A., Brummit, A., Brunet, G., Bullington, A., Buonanno, A., Burmeister, O., Byer, R. L., Cadonati, L., Camp, J. B., Cannizzo, J., Cannon, K. C., Cao, J., Cardenas, L., Caride, S., Castaldi, G., Caudill, S., Cavaglià, M., Cepeda, C., Chalermsongsak, T., Chalkley, E., Charlton, P., Chatterji, S., Chelkowski, S., Chen, Y., Christensen, N., Chung, C. T. Y., Clark, D., Clark, J., Clayton, J. H., Cokelaer, T., Colacino, C. N., Conte, R., Cook, D., Corbitt, T. R. C., Cornish, N., Coward, D., Coyne, D. C., Creighton, J. D. E., Creighton, T. D., Cruise, A. M., Culter, R. M., Cumming, A., Cunningham, L., Danilishin, S. L., Danzmann, K., Daudert, B., Davies, G., Daw, E. J., DeBra, D., Degallaix, J., Dergachev, V.,

Desai, S., DeSalvo, R., Dhurandhar, S., Díaz, M., Dietz, A., Donovan, F., Dooley, K. L., Doomes, E. E., Drever, R. W. P., Dueck, J., Duke, I., Dumas, J.-C., Dwyer, J. G., Echols, C., Edgar, M., Effler, A., Ehrens, P., Espinoza, E., Etzel, T., Evans, M., Evans, T., Fairhurst, S., Faltas, Y., Fan, Y., Fazi, D., Fehrmenn, H., Finn, L. S., Flasch, K., Foley, S., Forrest, C., Fotopoulos, N., Franzen, A., Frede, M., Frei, M., Frei, Z., Freise, A., Frey, R., Fricke, T., Fritschel, P., Frolov, V. V., Fyffe, M., Galdi, V., Garofoli, J. A., Gholami, I., Giaime, J. A., Giampanis, S., Giardina, K. D., Goda, K., Goetz, E., Goggin, L. M., González, G., Gorodetsky, M. L., Goßler, S., Gouaty, R., Grant, A., Gras, S., Gray, C., Gray, M., Greenhalgh, R. J. S., Gretarsson, A. M., Grimaldi, F., Grosso, R., Grote, H., Grunewald, S., Guenther, M., Gustafson, E. K., Gustafson, R., Hage, B., Hallam, J. M., Hammer, D., Hammond, G. D., Hanna, C., Hanson, J., Harms, J., Harry, G. M., Harry, I. W., Harstad, E. D., Haughian, K., Hayama, K., Heefner, J., Heng, I. S., Heptonstall, A., Hewitson, M., Hild, S., Hirose, E., Hoak, D., Hodge, K. A., Holt, K., Hosken, D. J., Hough, J., Hoyland, D., Hughey, B., Huttner, S. H., Ingram, D. R., Isogai, T., Ito, M., Ivanov, A., Johnson, B., Johnson, W. W., Jones, D. I., Jones, G., Jones, R., Ju, L., Kalmus, P., Kalogera, V., Kandhasamy, S., Kanner, J., Kasprzyk, D., Katsavounidis, E., Kawabe, K., Kawamura, S., Kawazoe, F., Kells, W., Keppel, D. G., Khalaidovski, A., Khalili, F. Y., Khan, R., Khazanov, E., King, P., Kissel, J. S., Klimenko, S., Kokeyama, K., Kondrashov, V., Kopparapu, R., Koranda, S., Kozak, D., Krishnan, B., Kumar, R., Kwee, P., Lam, P. K., Landry, M., Lantz, B., Lazzarini, A., Lei, H., Lei, M., Leindecker, N., Leonor, I., Li, C., Lin, H., Lindquist, P. E., Littenberg, T. B., Lockerbie, N. A., Lodhia, D., Longo, M., Lormand, M., Lu, P., Lubinski, M., Lucianetti, A., Lück, H., Machenschalk, B., MacInnis, M., Mageswaran, M., Mailand, K., Mandel, I., Mandic, V., Márka, S., Márka, Z., Markosyan, A., Markowitz, J., Maros, E., Martin, I. W., Martin, R. M., Marx, J. N., Mason, K., Matichard, F., Matone, L., Matzner, R. A., Mavalvala, N., McCarthy, R., McClelland, D. E., McGuire, S. C., McHugh, M., McIntyre, G., McKechan, D. J. A., McKenzie, K., Mehmet, M., Melatos, A., Melissinos, A. C., Menéndez, D. F., Mendell, G.,

Mercer, R. A., Meshkov, S., Messenger, C., Meyer, M. S., Miller, J., Minelli, J., Mino, Y., Mitrofanov, V. P., Mitselmakher, G., Mittleman, R., Miyakawa, O., Moe, B., Mohanty, S. D., Mohapatra, S. R. P., Moreno, G., Morioka, T., Mors, K., Mossavi, K., MowLowry, C., Mueller, G., Müller-Ebhardt, H., Muhammad, D., Mukherjee, S., Mukhopadhyay, H., Mullavey, A., Munch, J., Murray, P. G., Myers, E., Myers, J., Nash, T., Nelson, J., Newton, G., Nishizawa, A., Numata, K., O'Dell, J., O'Reilly, B., O'Shaughnessy, R., Ochsner, E., Ogin, G. H., Ottaway, D. J., Ottens, R. S., Overmier, H., Owen, B. J., Pan, Y., Pankow, C., Papa, M. A., Parameshwaraiah, V., Patel, P., Pedraza, M., Penn, S., Perraca, A., Pierro, V., Pinto, I. M., Pitkin, M., Pletsch, H. J., Plissi, M. V., Postiglione, F., Principe, M., Prix, R., Prokhorov, L., Punken, O., Quetschke, V., Raab, F. J., Rabeling, D. S., Radkins, H., Raffai, P., Raics, Z., Rainer, N., Rakhmanov, M., Raymond, V., Reed, C. M., Reed, T., Rehbein, H., Reid, S., Reitze, D. H., Riesen, R., Riles, K., Rivera, B., Roberts, P., Robertson, N. A., Robinson, C., Robinson, E. L., Roddy, S., Röver, C., Rollins, J., Romano, J. D., Romie, J. H., Rowan, S., Rüdiger, A., Russell, P., Ryan, K., Sakata, S., de la Jordana, L. S., Sandberg, V., Sannibale, V., Santamaría, L., Saraf, S., Sarin, P., Sathyaprakash, B. S., Sato, S., Satterthwaite, M., Saulson, P. R., Savage, R., Savov, P., Scanlan, M., Schilling, R., Schnabel, R., Schofield, R., Schulz, B., Schutz, B. F., Schwinberg, P., Scott, J., Scott, S. M., Searle, A. C., Sears, B., Seifert, F., Sellers, D., Sengupta, A. S., Sergeev, A., Shapiro, B., Shawhan, P., Shoemaker, D. H., Sibley, A., Siemens, X., Sigg, D., Sinha, S., Sintes, A. M., Slagmolen, B. J. J., Slutsky, J., Smith, J. R., Smith, M. R., Smith, N. D., Somiya, K., Sorazu, B., Stein, A., Stein, L. C., Steplewski, S., Stochino, A., Stone, R., Strain, K. A., Strigin, S., Stroeer, A., Stuver, A. L., Summerscales, T. Z., Sun, K.-X., Sung, M., Sutton, P. J., Szokoly, G. P., Talukder, D., Tang, L., Tanner, D. B., Tarabrin, S. P., Taylor, J. R., Taylor, R., Thacker, J., Thorne, K. A., Thüring, A., Tokmakov, K. V., Torres, C., Torrie, C., Traylor, G., Trias, M., Ugolini, D., Ulmen, J., Urbanek, K., Vahlbruch, H., Vallisneri, M., Broeck, C. V. D., van der Sluys, M. V., van Veggel, A. A., Vass, S., Vaulin, R., Vecchio, A., Veitch, J., Veitch, P., Veltkamp, C., Villar, A., Vorvick,

C., Vyachanin, S. P., Waldman, S. J., Wallace, L., Ward, R. L., Weidner, A., Weinert, M., Weinstein, A. J., Weiss, R., Wen, L., Wen, S., Wette, K., Whelan, J. T., Whitcomb, S. E., Whiting, B. F., Wilkinson, C., Willems, P. A., Williams, H. R., Williams, L., Willke, B., Wilmut, I., Winkelmann, L., Winkler, W., Wipf, C. C., Wiseman, A. G., Woan, G., Wooley, R., Worden, J., Wu, W., Yakushin, I., Yamamoto, H., Yan, Z., Yoshida, S., Zanolin, M., Zhang, J., Zhang, L., Zhao, C., Zotov, N., Zucker, M. E., zur Mühlen, H., and Zweizig, J. (2009). LIGO: The Laser Interferometer Gravitational-Wave Observatory. *Reports on Progress in Physics*, 72(7):076901.

[Ahmadipour and Alam, 2017] Ahmadipour, M. and Alam, M. S. (2017). Sensitivity analysis on mechanical characteristics of lead-core steel-reinforced elastomeric bearings under cyclic loading. *Engineering Structures*, 140:39–50.

[Alanoly and Sankar, 1987] Alanoly, J. and Sankar, S. (1987). A New Concept in Semi-Active Vibration Isolation. *Journal of Mechanisms Transmissions and Automation in Design*, 109(2):242.

[Allaoua and Guenfaf, 2019] Allaoua, S. and Guenfaf, L. (2019). LQG vibration control effectiveness of an electric active mass damper considering soil–structure interaction. *International Journal of Dynamics and Control*, 7(1):185–200.

[Alleyne and Hedrick, 1995] Alleyne, A. and Hedrick, J. (1995). Nonlinear adaptive control of active suspensions. *IEEE Transactions on Control Systems Technology*, 3(1):94–101.

[Alujević et al., 2018] Alujević, N., Čakmak, D., Wolf, H., and Jokić, M. (2018). Passive and active vibration isolation systems using inerter. *Journal of Sound and Vibration*, 418:163–183.

[Alujević et al., 2019] Alujević, N., Senjanović, I., Ćatipović, I., and Vladimir, N. (2019). The absence of reciprocity in active structures using direct velocity feedback. *Journal of Sound and Vibration*, 438:251–256.

[Aly and Salem, 2013] Aly, A. A. and Salem, F. A. (2013). Vehicle Suspension Systems Control: A Review. *INTERNATIONAL JOURNAL OF CONTROL*, page 9.

[Anvar et al., 2017] Anvar, V., Alexey, Z., and Artem, T. (2017). Study of Application of Vibration Isolators with Quasi-zero Stiffness for Reducing Dynamics Loads on the Foundation. *Procedia Engineering*, 176:137–143.

[Autodesk, 2020] Autodesk, R. S. (2020). Autodesk Robot Structural Analysis Professional. Autodesk.

[Balas, 1978] Balas, M. (1978). Feedback control of flexible systems. *IEEE Transactions on Automatic Control*, 23(4):673–679.

[Balas, 1979] Balas, M. J. (1979). Direct Velocity Feedback Control of Large Space Structures. *Journal of Guidance, Control, and Dynamics*, 2(3):252–253.

[Bastaits et al., 2009] Bastaits, R., Rodrigues, G., Mokrani, B., and Preumont, A. (2009). Active Optics of Large Segmented Mirrors: Dynamics and Control. *Journal of Guidance, Control, and Dynamics*, 32(6):1795–1803.

[Beijen, 2018] Beijen, M. (2018). *Disturbance Feedforward Control for Vibration Isolation Systems: Analysis, Design, and Implementation*. PhD thesis, Technische Universiteit Eindhoven.

[Beijen et al., 2017] Beijen, M., Heertjes, M., Butler, H., and Steinbuch, M. (2017). H $\infty$ feedback and feedforward controller design for active vibration isolators. *IFAC-PapersOnLine*, 50(1):13384–13389.

[Beijen et al., 2018] Beijen, M., Heertjes, M., Van Dijk, J., and Hakvoort, W. (2018). Self-tuning MIMO disturbance feedforward control for active hard-mounted vibration isolators. *Control Engineering Practice*, 72:90–103.

[Beijen et al., 2019] Beijen, M. A., Heertjes, M. F., Butler, H., and Steinbuch, M. (2019). Mixed feedback and feedforward control design for multi-axis vibration isolation systems. *Mechatronics*, 61:106–116.

[Benassi and Elliott, 2004] Benassi, L. and Elliott, S. (2004). Active vibration isolation using an inertial actuator with local displacement feedback control. *Journal of Sound and Vibration*, 278(4-5):705–724.

[Benassi et al., 2004] Benassi, L., Elliott, S., and Gardonio, P. (2004). Active vibration isolation using an inertial actuator with local force feedback control. *Journal of Sound and Vibration*, 276(1-2):157–179.

[Bendat and Piersol, 1993] Bendat, J. and Piersol, A. (1993). *Engineering Applications of Correlation and Spectral Analysis*. Wiley, New York, NY.

[Bermejo et al., 2018] Bermejo, E., Chica, M., Damas, S., Salcedo-Sanz, S., and Cordón, O. (2018). Coral Reef Optimization with substrate layers for medical Image Registration. *Swarm and Evolutionary Computation*, 42:138–159.

[Bhandari et al., 2018] Bhandari, M., Bharti, S., Shrimali, M., and Datta, T. (2018). Assessment of proposed lateral load patterns in pushover analysis for base-isolated frames. *Engineering Structures*, 175:531–548.

[Blackwood, 1994] Blackwood, H., G. (1994). *Active Vibration Isolation for Controlled Flexible Structures*. PhD thesis, Massachusetts Institute of Technology. Stamford University.

[Bradaschia et al., 1990] Bradaschia, C., Fabbro, R. D., Virgilio, A. D., Giazotto, A., Kautzky, H., Montelatici, V., Passuello, D., Brillet, A., Cregut, O., Hello, P., Man, C. N., Manh, P. T., Marraud, A., Shoemaker, D., Vinet, J. Y., Barone, F., Fiore, L. D., Milano, L., Russo, G., Aguirregabiria, J. M., Bel, H., Di, J. P., Denmat, G. L., Tourrenc, P., Capozzi, M., Longo, M., Lops, M., Pinto, I., Rotoli, G., Damour, T., Bonazzola, S., Marck, J. A., Gourghoulon, Y., and Holloway, L. E. (1990). VIRGO project: A wide band antenna for gravitationa wave detection. *Nuclear Instruments and Methods in Physical Research*, 289:518–525.

[Brennan et al., 2006] Brennan, M. J., Elliott, S. J., and Huang, X. (2006). A demonstration of active vibration isolation using decentralized velocity feedback control. *Smart Materials and Structures*, 15(1):N19–N22.

[Camacho-Gómez et al., 2019] Camacho-Gómez, C., Marsa-Maestre, I., Gimenez-Guzman, J. M., and Salcedo-Sanz, S. (2019). A Coral Reefs Optimization algorithm with substrate layer for robust Wi-Fi channel assignment. *Soft Computing*, 23(23):12621–12640.

[Camacho-Gómez et al., 2018] Camacho-Gómez, C., Wang, X., Pereira, E., Díaz, I., and Salcedo-Sanz, S. (2018). Active vibration control design using the Coral Reefs Optimization with Substrate Layer algorithm. *Engineering Structures*, 157:14–26.

[Carpani, 2017] Carpani, B. (2017). Base isolation from a historical perspective. In *16th World Conference on Earthquake,16WCEE 2017*, page 13, Santiago Chile.

[Chanan et al., 2004] Chanan, G., MacMartin, D. G., Nelson, J., and Mast, T. (2004). Control and alignment of segmented-mirror telescopes: Matrices, modes, and error propagation. *Applied Optics*, 43(6):1223.

[Chang and Spencer, 2010] Chang, C.-M. and Spencer, B. F. (2010). Active base isolation of buildings subjected to seismic excitations. *Earthquake Engineering & Structural Dynamics*, 39(13):1493–1512.

[Chen et al., 2005] Chen, H., Liu, Z. Y., and Sun, P. Y. (2005). Application of Constrained H$\infty$ Control to Active Suspension Systems on Half-Car Models. *Journal of Dynamic Systems, Measurement, and Control*, 127(3):345–354.

[Chopra, 2011] Chopra, K., A. (2011). *Dynamic of Structures.* Pearson, fourth edition.

[Cobb et al., 1999] Cobb, R. G., Sullivan, J. M., Das, A., Davis, L. P., Hyde, T. T., Davis, T., Rahman, Z. H., and Spanos, J. T. (1999). Vibration isolation and suppression system for precision payloads in space. *Smart Materials and Structures*, 8(6):798–812.

[Colgate et al., 1995] Colgate, J., Chang, C.-T., Chiou, Y.-C., Liu, W., and Keer, L. (1995). Modelling of a hydraulic engine mount focusing on response to sinusoidal and composite excitations. *Journal of Sound and Vibration*, 184(3):503–528.

[Collette et al., 2011] Collette, C., Janssens, S., and Artoos, K. (2011). Review of Active Vibration Isolation Strategies. *Recent patents on Mechanical engineering*, 4:212–219.

[Davis et al., 1995] Davis, L. P., Carter, D., and Hyde, T. (1995). Second-generation hybrid D-strut. In *Smart Structures and Materials 1995: Passive Damping*, volume 2445 of *Society of Photo-Optical Instrumentation Engineers (SPIE) Conference Series*, pages 161–175.

[Davis et al., 1994] Davis, P., Cunningham, D., and Harrell, J. (1994). Advanced 1.5 Hz passive viscous isolation system. In *35th AIAA SDM Conference Hilton Head*, South Carolina.

[De Domenico and Ricciardi, 2018] De Domenico, D. and Ricciardi, G. (2018). Optimal design and seismic performance of tuned mass damper inerter (TMDI) for structures with nonlinear base isolation systems. *Earthquake Engineering & Structural Dynamics*.

[D'Errico, 2020] D'Errico, J. (2020). Fminsearchbnd, fminsearchcon. MathWorks.

[Díaz and Reynolds, 2010] Díaz, I. M. and Reynolds, P. (2010). On-off nonlinear active control of floor vibrations. *Mechanical Systems and Signal Processing*, 24(6):1711–1726.

[Ding et al., 2019] Ding, H., Ji, J., and Chen, L.-Q. (2019). Nonlinear vibration isolation for fluid-conveying pipes using quasi-zero stiffness characteristics. *Mechanical Systems and Signal Processing*, 121:675–688.

[Dyke et al., 1996] Dyke, S. J., Spencer, B. F., Sain, M. K., and Carlson, J. D. (1996). Modeling and control of magnetorheological dampers for seismic response reduction. *Smart Materials and Structures*, 5(5):565–575.

[Eiben and Smith, 2003] Eiben, A. E. and Smith, J. E. (2003). *Introduction to Evolutionary Computing*. Springer-Verlag, Berlin.

[Elliott et al., 2004] Elliott, S., Benassi, L., Brennan, M., Gardonio, P., and Huang, X. (2004). Mobility analysis of active isolation systems. *Journal of Sound and Vibration*, 271(1-2):297–321.

[Fan et al., 2020] Fan, H., Yang, L., Tian, Y., and Wang, Z. (2020). Design of metastructures with quasi-zero dynamic stiffness for vibration isolation. *Composite Structures*, 243:112244.

[Farshidianfar et al., 2012] Farshidianfar, A., Saghafi, A., Kalami, S. M., and Saghafi, I. (2012). Active vibration isolation of machinery and sensitive equipment using H $\infty$ control criterion and particle swarm optimization method. *Meccanica*, 47(2):437–453.

[Fichter, 1986] Fichter, E. (1986). A Stewart Platform- Based Manipulator: General Theory and Practical Construction. *The International Journal of Robotics Research*, 5(2):157–182.

[Foda, 2000] Foda, S. (2000). Fuzzy control of a quarter-car suspension system. In *ICM 2000. Proceedings of the 12th International Conference on Microelectronics. (IEEE Cat. No.00EX453)*, pages 231–234, Tehran, Iran. Univ. Tehran.

[Fujita, 1991] Fujita, T. (1991). Seismic isolation rubber bearings for nuclear facilities. *Nuclear Engineering and Design*, 127(3):379–391.

[Fuller et al., 1997] Fuller, K. N. G., Gough, J., Pond, T. J., and Ahmadi, H. R. (1997). High damping natural rubber seismic isolators. *Journal of Structural Control*, 4(2):19–40.

[Gao et al., 2019] Gao, H., Zhang, S., Su, Y., and Diao, M. (2019). Joint Resource Allocation and Power Control Algorithm for Cooperative D2D Heterogeneous Networks. *IEEE Access*, 7:20632–20643.

[Garcia et al., 1992] Garcia, J. G., Sievers, L. A., and von Flotow, A. (1992). High-bandwidth positioning control of small payloads mounted on a flexible structure. *Journal of Guidance, Control, and Dynamics*, 15(4):928–934.

[Garcia-Hernandez et al., 2020] Garcia-Hernandez, L., Garcia-Hernandez, J., Salas-Morera, L., Carmona-Muñoz, C., Alghamdi, N., de Oliveira, J. V., and Salcedo-Sanz, S. (2020). Addressing Unequal Area Facility Layout Problems with the Coral Reef Optimization algorithm with Substrate Layers. *Engineering Applications of Artificial Intelligence*, 93:103697.

[Gardonio et al., 1997a] Gardonio, P., Elliott, S., and Pinnington, R. (1997a). Active isolation of structural vibration on a multiple-degree-of-freedom system. Part I: The dynamics of the system. *Journal of Sound and Vibration*, 207(1):61–93.

[Gardonio et al., 1997b] Gardonio, P., Elliott, S., and Pinnington, R. (1997b). Active isolation of structural vibration on a multiple-degree-of-freedom system. Part II: Effectiveness of active control strategies. *Journal of Sound and Vibration*, 207(1):95–121.

[Gaspar et al., 2003] Gaspar, P., Szaszi, I., and Bokor, J. (2003). Design of Robust Controllers for Active Vehicle Suspension Using the Mixed µ Synthesis. *Vehicle System Dynamics*, 40(4):193–228.

[Geem et al., 2001] Geem, Z. W., Kim, J. H., and Loganathan, G. (2001). A new heuristic optimization algorithm: Harmony search. *SIMULATION*, 76(2):60–68.

[Geng and Haynes, 1992] Geng, Z. and Haynes, L. (1992). Six degree-of-freedom active vibration control using the Stewart platforms. *IEEE Transactions on Control Systems Technology*, 2(1):45–53.

[George W. Wilson and Patrick J. Wolke, 1997] George W. Wilson and Patrick J. Wolke (1997). Performance prediction of D-Strut isolation systems. In *Proc.SPIE*, volume 3045.

[Golnaraghi and Nakhaie Jazar, 2001] Golnaraghi, M. F. and Nakhaie Jazar, G. (2001). Development and Analysis of a Simplified Nonlinear Model of a Hydraulic Engine Mount. *Journal of Vibration and Control*, 7(4):495–526.

[Ho et al., 2013] Ho, C., Lang, Z. Q., Sapiński, B., and Billings, S. A. (2013). Vibration isolation using nonlinear damping implemented by a feedback-controlled MR damper. *Smart Materials and Structures*, 22(10):105010.

[Hua et al., 2004] Hua, W., Adhikari, R., DeBra, D. B., Giaime, J. A., Hammond, G. D., Hardham, C., Hennessy, M., How, J. P., Lantz, B. T., Macinnis, M., et al. (2004). Low-frequency active vibration isolation for advanced LIGO. In *Gravitational Wave and Particle Astrophysics Detectors*, volume 5500, pages 194–205. International Society for Optics and Photonics.

[Huang et al., 2003] Huang, X., Elliott, S., and Brennan, M. (2003). Active isolation of a flexible structure from base vibration. *Journal of Sound and Vibration*, 263(2):357–376.

[Ibrahim, 2008] Ibrahim, R. (2008). Recent advances in nonlinear passive vibration isolators. *Journal of Sound and Vibration*, 314(3-5):371–452.

[Inman, 1990] Inman, D. (1990). Control/structure interaction - Effects of actuator dynamics. In *Dynamics Specialists Conference*, Long Beach,CA,U.S.A. American Institute of Aeronautics and Astronautics.

[Jiang et al., 2020] Jiang, D., Li, J., Li, X., Deng, C., and Liu, P. (2020). Modeling identification and control of a 6-DOF active vibration isolation system driving by voice coil motors with a Halbach array magnet. *Journal of Mechanical Science and Technology*, 34(2):617–630.

[Jiang et al., 2018] Jiang, J., Gao, W., Wang, L., Teng, Z., and Liu, Y. (2018). Active vibration control based on modal controller considering structure-actuator interaction. *Journal of Mechanical Science and Technology*, 32(8):3515–3521.

[Jung et al., 2006] Jung, H.-J., Choi, K.-M., Spencer, B. F., and Lee, I.-W. (2006). Application of some semi-active control algorithms to a smart base-isolated building employing MR dampers. *Structural Control and Health Monitoring*, 13(2-3):693–704.

[Kamesh et al., 2012] Kamesh, D., Pandiyan, R., and Ghosal, A. (2012). Passive vibration isolation of reaction wheel disturbances using a low frequency flexible space platform. *Journal of Sound and Vibration*, 331(6):1310–1330.

[Kaplow and Velman, 1980] Kaplow, C. and Velman, J. (1980). Active Local Vibration Isolation Applied to a Flexible Space Telescope. *Journal of Guidance, Control, and Dynamics*, 3(3):227–233.

[Karnopp et al., 1974] Karnopp, D., Crosby, M. J., and Harwood, R. A. (1974). Vibration Control Using Semi-Active Force Generators. *Journal of Engineering for Industry*, 96(2):619.

[Kim and Singh, 1993] Kim, G. and Singh, R. (1993). Nonlinear Analysis of Automotive Hydraulic Engine Mount. *Journal of Dynamic Systems, Measurement, and Control*, 115(3):482–487.

[Kim et al., 2001] Kim, S.-M., Elliott, S. J., and Brennan, M. J. (2001). Decentralized Control for Multichannel Active Vibration Isolation. *IEEE TRANSACTIONS ON CONTROL SYSTEMS TECHNOLOGY*, 9(1):8.

[Kirpatrick et al., 1983] Kirpatrick, S., Gerlatt, C. D., and Vecchi, M. P. (1983). Optimization by simulated annealing. *Science*, 220:671–680.

[Klement et al., 1999] Klement, E. P., Koczy, L. T., and Moser, B. (1999). ARE FUZZY SYSTEMS UNIVERSAL APPROXIMATORS? *International Journal of General Systems*, 28(2-3):259–282.

[Kong and Huang, 2018] Kong, Y. and Huang, H. (2018). Vibration isolation and dual-stage actuation pointing system for space precision payloads. *Acta Astronautica*, 143:183–192.

[Kuo et al., 2005] Kuo, C.-L., Li, T.-H. S., and Guo, N. R. (2005). Design of a Novel Fuzzy Sliding-Mode Control for Magnetic Ball Levitation System. *Journal of Intelligent and Robotic Systems*, 42(3):295–316.

[Lagarias et al., 1998] Lagarias, J. C., Reeds, J. A., Wright, M. H., and Wright, P. E. (1998). Convergence Properties of the Nelder–Mead Simplex Method in Low Dimensions. *SIAM Journal on Optimization*, 9(1):112–147.

[Li et al., 2018] Li, M., Zhang, Y., Wang, Y., Hu, Q., and Qi, R. (2018). The Pointing and Vibration Isolation Integrated Control Method for Optical Payload. *Journal of Sound and Vibration*.

[Li and Xu, 2017] Li, Y. and Xu, D. (2017). Vibration attenuation of high dimensional quasi-zero stiffness floating raft system. *International Journal of Mechanical Sciences*, 126:186–195.

[Liao and Lai, 2002] Liao, W. H. and Lai, C. Y. (2002). Harmonic analysis of a magnetorheological damper for vibration control. *Smart Materials and Structures*, 11(2):288–296.

[Liu et al., 2015] Liu, C., Jing, X., Daley, S., and Li, F. (2015). Recent advances in micro-vibration isolation. *Mechanical Systems and Signal Processing*, 56-57:55–80.

[Liu et al., 2012] Liu, J., Liu, H. J., and Dyke, S. J. (2012). Control–structure interaction for micro-vibration structural control. *Smart Materials and Structures*, 21(10):105021.

[Liu et al., 2008] Liu, Y., Matsuhisa, H., and Utsuno, H. (2008). Semi-active vibration isolation system with variable stiffness and damping control. *Journal of Sound and Vibration*, 313(1-2):16–28.

[Loix et al., 2002] Loix, N., Hanieh, A. A., and Preumont, A. (2002). Piezoelectric Stewart platform for general purpose active damping interface and precision control. In *3rd International Conference of the European Society for Precision Engineering and Nanotechnology*.

[Makihara et al., 2006] Makihara, K., Onoda, J., and Minesugi, K. (2006). New approach to semi-active vibration isolation to improve the pointing performance of observation satellites. *Smart Materials and Structures*, 15(2):342–350.

[Marjoram, 1985] Marjoram, R. H. (1985). Pressurized Hydraulic Mounts for Improved Isolation of Vehicle Cabs. In *3rd International Pacific Conference on Automotive Engineering (1985)*, page 852349.

[Markou and Manolis, 2016] Markou, A. A. and Manolis, G. D. (2016). Mechanical models for shear behavior in high damping rubber bearings. *Soil Dynamics and Earthquake Engineering*, 90:221–226.

[Matichard et al., 2015a] Matichard, F., Lantz, B., Mason, K., Mittleman, R., Abbott, B., Abbott, S., Allwine, E., Barnum, S., Birch, J., Biscans, S., Clark, D., Coyne, D., DeBra, D., DeRosa, R., Foley, S., Fritschel, P., Giaime, J., Gray, C., Grabeel, G., Hanson, J., Hillard, M., Kissel, J., Kucharczyk, C., Le Roux, A., Lhuillier, V., Macinnis, M., O'Reilly, B., Ottaway, D., Paris, H., Puma, M., Radkins, H., Ramet, C., Robinson, M., Ruet, L., Sareen, P., Shoemaker, D., Stein, A., Thomas, J., Vargas, M., and Warner, J. (2015a). Advanced LIGO two-stage twelve-axis vibration isolation and positioning platform. Part 2: Experimental investigation and tests results. *Precision Engineering*, 40:287–297.

[Matichard et al., 2015b] Matichard, F., Lantz, B., Mason, K., Mittleman, R., Abbott, B., Abbott, S., Allwine, E., Barnum, S., Birch, J., Biscans, S., Clark, D., Coyne, D., DeBra, D., DeRosa, R., Foley, S., Fritschel, P., Giaime, J., Gray, C., Grabeel, G., Hanson, J., Hillard, M., Kissel, J., Kucharczyk, C., Le Roux, A., Lhuillier, V., Macinnis, M., O'Reilly, B., Ottaway, D., Paris, H., Puma, M., Radkins, H., Ramet, C., Robinson, M., Ruet, L., Sareen, P., Shoemaker, D., Stein, A., Thomas, J., Vargas, M., and Warner, J. (2015b). Advanced LIGO two-stage twelve-axis vibration isolation and positioning platform. Part 1: Design and production overview. *Precision Engineering*, 40:273–286.

[Mikhailov and Bazinenkov, 2017] Mikhailov, V. P. and Bazinenkov, A. M. (2017). Active vibration isolation platform on base of magnetorheological elastomers. *Journal of Magnetism and Magnetic Materials*, 431:266–268.

[Miller and Nobles, 1990] Miller, L. R. and Nobles, C. M. (1990). Methods for Eliminating Jerk and Noise in Semi-Active Suspensions. In *International Truck & Bus Meeting & Exposition*, page 902284. SAE International.

[Naeim and Kelly, 1999] Naeim, F. and Kelly, J. M. (1999). *Design of Seismic Isolated Structures: From Theory to Practice*. John Wiley & Sons, New York.

[Nagarajaiah and Narasimhan, 2006] Nagarajaiah, S. and Narasimhan, S. (2006). Smart base-isolated benchmark building. Part II: Phase I sample controllers for linear isolation systems. *Structural Control and Health Monitoring*, 13(2-3):589–604.

[Nagarajaiah et al., 1993] Nagarajaiah, S., Riley, M. A., and Reinhorn, A. (1993). Control of Sliding-Isolated Bridge with Absolute Acceleration Feedback. *Journal of Engineering Mechanics*, 119(11):2317–2332.

[Narasimhan et al., 2006] Narasimhan, S., Nagarajaiah, S., Johnson, E., and Gavin, H. (2006). Smart base-isolated benchmark building. Part I: Problem definition. *Structural Control and Health Monitoring*, 13(2-3):573–588.

[Nelson, 1991] Nelson, P. G. (1991). An active vibration isolation system for inertial reference and precision measurement. *Review of Scientific Instruments*, 62(9):2069–2075.

[Ogata, 2010] Ogata, K. (2010). *Modern Control Engineering*. Prentice-Hall Electrical Engineering Series. Instrumentation and Controls Series. Prentice-Hall, Boston, 5th ed edition.

[Oh et al., 2000] Oh, H. ., Onoda, J., and Minesugi, K. (2000). Characteristics of a liquid-crystal type ER-fluid variable damper for semiactive vibration suppression. *Journal of Vibration and Acoustics, Transactions of the ASME*, 122(4):412–419.

[Oh et al., 2004] Oh, H.-U., Onoda, J., and Minesugi, K. (2004). Semiactive Isolator With Liquid-Crystal Type ER Fluid for Momentum-Wheel Vibration Isolation. *Journal of Vibration and Acoustics*, 126(2):272–277.

[Oliveto et al., 2019] Oliveto, N. D., Markou, A. A., and Athanasiou, A. (2019). Modeling of high damping rubber bearings under bidirectional shear loading. *Soil Dynamics and Earthquake Engineering*, 118:179–190.

[Parthasarathy and Klingenberg, 1996] Parthasarathy, M. and Klingenberg, D. (1996). Electrorheology: Mechanisms and models. *Materials Science and Engineering: R: Reports*, 17(2):57–103.

[Perez-Aracil et al., 2020] Perez-Aracil, J., Camacho-Gomez, C., Hernandez-Diaz, A. M., Pereira, E., and Salcedo-Sanz, S. (2020). Submerged Arches Optimal Design With a Multi-Method Ensemble Meta-Heuristic Approach. *IEEE Access*, 8:215057–215072.

[Pérez-Aracil et al., 2021] Pérez-Aracil, J., Pereira, E., Díaz, I. M., and Reynolds, P. (2021). Study on the Isolator-Structure Interaction. Influence on the Supporting Structure. In Gonçalves, J. A., Braz-César, M., and Coelho, J. P., editors, *CONTROLO 2020*, pages 394–403, Cham. Springer International Publishing.

[Platus, 1992] Platus, D. L. (1992). Negative-stiffness-mechanism vibration isolation systems. In Gordon, C. G., editor, *San Jose - DL Tentative*, pages 44–54, San Jose, CA.

[Plunkett, 1958] Plunkett, R. (1958). Vibratory Machine and Its Foundation. *NOISE Control*, page 5.

[Preumont, 2018a] Preumont, A. (2018a). *Active Control of Large Telescopes: Active Optics*, volume 246, pages 449–468. Springer International Publishing, Cham.

[Preumont, 2018b] Preumont, A. (2018b). *Vibration Control of Active Structures*. Springer Berlin Heidelberg, New York, NY.

[Preumont et al., 2002] Preumont, A., FrançOis, A., Bossens, F., and Abu-Hanieh, A. (2002). Force feedback versus acceleration feedback in active vibration isolation. *Journal of Sound and Vibration*, 257(4):605–613.

[Preumont et al., 2007] Preumont, A., Horodinca, M., Romanescu, I., de Marneffe, B., Avraam, M., Deraemaeker, A., Bossens, F., and Abu Hanieh, A. (2007). A six-axis single-stage active vibration isolator based on Stewart platform. *Journal of Sound and Vibration*, 300(3-5):644–661.

[Pu et al., 2019] Pu, H., Yuan, S., Peng, Y., Meng, K., Zhao, J., Xie, R., Huang, Y., Sun, Y., Yang, Y., Xie, S., Luo, J., and Chen, X. (2019). Multi-layer electromagnetic spring with tunable negative stiffness for semi-active vibration isolation. *Mechanical Systems and Signal Processing*, 121:942–960.

[Qiu et al., 2009] Qiu, J., Ji, H., and Zhu, K. (2009). Semi-active vibration control using piezoelectric actuators in smart structures. *Frontiers of Mechanical Engineering in China*.

[Rahman et al., 1998] Rahman, Z. H., Spanos, J. T., and Laskin, R. A. (1998). Multiaxis vibration isolation, suppression, and steering system for space observational applications. In Lewis, H., editor, *Astronomical Telescopes & Instrumentation*, pages 73–81, Kona, HI.

[Rakheja and Sankar, 1985] Rakheja, S. and Sankar, S. (1985). Vibration and Shock Isolation Performance of a Semi-Active "On-Off" Damper. *Journal of Vibration Acoustics Stress and Reliability in Design*, 107(4):398.

[Rivin, 2003] Rivin, E. I. (2003). *Passive Vibration Isolation*. ASME Press [u.a.], New York.

[Robinson, 1982] Robinson, W. H. (1982). Lead-rubber hysteretic bearings suitable for protecting structures during earthquakes. *Earthquake Engineering & Structural Dynamics*, 10(4):593–604.

[Rosaria, 2008] Rosaria, A. M. M. (2008). *Seismic Isolation and Energy Dissipation:Theoretical Basis and Applications*. PhD thesis, Università degli Studi di Napoli Federico II, Italy.

[Rutledge et al., 1996] Rutledge, D., Hubbard, M., and Hrovat, D. (1996). A Two DOF Model for Jerk Optimal Vehicle Suspensions. *Vehicle System Dynamics*, 25(2):113–136.

[Ruzicka, 1968] Ruzicka, J. E. (1968). Active Vibration and Shock Isolation. In *National Aeronautic and Space Engineering and Manufacturing Meeting*.

[Salcedo-Sanz, 2016] Salcedo-Sanz, S. (2016). Modern meta-heuristics based on non-linear physics processes: A review of models and design procedures. *Physics Reports*, 655:1–70.

[Salcedo-Sanz, 2017] Salcedo-Sanz, S. (2017). A review on the coral reefs optimization algorithm: New development lines and current applications. *Progress in Artificial Intelligence*, 6(1):1–15.

[Salcedo-Sanz et al., 2017a] Salcedo-Sanz, S., Camacho-Gómez, C., Magdaleno, A., Pereira, E., and Lorenzana, A. (2017a). Structures vibration control via Tuned Mass Dampers using a co-evolution Coral Reefs Optimization algorithm. *Journal of Sound and Vibration*, 393:62–75.

[Salcedo-Sanz et al., 2016] Salcedo-Sanz, S., Camacho-Gomez, C., Molina, D., and Herrera, F. (2016). A coral reefs optimization algorithm with substrate layers and local search for large scale global optimization. In *2016 IEEE Congress on Evolutionary Computation (CEC)*, pages 3574–3581, Vancouver, BC, Canada. IEEE.

[Salcedo-Sanz et al., 2014a] Salcedo-Sanz, S., Del Ser, J., Landa-Torres, I., Gil-López, S., and Portilla-Figueras, J. A. (2014a). The Coral Reefs Optimization Algorithm: A Novel Metaheuristic for Efficiently Solving Optimization Problems. *The Scientific World Journal*, 2014:1–15.

[Salcedo-Sanz et al., 2019] Salcedo-Sanz, S., García-Herrera, R., Camacho-Gómez, C., Alexandre, E., Carro-Calvo, L., and Jaume-Santero, F. (2019). Near-optimal selection of representative measuring points for robust temperature field recon-

struction with the CRO-SL and analogue methods. *Global and Planetary Change*, 178:15–34.

[Salcedo-Sanz et al., 2017b] Salcedo-Sanz, S., Muñoz-Bulnes, J., and Vermeij, M. J. A. (2017b). New coral reefs-based approaches for the model type selection problem: A novel method to predict a nation's future energy demand. *Int. J. Bio-Inspired Comput.*, 10(3):145–158.

[Salcedo-Sanz et al., 2014b] Salcedo-Sanz, S., Pastor-Sánchez, A., Prieto, L., Blanco-Aguilera, A., and García-Herrera, R. (2014b). Feature selection in wind speed prediction systems based on a hybrid coral reefs optimization – Extreme learning machine approach. *Energy Conversion and Management*, 87:10–18.

[Sánchez-Montero et al., 2018] Sánchez-Montero, R., Camacho-Gómez, C., López-Espí, P.-L., and Salcedo-Sanz, S. (2018). Optimal Design of a Planar Textile Antenna for Industrial Scientific Medical (ISM) 2.4 GHz Wireless Body Area Networks (WBAN) with the CRO-SL Algorithm. *Sensors*, 18(7):1982.

[Saulson, 1984] Saulson, P. R. (1984). Vibration isolation for broadband gravitational wave antennas. *Review of Scientific Instruments*, 55(8):1315–1320.

[Schmitt and Leingang, 1976] Schmitt, R. V. and Leingang, C. J. (1976). Design of Elastomeric Vibration Isolation Mounting Systems for Internal Combustion Engines. In *27th Annual Earthmoving Industry Conference*, page 760431.

[Sciulli and Inman, 1998] Sciulli, D. and Inman, D. J. (1998). Isolation Design for a Flexible System. *Journal of Sound and Vibration*, 216(2):251–267.

[Sciulli and Inman, 2000] Sciulli, D. and Inman, D. J. (2000). Isolation design for fully flexible systems. *Journal of Intelligent Material Systems and Structures*, 10(10):813–824.

[Scribner et al., 1993] Scribner, K. B., Sievers, L., and Flotow, A. H. (1993). Active narrow-band vibration isolation of machinery noise from resonant substructures. *Journal of Sound and Vibration*, 167:17–40.

[Shirahatti et al., 2008] Shirahatti, A., Prasad, P., Panzade, P., and Kulkarni, M. (2008). Optimal design of passenger car suspension for ride and road holding. *Journal of the Brazilian Society of Mechanical Sciences and Engineering*, 30(1):66–76.

[Shook et al., 2008] Shook, D. A., Roschke, P. N., and Ozbulut, O. E. (2008). Superelastic semi-active damping of a base-isolated structure. *Structural Control and Health Monitoring*, 15(5):746–768.

[Smith and Walker, 2000] Smith, M. C. and Walker, G. W. (2000). Performance Limitations and Constraints for Active and Passive Suspensions: A Mechanical Multi-port Approach. *Vehicle System Dynamics*, 33(3):137–168.

[Soliman and Hallam, 1968] Soliman, J. and Hallam, M. (1968). Vibration isolation between non-rigid machines and non-rigid foundations. *Journal of Sound and Vibration*, 8(2):329–351.

[Song et al., 2018] Song, C., Xiao, Y., Yu, C., Xu, W., and Zhang, J. (2018). H $_\infty$ active control of frequency-varying disturbances in a main engine on the floating raft vibration isolation system. *Journal of Low Frequency Noise, Vibration and Active Control*, 37(2):199–215.

[Spanos et al., 1992] Spanos, J., Rahman, Z., Chu, C., and O'Brien, J. (1992). Control Structure Interaction in Long Baseline Space Interferometers. *IFAC Proceedings Volumes*, 25(22):463–470.

[Stevenson, 1868] Stevenson, D. (1868). Notice of Aseismatic Arrangements, adapted to Structures in Countries subject to Earthquakes Shocks. *Transaction of the Royal Scottish Society of Arts*, 7:557–566.

[Stewart, 1965] Stewart, D. (1965). A Platform with Six Degrees of Freedom. *Proceedings of the Institution of Mechanical Engineers*, 180(1):371–386.

[Storn and Price, 1997] Storn, R. and Price, K. (1997). Differential Evolution – A Simple and Efficient Heuristic for global Optimization over Continuous Spaces. *Journal of Global Optimization*, 11(4):341–359.

[Sun et al., 2015a] Sun, L., Hansen, C., and Doolan, C. (2015a). Evaluation of the performance of a passive–active vibration isolation system. *Mechanical Systems and Signal Processing*, 50-51:480–497.

[Sun et al., 2015b] Sun, S., Yang, J., Li, W., Deng, H., Du, H., and Alici, G. (2015b). Development of a novel variable stiffness and damping magnetorheological fluid damper. *Smart Materials and Structures*, 24(8):085021.

[Symans and Constantinou, 1999] Symans, M. D. and Constantinou, M. C. (1999). Semi-active control systems for seismic protection of structures: A state-of-the-art review. *Engineering Structures*, 21(6):469–487.

[Symans and Kelly, 1999] Symans, M. D. and Kelly, S. W. (1999). Fuzzy logic control of bridge structures using intelligent semi-active seismic isolation systems. *Earthquake Engineering \& Structural Dynamics*, 28(1):37–60.

[Tang et al., 2019] Tang, J., Cao, D., and Yu, T. (2019). Decentralized vibration control of a voice coil motor-based Stewart parallel mechanism: Simulation and experiments. *Proceedings of the Institution of Mechanical Engineers, Part C: Journal of Mechanical Engineering Science*, 233(1):132–145.

[Thayer et al., 2002] Thayer, D., Campbell, M., Vagners, J., and von Flotow, A. (2002). Six-Axis Vibration Isolation System Using Soft Actuators and Multiple Sensors. *Journal of Spacecraft and Rockets*, 39(2):206–212.

[Thompson, 1970] Thompson, A. G. (1970). Design of Active Suspensions. *Proceedings of the Institution of Mechanical Engineers*, 185(1):553–563.

[Tsai et al., 2006] Tsai, C. S., Chen, W.-S., Chiang, T.-C., and Chen, B.-J. (2006). Component and shaking table tests for full-scale multiple friction pendulum system. *Earthquake Engineering & Structural Dynamics*, 35(13):1653–1675.

[Tsai et al., 2019] Tsai, C.-W., Chang, W.-Y., Wang, Y.-C., and Chen, H. (2019). A high-performance parallel coral reef optimization for data clustering. *Soft Computing*, 23(19):9327–9340.

[Tseng and Hedrick, 1994] Tseng, H. and Hedrick, J. (1994). Semi-Active Control Laws - Optimal and Sub-Optimal. *Vehicle System Dynamics*, 23(1):545–569.

[Venanzi et al., 2017] Venanzi, I., Ierimonti, L., and Ubertini, F. (2017). Effects of control-structure interaction in active mass driver systems with electric torsional servomotor for seismic applications. *Bulletin of Earthquake Engineering*, 15(4):1543–1557.

[Vervoordeldonk et al., 2004] Vervoordeldonk, M. J., Ruijl, T. A., and Rijs, R. M. (2004). Development of a novel active isolation concept. In *ASPE Spring Topical Meeting*.

[Wang et al., 2016a] Wang, C., Xie, X., Chen, Y., and Zhang, Z. (2016a). Active vibration isolation through a Stewart platform with piezoelectric actuators. *Journal of Physics: Conference Series*, 744:012006.

[Wang et al., 2016b] Wang, C., Xie, X., Chen, Y., and Zhang, Z. (2016b). Investigation on active vibration isolation of a Stewart platform with piezoelectric actuators. *Journal of Sound and Vibration*, 383:1–19.

[Wang et al., 2017] Wang, H., Wang, W., Zhou, X., Sun, H., Zhao, J., Yu, X., and Cui, Z. (2017). Firefly algorithm with neighborhood attraction. *Information Sciences*, 382-383:374–387.

[Warn et al., 2007] Warn, G. P., Whittaker, A. S., and Constantinou, M. C. (2007). Vertical Stiffness of Elastomeric and Lead–Rubber Seismic Isolation Bearings. *Journal of Structural Engineering*, 133(9):1227–1236.

[Wilson et al., 1986] Wilson, D. A., Sharp, R. S., and Hassan, S. A. (1986). The Application of Linear Optimal Control Theory to the Design of Active Automotive Suspensions. *Vehicle System Dynamics*, 15(2):105–118.

[Wu et al., 2019] Wu, G., Mallipeddi, R., and Suganthan, P. N. (2019). Ensemble strategies for population-based optimization algorithms – A survey. *Swarm and Evolutionary Computation*, 44:695–711.

[Wu et al., 1994] Wu, X. M., Wong, J. Y., Sturk, M., and Russel, D. L. (1994). Simulation and experimental study of a semi-active suspension with an electrorheological damper. *International Journal of Modern Physics*, 8:2987–3003.

[Xie et al., 2018] Xie, Y., Shi, H., Bi, F., and Shi, J. (2018). A MIMO data driven control to suppress structural vibrations. *Aerospace Science and Technology*, 77:429–438.

[Xu and Weng, 2013] Xu, Z.-d. and Weng, C.-h. (2013). Track-position and vibration control simulation for strut of the Stewart platform. *Journal of Zhejiang University SCIENCE A*, 14(4):281–291.

[Yan et al., 2006] Yan, B., Brennan, M., Elliott, S., and Ferguson, N. (2006). Velocity feedback control of vibration isolation systems. *ISVR Technical Memorandum 962*.

[Yan et al., 2010] Yan, B., Brennan, M., Elliott, S., and Ferguson, N. (2010). Active vibration isolation of a system with a distributed parameter isolator using absolute velocity feedback control. *Journal of Sound and Vibration*, 329(10):1601–1614.

[Yan et al., 2019] Yan, C., Ma, J., Luo, H., and Patel, A. (2019). Hybrid binary Coral Reefs Optimization algorithm with Simulated Annealing for Feature Selection in high-dimensional biomedical datasets. *Chemometrics and Intelligent Laboratory Systems*, 184:102–111.

[Yang, 1994] Yang, B. (1994). Distributed Transfer Function Analysis of Complex Distributed Parameter Systems. *Journal of Applied Mechanics*, 61(1):84–92.

[Yang et al., 2017] Yang, X., Wu, H., Li, Y., and Chen, B. (2017). Dynamic isotropic design and decentralized active control of a six-axis vibration isolator via Stewart platform. *Mechanism and Machine Theory*, 117:244–252.

[Yang, 2008] Yang, X. S. (2008). Firefly algorithm. *Nature-inspired metaheuristic algorithms*, 20:79–90.

[Yang et al., 2018] Yang, Y., Yang, B., and Niu, M. (2018). Adaptive infinite impulse response system identification using opposition based hybrid coral reefs optimization algorithm. *Applied Intelligence*, 48(7):1689–1706.

[Yang et al., 2016] Yang, Z., Zhang, T., and Zhang, D. (2016). A novel algorithm with differential evolution and coral reef optimization for extreme learning machine training. *Cognitive Neurodynamics*, 10(1):73–83.

[Yao et al., 2002] Yao, G., Yap, F., Chen, G., Li, W., and Yeo, S. (2002). MR damper and its application for semi-active control of vehicle suspension system. *Mechatronics*, 12(7):963–973.

[Yu et al., 2001] Yu, Y., Naganathan, N. G., and Dukkipati, R. V. (2001). A literature review of automotive vehicle engine mounting systems. *Mechanism and Machine Theory*, 36(1):123–142.

[Zapateiro et al., 2012] Zapateiro, M., Pozo, F., Karimi, H. R., and Luo, N. (2012). Semiactive Control Methodologies for Suspension Control With Magnetorheological Dampers. *IEEE/ASME Transactions on Mechatronics*, 17(2):370–380.

[Zhang et al., 2009] Zhang, X. Z., Wang, X. Y., Li, W. H., and Kostidis, K. (2009). Variable stiffness and damping MR isolator. *Journal of Physics: Conference Series*, 149:012088.

[Zhang et al., 2014] Zhang, Z., Karimi, H. R., Huang, H., and Robbersmyr, K. G. (2014). Vibration Control of a Semiactive Vehicle Suspension System Based on Extended State Observer Techniques. *Journal of Applied Mathematics*, 2014:1–10.

[Zhao et al., 2019] Zhao, Z., Zhang, R., Jiang, Y., and Pan, C. (2019). Seismic response mitigation of structures with a friction pendulum inerter system. *Engineering Structures*, 193:110–120.

[Zheng, 2015] Zheng, Y.-J. (2015). Water wave optimization: A new nature-inspired metaheuristic. *Computers & Operations Research*, 55:1–11.

[Zhou et al., 2009] Zhou, Y., Wang, X., Zhang, X., and Li, W. (2009). Variable stiffness and damping magnetorheological isolator. *Frontiers of Mechanical Engineering in China*.